N84-28892

HOWARD UNIVERSITY
SCHOOL OF ENGINEERING
DEPARTMENT OF MECHANICAL ENGINEERING
WASHINGTON, D.C. 20059

FINAL REPORT

NASA GRANT: NSG-1414, Suppl. 6

THE DYNAMICS AND CONTROL OF LARGE FLEXIBLE SPACE STRUCTURES - VII

by

Peter M. Bainum
Professor of Aerospace Engineering
Principal Investigator

and

A.S.S.R. Reddy
Assistant Professor
Co-Investigator

and

R. Krishna, Cheick M. Diarra, and S. Ananthakrishnan

Graduate Research Assistants

June 1984

TABLE OF CONTENTS

ABSTRACT

A preliminary Eulerian formulation of the in-plane dynamics of the proposed SCOLE configuration is undertaken when the mast is treated as a cantilever - type beam and the reflector as a lumped mass at the end of the beam. Frequencies and mode shapes are obtained for the open loop model of the beam system. The inherent time delay due to actuators is taken into consideration to analyze the stability of closed-loop control systems by both frequency and time domain techniques. Environmental disturbances due to solar radiation pressure are incorporated into the previously developed models of controlled large flexible orbiting platforms nominally oriented along the local vertical (with the major surface normal to the orbital plane) or oriented with the major surface lying in the local horizontal plane. For extremely flexible platforms the need to redesign previously synthesized control laws is indicated. Thermally induced deformations of simple beam and platform type structures are modelled and expressions developed for the disturbance torques resulting from the interaction of solar radiation pressure. Such thermal deformations may give rise to larger disturbance torques than the interaction of solar pressure with the vibrating structure (ignoring the thermal distortions). Noise effects in the previously designed deterministic model of the Hoop/Column antenna system are found to cause a degradation in system performance. Improved transient and steady state performance can be obtained by appropriate changes in the ratio of plant noise to the measurement noise and/or changes in the control weighting matrix elements.

LIST OF FIGURES

LIST OF FIGURES

LIST OF FIGURES

LIST OF FIGURES

I. INTRODUCTION

The present grant extends the research effort initiated in previous grant years (May 1977 - May 1983) and reported in Refs. 1-9*. Techniques for controlling both the shape and orientation of very large inherently flexible proposed future spacecraft systems are being studied. Possible applications of such large structures in orbit include: large scale multi-beam communication systems; earth observation and resource sensing systems; orbitally based electronic mail transmission; and as orbital platforms for the collection of solar energy and transmission (via microwave) to earth based receivers.

This report is subdivided into seven chapters. Chapter II presents a preliminary development of a two dimensional model of the rotational equations of motion for the proposed Spacecraft Control Laboratory Experiment - (SCOLE)[10]. This development is based on the expansion of the Eulerian moment equations assuming the Shuttle and the reflector are rigid bodies and modelling the mast as a flexible cantilever type beam. A preliminary calculation is performed to obtain the frequencies of the fundamental and first few in-plane bending modes as well as the corresponding modal shape functions.

In the following chapter a preliminary review is given of stability techniques that can be applied when time delays are present in the implementation of the control inputs.

---

*References cited in this report are listed separately at the end of each chapter.

Both time domain and frequency domain techniques are described with emphasis placed on applications to large order systems typical of large space structures. The major question to be answered is whether marginally stable or oscillatory systems could be stabilized by using delayed feedback techniques.

Chapter IV is based on a paper to be presented at the Fourteenth International Symposium on Space Technology and Science and examines the control of a thin orbiting flexible square platform in the presence of solar radiation. The disturbance torques resulting from the interaction of solar pressure with the vibrating plate analog of the platform are modelled and incorporated in the dynamic model of a square plate nominally oriented along the local vertical with the major surface normal to the orbital plane and also nominally oriented with the major surface lying in the local horizontal plane. Transient responses and control requirements are examined for both nominal orientations.

The effect of environmental disturbances on the dynamics of large orbiting systems is extended in Chapter V to also include solar heating effects. A paper to be presented at the 1984 AIAA/AAS Astrodynamics Conference forms the basis of this chapter. The evaluation of the effect of solar radiation pressure on flexible beams and plates which are subject to thermal deflections (in addition to vibrations) is the objective of this paper. For very flexible system where the previously developed control laws may not be adequate to account for environmental disturbances, the versatility of the linear quadratic regulator techniques provided by the ORACLS software package[11] can be utilized to

redesign the control strategies in order to reach a compromise between reducing the excess vibrational and rotational energy while at the same time maintaining the control effect at an acceptable level.

Partial support from this grant was provided for one of the graduate research assistants during the Summer of 1983 only. This research was continued during the 1983-84 academic year sponsored by the University, and the results are presented in Chapter VI in the format of a paper presented at the recent 1984 AIAA Mid-Atlantic Regional Student Conference. In this paper, the work previously initiated during the last grant year[9] analyzing the dynamics and control of the proposed Hoop/Column orbiting antenna system is extended to incorporate the effects of both plant and measurement noise in the system. The results described here are based on co-located actuators and sensors assumed to be located on the column, electronic feed, and also on the hoop. The general degradation of the previously designed deterministic system is attributed to the incorporation of the uncorrelated zero-mean white noises assumed to be present in the plant and measurement sensors. The Kalman filter algorithm of the ORACLS package is used to develop control laws and simulate the estimate of the state in an optimal LQG manner. Studies are included showing the effect of increasing the elements in the state weighting matrix as well as varying the noise characteristics.

Chapter VII describes the main general conclusions together with future recommendations. The effort described in Chapters II and III is being continued during the 1984-85 grant period in accordance with our proposal[12] and subsequent discussions.

References

1. Bainum, P.M. and Sellappan, R., "The Dynamics and Control of Large Flexible Space Structures," Final Report NASA Grant: NSG-1414, Part A: Discrete Model and Modal Control, Howard University, May 1978.

2. Bainum, Peter M., Kumar, V.K., and James, Paul K., "The Dynamics and Control of Large Flexible Space Structures," Final Report, NASA Grant: NSG-1414, Part B: Development of Continuum Model and Computer Simulation, Howard University, May 1978.

3. Bainum, P.M. and Reddy, A.S.S.R., "The Dynamics and Control of Large Flexible Space Structures II," Final Report, NASA Grant NSG-1414, Suppl. I, Part A: Shape and Orientation Control Using Point Actuators, Howard University, June 1979.

4. Bainum, P.M., James, P.K., Krishna, R., and Kumar, V.K., "The Dynamics and Control of Large Flexible Space Structures II," Final Report, NASA Grant NSG-1414, Suppl. 1, Part B: Model Development and Computer Simulation, Howard University, June 1979.

5. Bainum, P.M., Krishna, R., and James, P.K., "The Dynamics and Control of Large Flexible Space Structures III," Final Report, NASA Grant NSG-1414, Suppl. 2, Part A: Shape and Orientation Control of a Platform in Orbit Using Point Actuators, Howard University, June 1980.

6. Bainum, P.M. and Kumar, V.K., "The Dynamics and Control of Large Flexible Space Structures III," Final Report, NASA Grant NSG-1414, Suppl. 2, Part B: The Modelling, Dynamics and Stability of Large Earth Pointing Orbiting Structures, Howard University, September 1980.

7. Bainum, P.M., Kumar, V.K., Krishna, R. and Reddy, A.S.S.R., "The Dynamics and Control of Large Flexible Space Structures IV," Final Report, NASA Grant NSG-1414, Suppl. 3, NASA CR-165815, Howard University, August 1981.

8. Bainum, P.M., Reddy, A.S.S.R., Krishna, R., Diarra, C.M., and Kumar, V.K., "The Dynamics and Control of Large Flexible Space Structures V", Final Report, NASA Grant NSG-1414, Suppl. 4, NASA CR-169360, Howard University, August 1982.

9. Bainum, P.M., Reddy, A.S.S.R., Krishna, R., and Diarra, C.M., "The Dynamics and Control of Large Flexible Space Sturctures VI," Final Report NASA Grant NSG-1414, Suppl. 5, Howard University, Sept. 1983.

10. Taylor, L.W. and Balskrishnan, A.V., "A Mathematical Problem and a Spacecraft Control Laboratory Experiment (SCOLE) Used to Evaluate Control Laws for Flexible Spacecraft ... NASA/ IEEE Design Challenge," (Rev.), January 1984. (originally presented at AIAA/VPI&SU Symposium on Dynamics and Control of Large Structures," June 6-8, 1983).

11. Armstrong, E.S., "ORACLS - A System for Linear Quadratic-Gaussian Control Law Design," NASA Technical Paper 1106, April 1978.

12. Bainum, P.M. and Reddy, A.S.S.R., "Proposal for Research Grant on: "The Dynamics and Control of Large Flexible Space Structures VII," Howard University (submitted to NASA), Nov. 10, 1983.

II. MODELLING TECHNIQUES AND CONTROL SYNTHESIS FOR THE SPACECRAFT CONTROL LABORATORY EXPERIENT - PRELIMINARY RESULTS

The transfer of large, massive payloads into Earth orbit is currently accomplished with considerable propulsive and control effort. As a result, spacecraft designers must strive to minimize a large structure's mass. Consequently, many of the future spacecraft will be very flexible and will require that their shape and orientation be controlled.[1] The problem of controlling large, flexible space systems has been the subject of considerable research. Many approaches to control system synthesis have been evaluated using computer simulations including a preliminary synthesis of control laws for the proposed Hoop/Column System.[2,3] Ground experiments have also been used to validate system performance under more realistic conditions but based on simple structures such as beams and plates.[4] In a recent paper, SCOLE (Spacecraft Control Laboratory Experiment), Lawrence W. Taylor Jr. and A.V. Balakrishnan described a proposed laboratory experiment based on a model of the Shuttle connected to a flexible beam with a reflecting grillage mounted at the end of the beam[5] (Fig. 2.1). The authors stressed the need to directly compare competing control design techniques, and discussed the feasibility of such direct comparison. Concern would be given to modelling order reduction, fault management, stability, and dynamic system performance.

With this paper[5] as a background, the purpose of the study proposed here is to model the system in different phases where each successive phase would represent a mathematical model successively closer to that of the actual laboratory system.

It is anticipated that this (multi-year) study would consist of five parts, the first of which would consist of a literature survey during which the investigators would familiarize themselves with different mathematical modelling techniques.

During the second part, the system would be successively modelled as follows:

a) The Space Shuttle as a rigid body; the reflector mast as a flexible beam type appendage; and the reflector as a rigid plate. The mast shape functions are actually solved from the fourth order non-linear flexural beam equation with different boundary conditions imposed on both the Shuttle and grillage ends. b) Here the Space Shuttle would be treated as a rigid body body; the composite appendage consisting of the flexible reflector mast and also the continuous rigid reflector (grillage) could be modelled using finite element techniques. Then the composite system dynamics can be modelled using the hybrid coordinate technique[6] which involves sets of matrix equations describing the motion of the main vehicle as well as that of any attached appendages. It is anticipated that within the second part of this study these different mathematical models would be developed in a form suitable for numerical simulation.

During the third part, each of these models could be directly compared with the model proposed in the SCOLE paper[5], beginning with the simulation of the open-loop system dynamics. The fourth part of the effort would consist of the control law synthesis when the model can be described by linear system dynamics - i.e., in response to small perturbations induced on the system about the nominal laboratory configuration and orientation, or after a major slewing maneuver, to remove the

remaining transients which exist in a neighborhood of the new equilibrium orientation. Such a construction of control laws will probably be based on the ORACLS software package.[7] Strategies would be developed to control the shape and orientation of the beam/grillage.

First the controllability of the system could be examined based on the graph theoretic techniques already employed for a similar analysis of the Hoop/Column system[3], for different combinations of numbers and locations of the actuators. Next, control laws can be constructed based on the techniques of optimal control theory, and studies can be performed comparing transient and control effort characteristics for a variety of system parameters and weighting matrix elements.

Finally, the fifth part would focus on the slewing maneuvers to accurately point the reflector at a specific target in a minimum lapse of time. For simple maneuvers (single axis) attempts would be made to analytically determine the slewing control law; for more general maneuvers, numerical techniques would be implemented.

II. A Development of the Two Dimensional Model - (Eulerian Moment Equations)

The SCOLE system is assumed to be comprised of three main parts (Fig. 2.1):

i) the Space Shuttle Orbiter with its center of mass located at point O_1;

ii) the mast, treated as a 130 ft long beam, connected to the Shuttle at O_2 and to the reflector at O_3;

iii) the reflector, considered to be a flat plate with its center of mass at O_4.

The preliminary analysis presented here started before it was specified[8] that the interface point between the mast and the Shuttle is at O_1.[8] Therefore, in what follows, a position vector $\vec{R}_1$ appears which defines $\vec{O_1O_2}$, where O_2 is the assumed interface point.

In the following analysis, the angular momentum of the entire system is evaluated at point O_1 and the dynamics include the lateral displacements of the beam.

II. A.1 Angular Momentum of the Shuttle with Respect to Point O_1

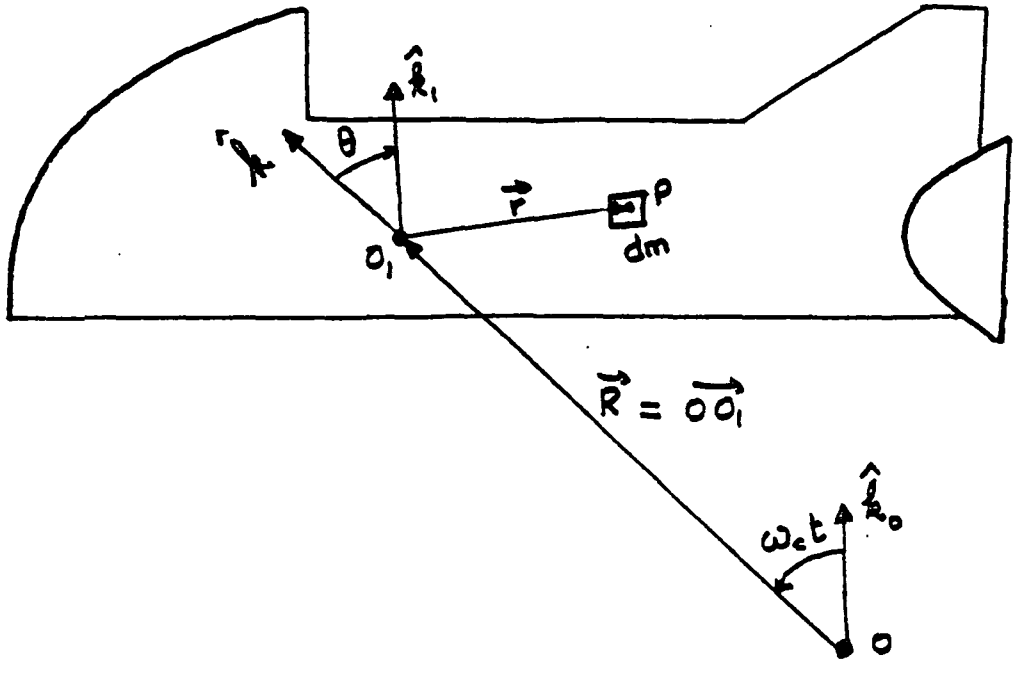

Consider a point, P, of mass, dm, at an arbitrary position in the Shuttle such that $\vec{O_1P} = \vec{r}$. The elemental angular momentum of the mass, dm, is given by:

$$d\vec{H}_{O_1} = \vec{r} \times \frac{d}{dt}\vec{OP}\Big|_{R_o} dm = \vec{r} \times \frac{d}{dt}(\vec{R}+\vec{r})\Big|_{R_o} dm$$
$$= \vec{r} \times \{\dot{R}\hat{k} + R\omega_c \hat{\imath} + (\omega_c - \dot{\theta})\hat{\jmath} \times \vec{r}\}\, dm \qquad (2.1)$$

The total angular momentum for the Shuttle is obtained by integrating Eq. (2.1) over the entire mass of Shuttle as:

$$\vec{H}_{S_{O_1}} = -\dot{R}\hat{k} \times \int_{M_S} \vec{r}\, dm - R\omega_c \hat{\imath} \times \int_{M_S} \vec{r}\, dm + \int_{M_S} \vec{r} \times \{(\omega_c - \dot{\theta})\hat{\jmath} \times \vec{r}\}\, dm \qquad (2.2)$$

The first and second integrals appearing in the right side of Eq. (2.2) vanish because the center of mass of the Shuttle is at point O_1.

Since $\vec{r} \cdot \vec{j} = 0$, Eq. (2.2) takes the form:

$$\vec{H}_{S/O_1} = (\omega_c - \dot{\theta})\hat{\jmath} \int_{M_S} r^2\, dm = \mathbb{I}_S\, \vec{\omega}_{R_1/R_o} \qquad (2.3)$$

where $\mathbb{I}_S$ is the Inertia tensor of the Shuttle at point O_1 and $\vec{\omega}_{R_1/R_0} = (\omega_c - \dot{\theta})\,\hat{j}$.

II. A.2 Angular Momentum of the Mast with Respect to Point O_1

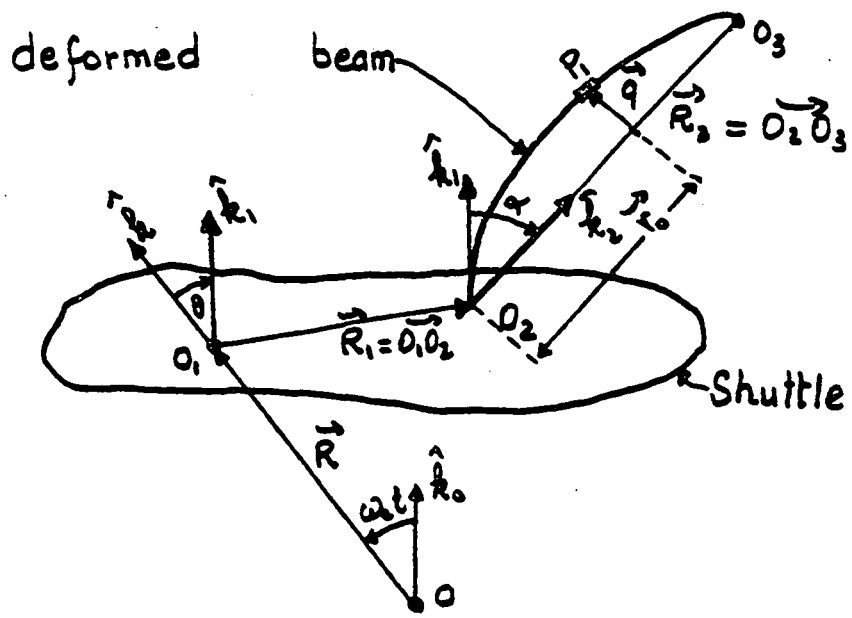

Consider here an element of the mast located at point, P_1, with mass, dm. The elemental angular momentum of such an element is given by:

$$d\vec{H}_{M/O_1} = \overrightarrow{O_1P_1} \times \frac{d}{dt}\overrightarrow{OP_1}\Big|_{\mathcal{R}_o} dm \qquad (2.4)$$

if one notes that

$$\left.\begin{aligned} \overrightarrow{O_1P_1} &= \vec{R}_1 + \vec{r}_o + \vec{q} \quad \text{and} \\ \overrightarrow{OP_1} &= \vec{R} + \overrightarrow{O_1P_1} \end{aligned}\right\} \qquad (2.5)$$

then, Eq. (2-4) may be expanded according to:

$$d\vec{H}_{M/O_1} = (\vec{R}_1 + \vec{r}_o + \vec{q}) \times \frac{d}{dt}(\vec{R} + \vec{R}_1 + \vec{r}_o + \vec{q})\Big|_{\mathcal{R}_o} dm \qquad (2.6)$$

$\frac{d}{dt}(\vec{R}+\vec{R}_1+\vec{r}_o+\vec{q})\Big|_{\mathcal{R}_o}$ is expressed using the relationship between the rate of change of a vector, $\vec{w}$, in an inertial (R_o) and rotating (R_i) frames, i.e.

$$\frac{d}{dt}\vec{W}\Big|_{\mathcal{R}_o} = \frac{d}{dt}\vec{W}\Big|_{\mathcal{R}_i} + \vec{\Omega}_{\mathcal{R}_i/\mathcal{R}_o} \times \vec{W} \qquad (2.7)$$

After substituion of Eq. (2.7) into Eq. (2.6) and integration term by term, one can develop:

$$\begin{aligned} \vec{H}_{M/O_1} = {} & \left[\vec{R}_1 \times \frac{d}{dt}(\vec{R}_1+\vec{R})\Big|_{\mathcal{R}_o}\right] M_m + \vec{R}_1 \times \int_{M_m} (\dot{r}_o\hat{k}_2 + \dot{q}\hat{i}_2)\, dm \\ & + (\omega_c - \dot{\theta} - \dot{\alpha})\hat{j}\left\{\vec{R}_1 \cdot \int_{M_m}(\vec{r}_o+\vec{q})\, dm\right\} - \frac{d}{dt}(\vec{R}+\vec{R}_1)\Big|_{\mathcal{R}_o} \times \int_{M_m}(\vec{r}_o+\vec{q})\, dm \\ & + \int_{M_m}(\vec{r}_o+\vec{q}) \times (\dot{r}_o\hat{k}_2 + \dot{q}\hat{i}_2)\, dm + (\omega_c - \dot{\theta} - \dot{\alpha})\hat{j}\int_{M_m}|\vec{r}_o+\vec{q}|^2 dm \end{aligned} \qquad (2.8)$$

II. A.3 Angular Momentum of the Rigid Reflector with Respect to Point O_1

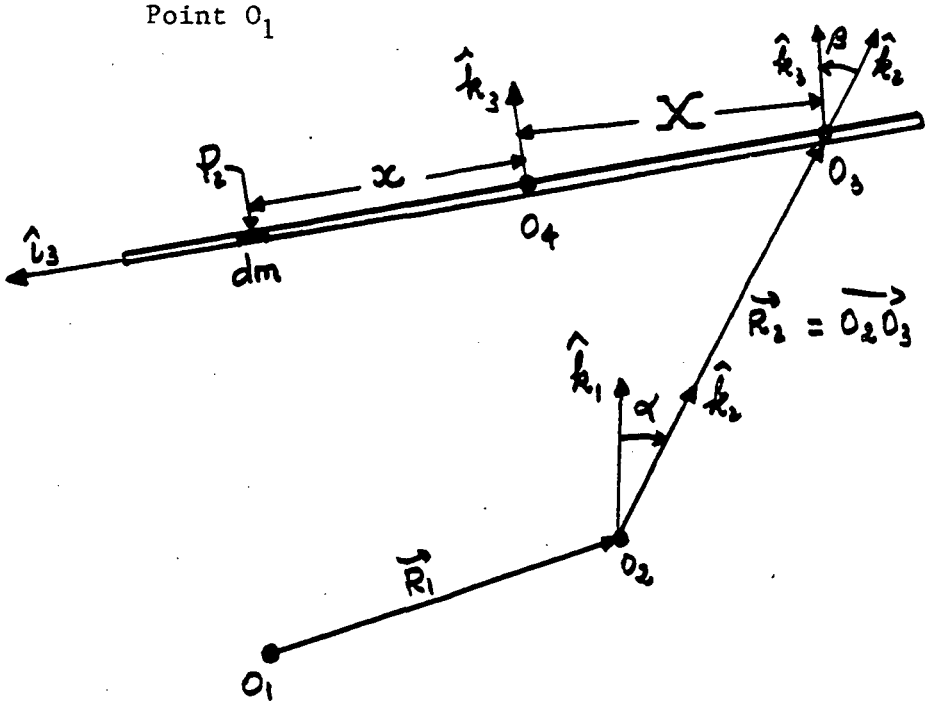

Let O_4 be the center of mass of the reflector, and O_3 the interface point between the reflector and the mast. The distance, X, between O_3 and O_4 is constant since the reflector is assumed to be rigid, at least for this analysis.

Let us now consider an element of mass, dm, of the reflector located at an arbitrary point, P_2. The elemental angular momentum of that element of mass can be expressed as:

$$d\vec{H}_{r/O_1} = \overrightarrow{O_1P_2} \times \frac{d}{dt}(\overrightarrow{OP_2})\Big|_{\mathcal{R}_0} dm \qquad (2.9)$$

$\vec{O_1P_2}$ and $\vec{O_2P_2}$ can be expressed as:

$$\left.\begin{aligned} \overrightarrow{O_1P_2} &= \vec{R}_1 + \vec{R}_2 + X\hat{\imath}_3 + x\hat{\imath}_3 \\ \overrightarrow{OP_2} &= \vec{R} + \overrightarrow{O_1P_2} \end{aligned}\right\} (2.10)$$

Eq. (2.9) may be expanded according to

$$\underline{d}\,\vec{H}_{r/O_1} = (\vec{R}_1+\vec{R}_2+(\mathcal{X}+x)\,\hat{i}_3) \times \frac{d}{dt}(\vec{R}_1+\vec{R}+\vec{R}_2+(\mathcal{X}+x)\,\hat{i}_3)\Big|_{\mathcal{R}_0} \qquad (2.11)$$

Once more, $\frac{d}{dt}(\vec{R}+\vec{R}_1+\vec{R}_2+(x+\mathcal{X})\,\hat{i}_3)\Big|_{\mathcal{R}_0}$ is expressed using Eq. (2.7): $\frac{d}{dt}\vec{w}\Big|_{\mathcal{R}_0} = \frac{d}{dt}\vec{w}\Big|_{\mathcal{R}_i} + \vec{\Omega}^{\mathcal{R}_i/\mathcal{R}_0} \times \vec{w}$

After substitution of Eq. (2.7) into Eq. (2.11) and integration term by term over the entire mass of the reflector, one arrives at

$$\vec{H}_{r/O_1} = M_r\left\{\vec{R}_1+\vec{R}_2\right\} \times \frac{d}{dt}\left\{\vec{R}+\vec{R}_1+\vec{R}_2\right\}\Big|_{\mathcal{R}_0} +$$

$$(\omega_c-\dot{\theta}-\dot{\alpha}+\dot{\beta})\left\{I_{2r}+\mathcal{X}^2 M_r\right\}\hat{j} +$$

$$(\omega_c-\dot{\theta}-\dot{\alpha}+\dot{\beta})\,M_r\left\{(\vec{R}_1+\vec{R}_2)\times\mathcal{X}\hat{k}_3\right\} +$$

$$M_r\mathcal{X}\,\hat{i}_3 \times \frac{d}{dt}\left\{\vec{R}+\vec{R}_1+\vec{R}_2\right\}_{\mathcal{R}_0} \qquad (2.12)$$

where I_{2r} is the moment of inertia of the reflector about the $\hat{j}$ axis taken at point O_4.

II. B.1 Moment Equation

The angular momentum of the entire system about O_1 is obtained by summing the angular momentum of each part about O_1, i.e.

$$\vec{H}_{T/O_1} = \sum_{i=1}^{3} \vec{H}_{i/O_1} \tag{2.13}$$

The moment equation

$$\frac{d}{dt} \vec{H}_{T/O_1} \Big|_{\mathcal{R}_0} = \vec{N} \tag{2.14}$$

where $\vec{N}$ is the sum of all the enternal torques, acting on the entire system, about an axis through point O_1.

At this stage of the analysis, it is assumed that the center of mass of the Shuttle moves in a circular orbit, ie.

$$\frac{d}{dt} \vec{R} \Big|_{\mathcal{R}} = \dot{\vec{R}} \Big|_{\mathcal{R}} = \vec{0} \tag{2.15}$$

Taking into consideration the coincidence between points O_1 and O_2, Eq. (2.14) is expanded using once more Eq. (2.7) and the following result is obtained:

$$\frac{d}{dt} \vec{H}_{T/O_1} \Big|_{\mathcal{R}_0} \cdot \hat{j} = \vec{N} \cdot \hat{j} = N_y =$$

$$- I_3 \ddot{\theta} + M_r \left[R \omega_e \dot{R}_2 (\cos\theta \cos\alpha - \sin\alpha \sin\theta) + \right.$$

$$\omega_2 \omega_e R R_2 (\cos\alpha \sin\theta + \sin\alpha \cos\theta) - \omega_3 \chi \{ \sin\theta (\sin\beta \cos\alpha$$

$$\left. - \cos\beta \sin\alpha) + \cos\theta (\sin\beta \sin\alpha + \cos\beta \cos\alpha) \} + R_2^2 \dot{\omega}_2 + \right.$$

$$2 R_2 \dot{R}_2 \omega_2 - R\omega_c^2 R_2 (\sin\alpha\cos\theta + \cos\alpha\sin\theta) -$$

$$R\omega_c^2 X \{\sin\theta(\cos\beta\sin\alpha - \sin\beta\cos\alpha) - \cos\theta(\cos\beta\cos\alpha + \sin\beta\sin\alpha)\}$$

$$+ 2\dot{R}_2 \omega_3 X \sin\beta - \omega_2\omega_3 X\cos\beta + X^2\dot{\omega}_3 \Big]$$

$$+ \dot{\omega}_3 I_{2r} - X\{\cos\beta(\ddot{R}_2 - \omega_2^2 R_2) +$$

$$\sin\beta(\dot{\omega}_2 R_2 + 2\omega_2\dot{R}_2)\} + \{R\omega_c\omega_2 - R\omega_c^2\} \times$$

$$(\cos\alpha\sin\theta + \sin\alpha\cos\theta)\int_{M_m} r_o\, dm +$$

$$\{R\omega_c\omega_2 - R\omega_c^2\}(\sin\alpha\sin\theta - \cos\alpha\cos\theta)\int_{M_m} q\, dm$$

$$+ R\omega_c(\cos\alpha\sin\theta + \sin\alpha\cos\theta)\int_{M_m}\dot{q}\, dm + \dot{\omega}_2\int_{M_m} r^2\, dm$$

$$+ \omega_2\int_{M_m}\frac{d}{dt}(r^2)\Big|_{\Omega_2} dm + \int_{M_m}(r_o\ddot{q} + q\dot{q}\omega_2)\, dm = N_y$$

(2.16)

II. B.2 Expression for $\vec{q}$

In the moment equation, Eq. (2.16), one notices integrals involving $\vec{q}$, the transverse displacement vector, and its first and and second derivatives with respect to time. It is, therefore, necessary to develop an expression for $\vec{q}$.

II.B.2.i Relation between q(x,t) and y(x,t)

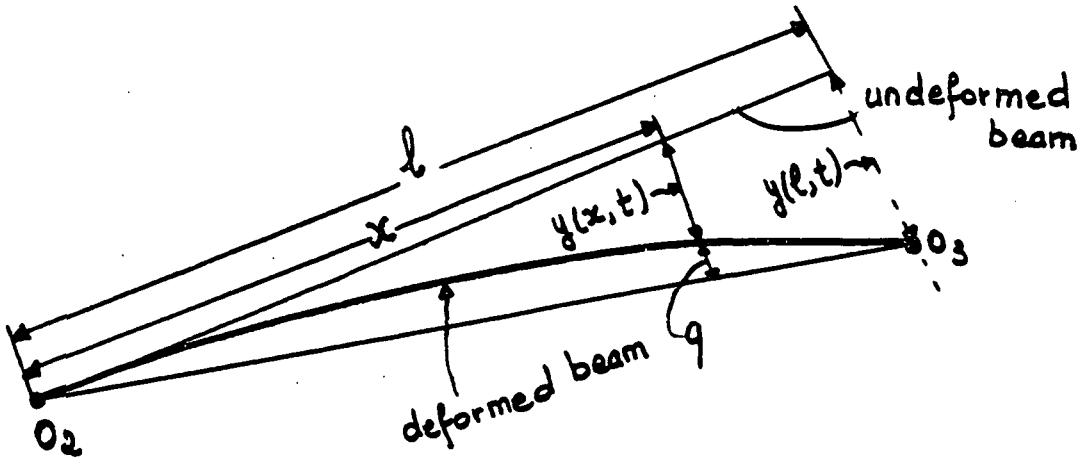

Consider the beam in its deflected configuration. $y(\ell,t)$ is the deflection of the reflector-end of the mast at an arbitrary time, t; $y(x,t)$, the deflection of an arbitrary point on the mast at the same time.

From Fig. (2.1), $\hat{k}_1 \cdot \hat{k}_2 = \cos\alpha$ (2.17)

Assuming α small, $\tan\alpha$ can be expressed as

$$\tan\alpha = \frac{y(\ell,t)}{\ell} \approx \alpha = \frac{y(x,t)+q(x,t)}{x} \qquad (2.18)$$

From Eq. (2.18) one derives

$$q(x,t) = \frac{x\, y(\ell,t)}{\ell} - y(x,t) \tag{2.19}$$

or

$$q(x,t) = \alpha x - y(x,t) \tag{2.20}$$

II.B.2.ii Evaluation of y(x,t)

Assuming separability of the variables, the beam equation,

$$+\frac{EI}{\rho A}\frac{\partial^4 y(x,t)}{\partial x^4} + \frac{\partial^2 y(x,t)}{\partial t^2} = 0 \tag{2.21}$$

is solved to yield solutions of the form:

$$y(x,t) = f(t)\,\phi(x) \tag{2.22}$$

where

$f(t)$ = E sinωt + F cosωt with ω = frequency of the vibration

and $\phi(x)$ = A cosβx + B sinβx + C coshβx + D sinhβx (2.23)

When the following boundary conditions are assumed:

a) $y(0,t) = 0$; b) $y'(0,t) = 0$

c) $EI\, y'''(\ell,t) = -Mr\, \ddot{y}(\ell,t)$; d) $EI\, y''(\ell,t) = 0$ (2.24)

where $y' = \frac{\partial y}{\partial x}$ and $\dot{y} = \frac{\partial y}{\partial t}$ (2.25)

these can be expressed in the form:

$$\left.\begin{aligned} \alpha A + \delta B &= 0 \\ \gamma A + \tau B &= 0 \end{aligned}\right\} \Leftrightarrow \underbrace{\begin{bmatrix} \alpha & \delta \\ \gamma & \tau \end{bmatrix}}_{C} \begin{bmatrix} A \\ B \end{bmatrix} = \begin{bmatrix} 0 \\ 0 \end{bmatrix} \tag{2.26}$$

where

$$\alpha = \sin\beta\ell - \sinh\beta\ell - \frac{M_r}{\rho A}\beta\,(\cos\beta\ell - \cosh\beta\ell)$$

$$\delta = -\cos\beta\ell - \cosh\beta\ell - \frac{M_r}{\rho A}\beta\,(\sin\beta\ell - \sinh\beta\ell) \qquad (2.26)$$

$$\gamma = \cos\beta\ell + \cosh\beta\ell$$

$$\sigma = \sin\beta\ell + \sinh\beta\ell$$

$$\beta^2 = \omega\sqrt{\frac{\rho A}{EI}} \qquad (2.28)$$

For the SCOLE system, the following parameters have been supplied[8]:

$\rho A = 0.09556$ slugs/ft

$EI = 4.0 \times 10^7$ lb-ft^2

$M_r = (400/32.2)$ slugs

$\ell = 130$ ft.

For non-trivial solutions for A and B, det C must vanish. The values of β for which det C = 0 are computed and substituted back into Eq. (2.28) to obtain the frequencies of the different vibrational modes (Table 2.1).

The same values of β are substituted into $\phi(x)$, (Eq. 2.23), which is normalized with respect to its maximum value and the normalized mode shapes plotted (see Table 2.1 and Figs. 2.2 - 2.6). Note that the ranges of frequencies obtained in Table 2.1 are higher then those prevously presented in the April 13, 1984 oral presentation due to previous inconsistencies in dimensional analysis of some physical units.

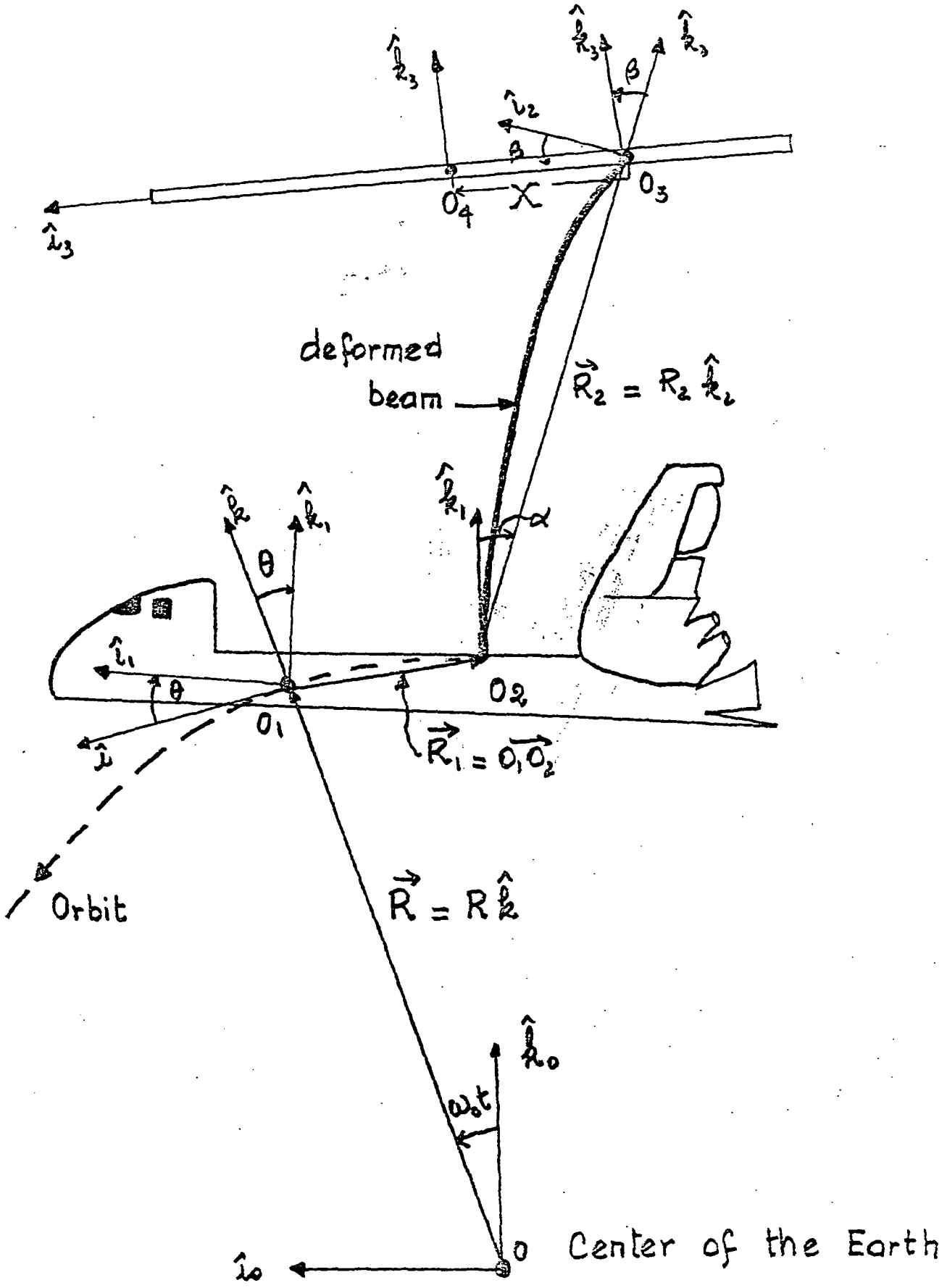

Fig. 2.1. SCOLE System Geometry in the Deformed State (2-D)

TABLE 2.1

Values of β and Natural Frequencies (HZ)
for the First 8 In-Plane (Pitch) Bending Modes

β	ω(Hz)
1.874599	.677828
4.6929	4.245
7.8519	11.884
10.997	23.3128
14.1309	38.4933
17.276	57.5283
20.4229	80.4045
23.555	106.958

References - Chapter II

1. Hale, A.L., and Lisowski, R.J., "Optimal Simultaneous Structural and Control Design of Maneuvering Flexible Spacecraft," Fourth VPI & SU/AIAA Symposium on the Dynamics and Control of Large Structures, Blacksburg, Virginia, June 6-8, 1983.

2. Bainum, P.M., Reddy, A.S.S.R., Krishna, R. and Diarra, C.M., "The Dynamics and Control of Large Flexible Space Structures-VI," Final Report, NASA Grant: NSG-1414, Suppl. 5, September 1983.

3. Bainum, P.M., Reddy, A.S.S.R., and Krishna, R., "On the Controllability and Control Law Design for an Orbiting Large Flexible Antenna System," 34th International Astronautical Congress, Budapest, Hungary, October 10-15, 1983, Paper No. IAF 83-340.

4. Montgomery, R.C., Horner, G.C., and Cole, S.R., "Experimental Research on Structural Dynamics and Control," Proceedings of the Third VPI & SU/AIAA Symposium on the Dynamics and Control of Large Flexible Spacecraft, Blacksburg, Virginia, June 15-17, 1981, pp. 365-377.

5. Taylor, L.W., Jr., and Balakrishnan, A.V., "A Laboratory Experiment Uded to Evaluate Control Laws for Flexible Spacecraft...NASA/IEEE Design Challene (SCOLE)," Fourth VPI & SU/AIAA Symposium on Dynamics and Control of Large Structures, Blacksburg, Virginia, June 6-8, 1983.

6. Likins, P.W., "Dynamics and Control of Flexible Space Vehicles," Technical Report 32-1329, Revision I, Jet Propulsion Laboratory Pasadena, California, January 15, 1970.

7. Armstrong, E.S., ORACLS, A Design System for Linear Multivariable Control, Marcel Dekker, Inc., New York and Basel, 1980.

8. Taylor, L.W., Jr., and Balakrishnan, A.V., "A Mathematical Problem and a Spacecraft Control Laboratory Experiment (SCOLE) used to Evaluate Control Laws for Flexible Spacecraft... NASA/IEEE Design Challenge, January 1984.

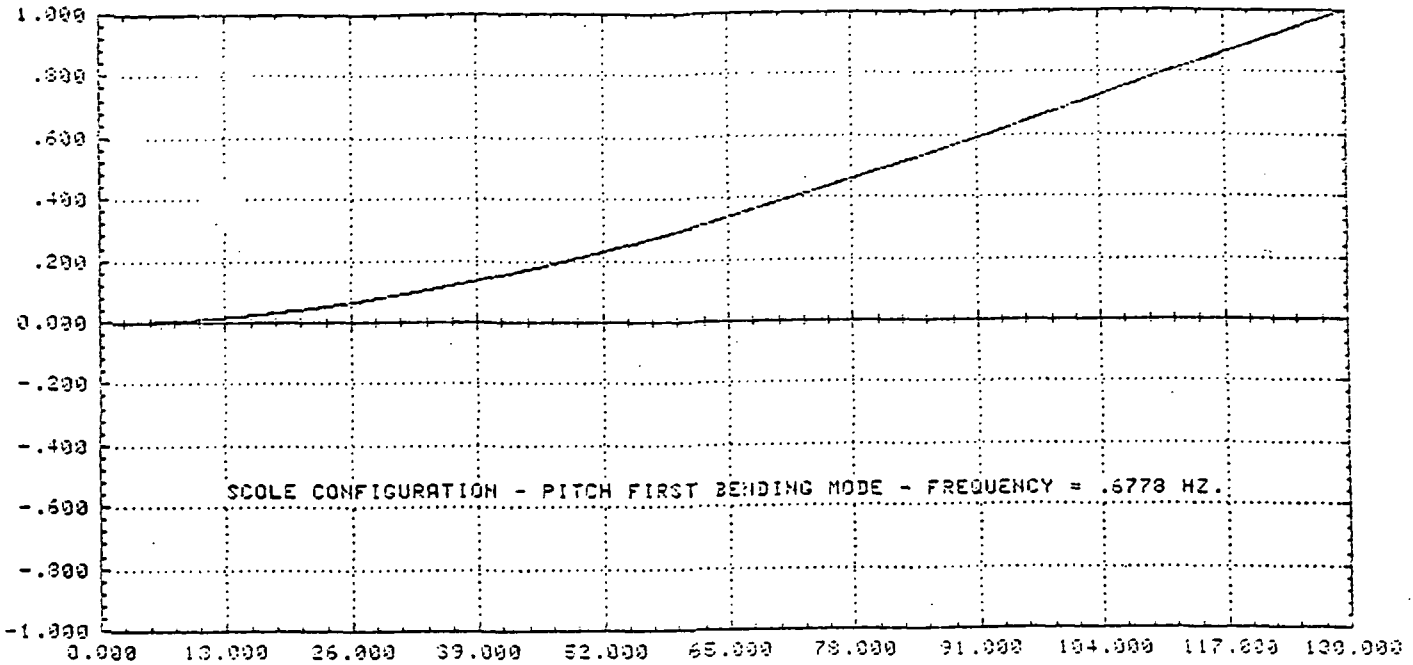
1.000
.800
.600
.400
.200
0.000
-.200
-.400
-.600
-.800
-1.000
SCOLE CONFIGURATION - PITCH FIRST BENDING MODE - FREQUENCY = .6778 HZ.
0.000
13.000
26.000
39.000
52.000
65.000
78.000
91.000
104.000
117.000
130.000

Fig. 2.2

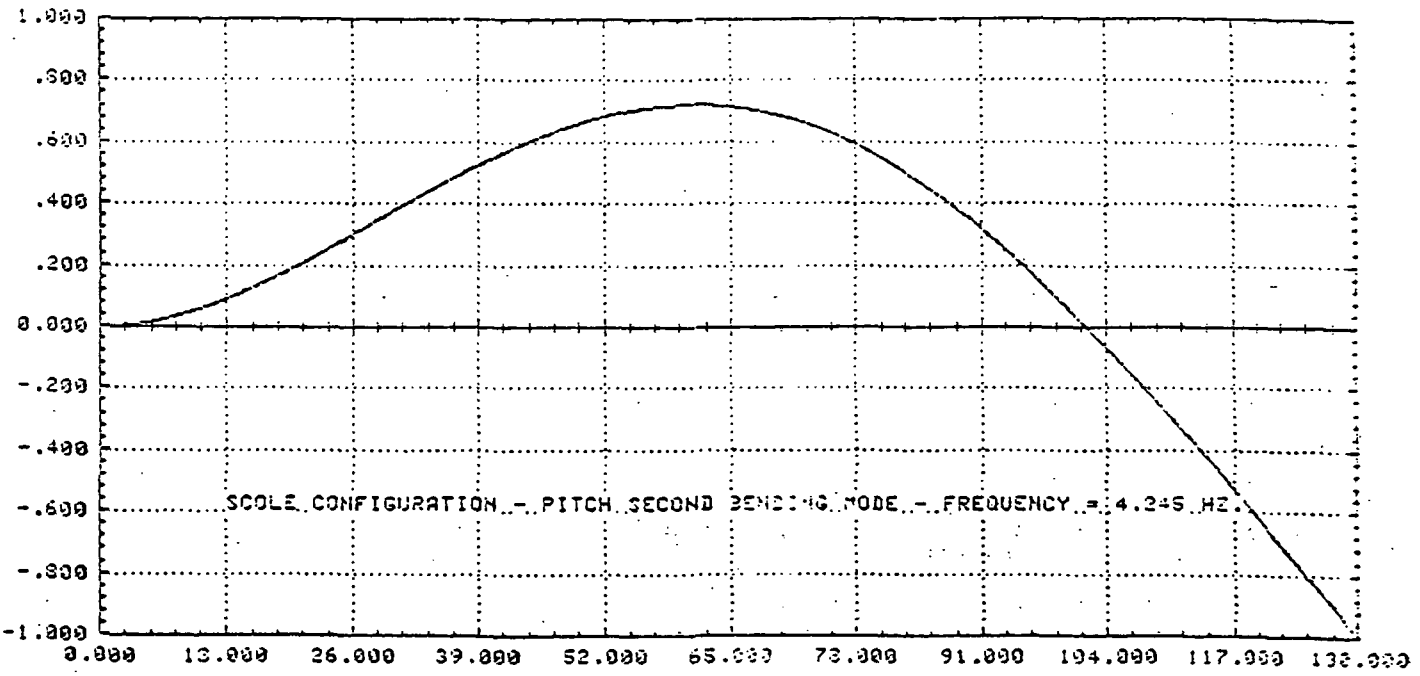
1.000
.800
.600
.400
.200
0.000
-.200
-.400
-.600
-.800
-1.000
SCOLE CONFIGURATION - PITCH SECOND BENDING MODE - FREQUENCY = 4.245 HZ.
0.000
13.000
26.000
39.000
52.000
65.000
78.000
91.000
104.000
117.000
130.000

Fig. 2.3

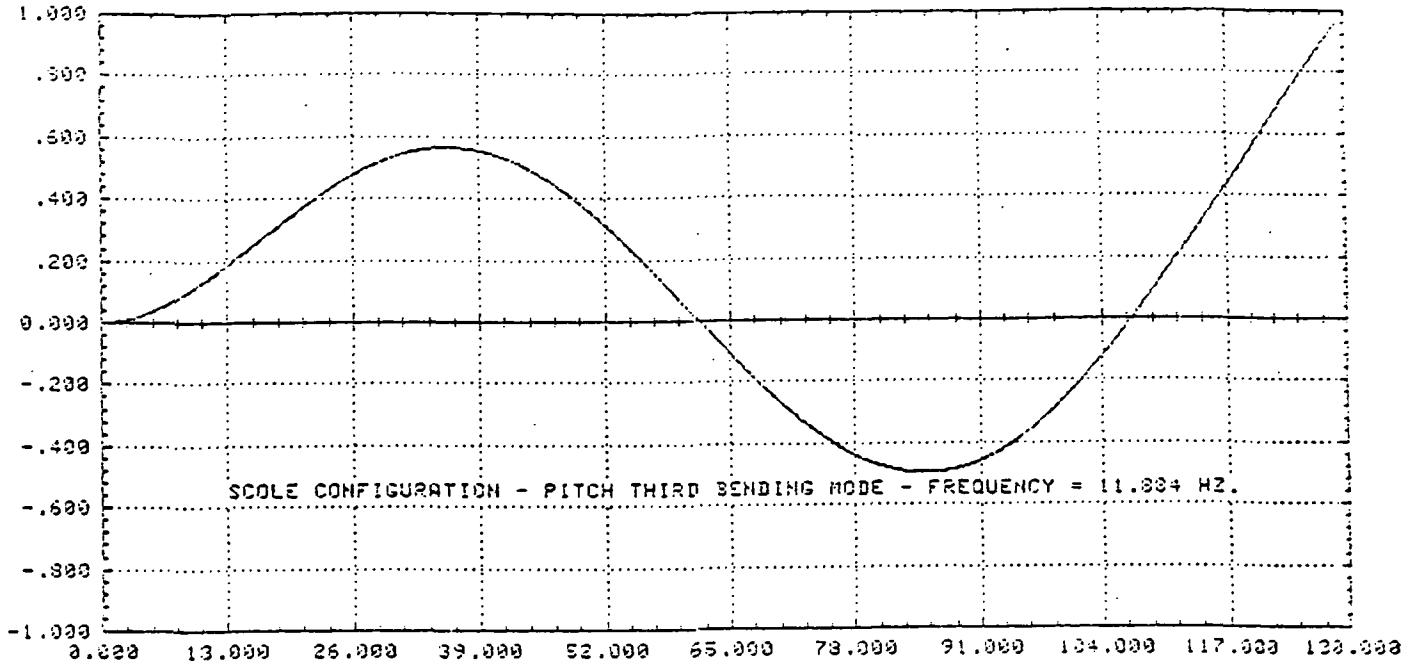
1.000
.800
.600
.400
.200
0.000
-.200
-.400
-.600
-.800
-1.000
0.000
13.000
26.000
39.000
52.000
65.000
78.000
91.000
104.000
117.000
130.000
SCOLE CONFIGURATION - PITCH THIRD BENDING MODE - FREQUENCY = 11.884 HZ.

Fig. 2.4

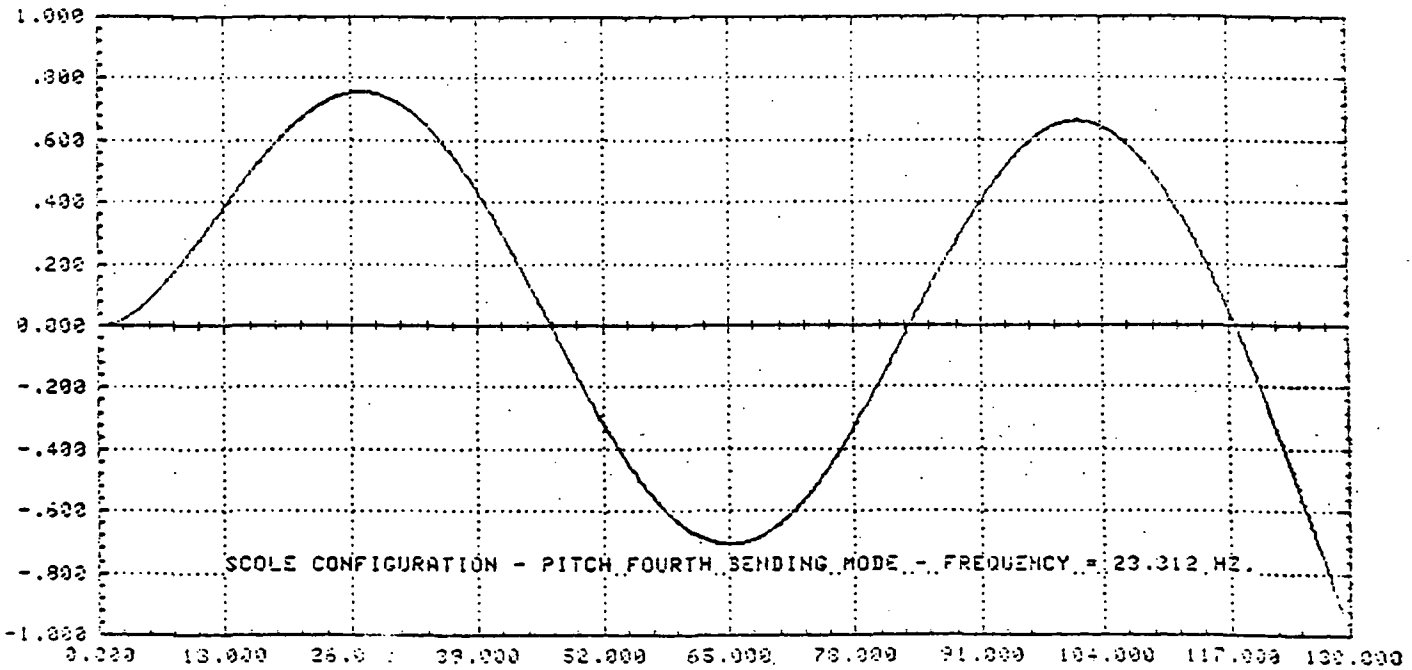
1.000
.800
.600
.400
.200
0.000
-.200
-.400
-.600
-.800
-1.000
13.000
39.000
52.000
65.000
78.000
91.000
104.000
117.000
SCOLE CONFIGURATION - PITCH FOURTH BENDING MODE - FREQUENCY = 23.312 HZ.

Fig. 2.5

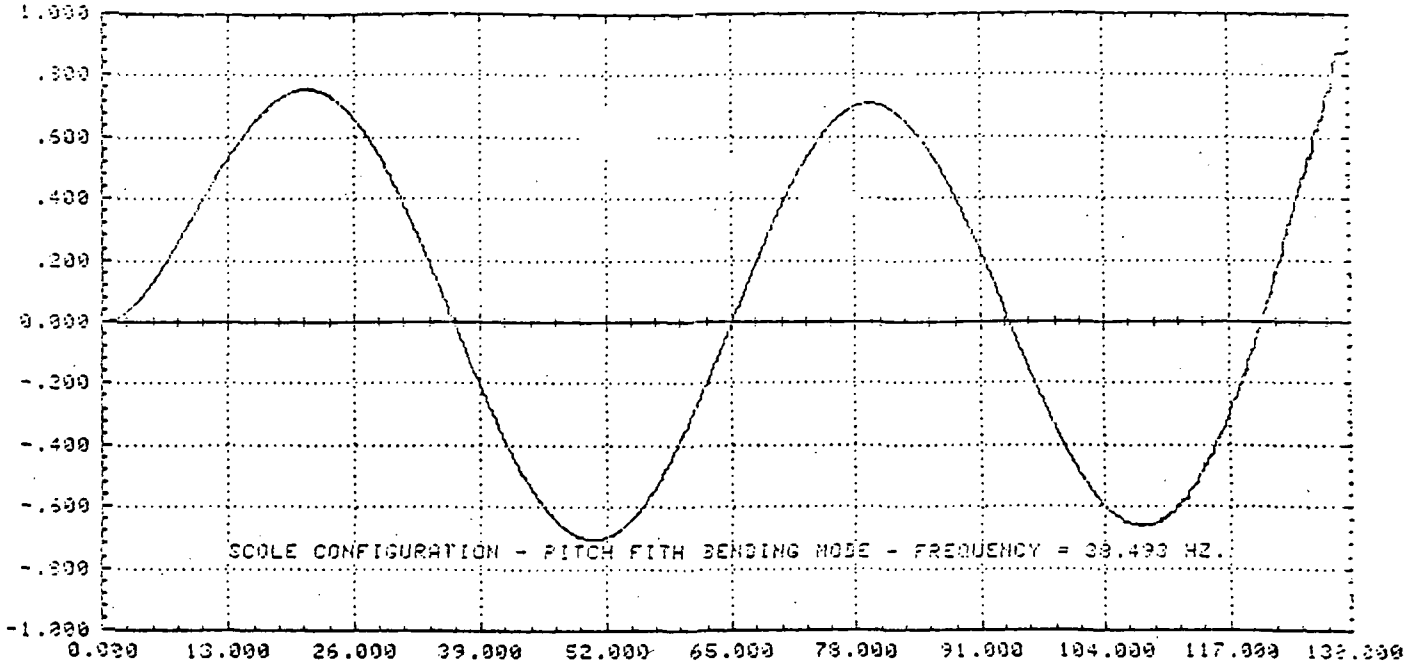
1.000
.800
.600
.400
.200
0.000
-.200
-.400
-.600
-.800
-1.000
0.000
13.000
26.000
39.000
52.000
65.000
78.000
91.000
104.000
117.000
SCALE CONFIGURATION - PITCH FITH BENDING MODE - FREQUENCY = 38.493 HZ.

Fig. 2.6

III. STABILITY OF LARGE SPACE STRUCTURES WITH INPUT DELAYS

The linear equations of motion of any large space structure can be developed in the standard state space form as:

$$\dot{X}(t) = AX(t) + BU(t) \tag{3.1}$$

where

X = nx1 state vector representing attitude angles, modal coordinates for vibration problems, etc.,

U = mx1 control vector

A = nxn system matrix

B = nxm control influence matrix.

Using modern control theory, a state variable feedback control law of the form

$$U(t) = -KX(t) \tag{3.2}$$

can be developed by proper selection of the feedback gain matrix, K, such that system (1) with control will exhibit required characteristics in terms of transient response, pole location or some performance under optimization.

One of the main characteristics of large space structures is the large value of n (in the range of 100's). This large value of n will dictate the use of on-board computers to evaluate u at every instant of time. In theory it is assumed the u at time $t= t_i$ can be instantaneously evaluated using X's at $t = t_i$. In reality there will be a finite time lag between the determination of the X's and the realization of the corresponding U's. Taking into account this delay, the equations of motion with control can be written more realistically as:

$$\dot{X}(t) = AX(t) - BKX(t-\tau) \tag{3.3}$$

The delays considered here may as well account for actuator delays, control system delays, etc. in addition to computational delays. In this report, a preliminary investigation has been carried out to study the stability of the control law designed without taking these delays into consideration.

III.A Stability Analysis - Time Domain

Following the analysis developed in reference 3.1, the system given by equation (3.3) is asymptotically stable if and only if

$$-\mu(A) > ||\ B\ || \tag{3.4}$$

where $\mu(A)$ = largest characteristic root of $\frac{1}{2}(A+A^*)$

$||B||$ = square root of the largest characteristic root of B^*B

A^*, B^* are conjugate transposes of A and B.

This stability criteria can be extended to composite linear systems (since mathematical models of large space structures can be viewed as composite systems, as will be demonstrated later) as follows:

The system equations can be written as

$$\dot{X}_i(t) = A_i X_i(t) + B_i U_i(t) \qquad i = 1,2, \ldots m \tag{3.5}$$

with

$$U_i(t) = \sum_{j=1}^{m} C_{ij} X_j(t-\tau) \tag{3.6}$$

where

X_i is an n(i)x1 state vector

U_i is an ℓ(i)x1 control vector.

The closed loop equations can be written as:

$$\dot{X}_i(t) = A_i X_i(t) + \sum_{j=1}^{m} B_i C_{ij} X_j(t-\tau) \qquad (3.7)$$
$$i=1,2, \ldots m.$$

After identifying the following matrices as:

$$M = \text{Diag } [\mu(A_i)]$$

$$N = n_{ij}$$

where $n_{ij} = || B_i C_{ii} ||$, $i = j$

$|| B_i C_{ij} ||$, $i \neq j$,

the stability of the composite systems described by equation (3.5) with the control given in equation (3.6) can then be defined as follows:

The system (3.5) is asymptotically stabile if and only if any one of the following conditions is satisfied:

(1) all the leading principal minors of the matrix, $-(M+N)$, are positive

(2) $-\tilde{\mu} > P(N)$ where $\tilde{\mu} = \max_i \mu(A_i)$
and $P(N)$ denotes the Perron root of the matrix, N.

(3) $-\tilde{\mu} > || N ||$.

The Perron root of a matrix is defined as follows:

Let $A = (a_{ij})$ be an nxn matrix with all $a_{ij} > 0$. Then A has a positive eigenvalue, ρ, of multiplicity, one, with $\rho > |\lambda_i|$ for all the other eigenvalues of A. This eigenvalue, ρ, has an eigenvector all of whose components are positive. Then ρ is known as the Perron root of the matrix.

The stability criteria can be extended to the study of large space structures by identifying the cooresponding matrices as:

$$A_i = \begin{bmatrix} 0 & 1 \\ -\omega_i^2 & 0 \end{bmatrix} \qquad \text{where } \omega_i = i^{th} \text{ modal frequency}$$

$$B_i\, C_{ij} = \begin{bmatrix} 0 & 0 \\ -p_{ij} & -k_{ij} \end{bmatrix}$$

$$\mu(A_i) = \frac{1 - \omega_i^2}{2} \qquad \text{if } \omega_i^2 < 1$$

$$\mu(A_i) = \frac{\omega_i^2 - 1}{2} \qquad \text{if } \omega_i^2 > 1$$

$$||B_i C_{ij}|| = \sqrt{p_{ij}^2 + k_{ij}^2}$$

So the M and N matrices are given by:

$$M = \begin{bmatrix} \frac{1 - \omega_1^2}{2} \text{ or } \frac{\omega_1^2 - 1}{2} & & \\ & \ddots & \\ & & \frac{1 - \omega_m^2}{2} \text{ or } \frac{\omega_m^2 - 1}{2} \end{bmatrix}$$

$$N = \begin{bmatrix} \sqrt{p_{11}^2 + k_{11}^2} & \sqrt{p_{in}^2 + k_{in}^2} \\ \sqrt{p_{n1}^2 + k_{n1}^2} & \sqrt{p_{nn}^2 + k_{nn}^2} \end{bmatrix}$$

With the application of any one of the three stability conditions it can be concluded that the system can not be stable under a delayed input as the original system without feedback is an oscillatory system in the case of large space structures. In the literature [Ref. 3.1 and Ref. 3.3] it is concluded that for systems with delayed inputs to be stable, the systems without these delays must be stable. No comments were made on the systems which are originally marginally stable. This preliminary investigation shows that even the oscillatory systems whose state variable feedback control laws are designed without taking delays into consideration in the model may not be stable.

This preliminary conclusion has led us to examine other forms of stability considerations for systems with input delay. In the following pages, Routh-Hurwitz stability criteria as applied to delay systems will be considered for the case of the large space structures.

III.B Stability Analysis - Frequency Domain:

In the literature [Ref. 3.2 and 3.3] the stability analysis in the frequency domain is carried out either by approximating e^{-sh} by a rational function in s or evaluating the unknown parameters such as feedback gain, etc. such that stability is assured with the delays present.

The stability analysis in the frequency domain using Routh-Hurwitz criteria is performed as follows:

The characteristic equation of the system described by equation (3.3) is written as

$$\text{determinant of } [SI-A-Be^{-\tau s}] = 0 \qquad (3.8)$$

For the system (3.3) to be asymptotically stable equation (3.8) must have all the roots in the left hand side of the s plane. Equation (3.8) is a polynomial of infinite degree. One way to approximate equation (3.8) is to replace $e^{-\tau s}$ by a rational function of the type

$$e^{-\tau s} = \frac{1 - Ts^2}{1 + Ts} \tag{3.9}$$

where

$$\tau = \frac{4}{\hat{\omega}} \left(\tan^{-1} \hat{\omega}T + K \frac{\pi}{2}\right) \qquad K = 0, 1, 2, \ldots \tag{3.10}$$

with $\hat{\omega}$ being the root of equation (3.8) and equation (3.11) given below:

$$\left| SI - A - B \quad \frac{1 - Ts^2}{1 + Ts} \right| = 0 \tag{3.11}$$

The maximum delay that can be tolerated by the system can be obtained from the relation

$$h_{max} \triangleq \min_i \left\{\frac{4}{\omega_i} \tan^{-1} (\omega_i T_i)\right\} \tag{3.12}$$

where ω_i are all the roots of equation (3.11) and T_i are the corresponding values of T.

This technique can be applied to systems of moderate dimensionality. For large space structures the determination of the range of T for which the roots of equation (3.11) won't cross the imaginary axis into the right hand side of the s plane may become computationally prohibitive.

In Reference 3.3 stability analysis in the frequency domain with delay is approached in a slightly different manner. The characteristic equation of a system with delay is written as

$$e^{-\tau s} = \frac{KN(s)}{D(s)} \tag{3.13}$$

where K is the gain
N(s) is the numerator polynomial
D(s) is the denominator polynomial

A preselected value of s ($\sigma+j\omega$) which gives the required damping and frequency for the closed loop system and the corresponding values, K, and some other adjustable parameters of the system are evaluated. It is clearly stated in reference 3.3 that this analysis is valid only for systems which are stable without the feedback. The marginally stable systems are not considered.

Conclusions:

The time domain approach is easy to implement for analyzing the stability of systems with delay in feedback. The analysis shows that marginally stable or oscillatory systems can not be stabilized using feedback.

The Routh-Hurwitz criteria and the design approach of reference (3.3) may become computationally unattractive for large space structure systems which are characterized by hundreds of modes to describe vibrations adequately.

At this stage, it is not completely conclusive that oscillatory systems which characterize the vibrations of large space structural systems can be made stable or not with delayed feedback. A further literature survey and numerical computation will be carried out during the grant period of 1984-1985 to arrive at definitive conclusions about the stability of large space structures with input delays.

References

3.1 Mori, T., Fukuma, N. and Kuwahara, M., "Simple Stability Criteria for Single and Composite Linear Systems with time delays," Int. J. Control, Vol. 34, No. 6, 1981, pp. 1175-1184.

3.2 Thowsen, A., "The Routh-Hurwitz Method for Stability Determination of Linear Differential-Difference Systems," Int. J. Control, Vol. 33, No. 6, 1981, pp. 991-995.

3.3 Gates, Jr., O.B., and Schy, A.A., "A Theoretical Method of Determining the Control Gearing and Time Lag Necessary for a Specified Damping of an Aircraft Equipped with a Constant-Time Lag Auto Pilot," NACA Technical Note 2307, March 1951.

IV. CONTROL OF AN ORBITING FLEXIBLE SQUARE PLATFORM IN THE PRESENCE OF SOLAR RADIATION

Abstract

A mathematical model for the solar radiation forces and moments acting on a square plate (platform) in orbit is obtained by considering the plate mode shapes as combinations of free-free beam shape functions. The moment expressions for a plate of arbitrary reflectivity coefficient are obtained as a function of the solar incidence angle. It is seen that only the first three flexible modes of the plate generate a first order net moment about the center of mass, and that the solar radiation pressure does not influence the flexible modes of the plate for small amplitude vibrations. The solar radiation disturbance model is then included in the dynamic model of a square plate nominally oriented along the local vertical and having the major surface of the plate normal to the orbital plane. The roll angle of the plate is seen to increase steadily due to the solar radiation pressure whereas the pitch and yaw motions oscillate with an amplitude of approximately 0.2 degrees for a 100m square thin aluminum plate in synchronous orbit. To control the shape and orientation of the plate two point actuators are assumed - one whose force axis is normal to the plane of the plate, the second with a force axis in the plane of the plate. The control law and the feedback gain values are obtained based on linear quadratic Gaussian methods. Transient responses and control requirements are simulated for local vertical and horizontal orientations.

1. Introduction

Proposed future applications of large space structures require control of the shape and orientation of the structure in orbit. It has been shown previously (Ref. 1), considering a long, thin and uniform beam, that the principal environmental disturbance acting on these structures could be due to the solar radiation pressure. In the present work the dynamics of a more important basic structure, namely, a thin, homogeneous and flexible square plate exposed to solar radiation disturbance will be considered. The force and moment expressions as given by Karymov (Ref. 2) will be used to obtain the expressions for solar radiation disturbing forces and moments acting on the free-free square plate in orbit. The dynamics of such a plate nominally oriented along the local vertical was considered earlier, disregarding the environmental disturbances (Ref. 3). In the present study it is proposed to reconsider the dynamics of the plate nominally oriented along the local vertical/horizontal with the solar radiation force and moment expressions included in the dynamic model.

The mode shapes and the frequencies of the plate are obtained using the finite element program, STRUDL (Ref. 4). To obtain expressions for solar radiation forces and moments, it is convenient to express the mode shapes of the plate as a combination of the mode shapes of a free-free beam (Ref. 5). The first five modes of the

plate will be considered for study here. The plate is assumed to have only small transverse vibrations, so that the shadowing of the plate due to any deflected part of the plate can be neglected. The small deflection assumption also allows the superposition of the beam mode shapes in representing the deformations of the plate.

2. Solar Radiation Forces and Moments Acting on a Thin Homogeneous Flexible Square Plate

Fig. 1 shows a square plate exposed to solar radiation. Let $\bar{n}$ denote the outward unit vector normal to the surface, ds, and let $\bar{\tau}$ be the unit vector in the direction of solar radiation denoted as

$$\bar{\tau} = a_o \bar{i} + b_o \bar{j} + c_o \bar{k} \tag{1}$$

The direction cosines of $\bar{\tau}$, namely, a_o, b_o and c_o, can be expressed in terms of the solar incidence angles, θ_i and ψ_i, (defined in Fig. 1) as

$$a_o = \sin\theta_i \cos\psi_i \; ; \; b_o = \sin\theta_i \sin\psi_i \; ; \; c_o = \cos\theta_i \tag{2}$$

Then, the solar radiation force, $\bar{F}_a$, and the moment, $\bar{N}_a$, on a completely absorbing surface are given by (Ref. 2)

$$\bar{F}_a = -h_o \bar{\tau} \int_s \bar{\tau}\cdot\bar{n} \, ds \tag{3}$$

and $$\bar{N}_a = h_o \bar{\tau} \times \int_s \bar{R} \, (\bar{\tau}\cdot\bar{n}) \, ds \tag{4}$$

where, $h_o = 4.64 \times 10^{-6}$ Nt/m^2 is a constant for near earth space structures. The integration over the area, s, is bounded by the condition

$$\bar{\tau}\cdot\bar{n} \leq 0 \tag{5}$$

The force, $\bar{F}_r$, and moment, $\bar{N}_r$, acting on a completely reflecting surface can be developed as (Ref. 2)

$$\bar{F}_r = -2h_o \int_s \bar{n} \, (\bar{\tau}\cdot\bar{n})^2 \, ds \tag{6}$$

and $$\bar{N}_r = 2h_o \int_s \bar{n}\times\bar{r} \, (\bar{\tau}\cdot\bar{n})^2 \, ds \tag{7}$$

where, $\bar{R}$ is the position vector of ds with respect to the center of mass of the plate. For a surface with an arbitrary reflection coefficient, ε_r, the force and moment expressions become (Ref. 2):

$$\bar{F}_{\varepsilon r} = \bar{F}_a + \varepsilon_r \, (\bar{F}_r - \bar{F}_a); \; \bar{N}_{\varepsilon r} = \bar{N}_a + \varepsilon_r \, (\bar{N}_r - \bar{N}_a) \tag{8}$$

The shape function of a rectangular plate can be represented as a product of the two beam functions given by (Ref. 5), considering only the transverse vibration,

$$Z_{m,n}(x,y) = \theta_n(x) \, \psi_m(y) \tag{9}$$

θ and ψ are the free-free beam shape functions given by

$$\theta_n(x) = \sigma_n \, (\sin\Omega_n x + \sinh\Omega_n x) + \cos\Omega_n x + \cosh\Omega_n x \quad ; \text{ for } n = 2,3,4 \ldots. \tag{10}$$

where, $\sigma_n = (\cos\Omega_n - \cosh\Omega_n)/(\sinh\Omega_n - \sin\Omega_n)$; $\theta_n(x) \equiv \psi_n(y)$
and $\theta_n(x) = 1-2x$ for n=1
$= a$ constant for n=0

For a square plate, certain special modes which are combinations of the modes of a rectangular plate are of interest (Ref. 5). The frequency expressions for such modes are also given in Ref. 5. The first five modes of a square plate in which the second and third modes represent special combinations of "beam modes" (Fig. 2) are considered in the present study.

A unit normal to the surface, $\bar{n}$, is given by,

$$\bar{n} = a_1\bar{i} + b_1\bar{j} + c_1\bar{k} = [(\psi(d\theta/d\xi)\bar{i} + \theta(d\psi/d\eta)\bar{j} - \bar{k})] / \sqrt{(\psi d\theta/d\xi)^2 + \theta(d\psi/d\eta)^2 + 1} \quad (11)$$

((ξ,η,ζ) are non-dimensional coordinates in the x,y,z directions, respectively.) The position vector, $\bar{R}$, is represented as,

$$\bar{R} = (\xi - \tfrac{1}{2})\,\bar{i} + (\eta - \tfrac{1}{2})\,\bar{j} + z\,\bar{k} \quad (12)$$

Eqs. (1), (11) and (12) are substituted into Eq. (4) and then the resulting integrals are evaluated to obtain the expression for the moment acting on a plate having a completely absorbing surface as,

$$\bar{N}_a = -h_o\ell^2[\{b_o s_3 - c_o(s_2 - s_4/2)\}\,\bar{i} + \{c_o(s_1 - s_4/2) - a_o s_3\}\,\bar{j} + \{a_o(s_2 - s_4/2) - b_o\,(s_1 - s_4/2)\}\,\bar{k}\,] \quad (13)$$

where, $s_1 = \int_s \xi s_c d\xi d\eta \quad s_2 = \int_s \eta s_c d\xi d\eta \quad s_3 = \int_s \zeta s_c d\xi d\eta$

$$s_4 = \int_s s_c d\xi d\eta \quad s_c = \left(a_o\psi_m \frac{d\theta_n}{d\xi} + b_o\,\theta_n \frac{d\psi_m}{d\eta} - c_o\right)$$

The integrals s_1 to s_4 can be evaluated analytically. The moment expressions are obtained for the first five plate modes (Fig. 2) by evaluating s_1 to s_4 for combinations of corresponding (m,n) modes and are given as,

$$\bar{N}_a = \frac{h_o\ell^2}{3}\,[a_o c_o\bar{i} - b_o c_o\bar{j} + (b_o^2 - a_o^2)\bar{k}]\,z_1 \quad \text{(for mode I)}$$

$$= h_o\ell^2 c_o\,[b_o\bar{i} + a_o\bar{j}]\,z_2 \quad \text{(for mode II)}$$

$$= h_o\ell^2 c_o\,[b_o\bar{i} - a_o\bar{j}]\,z_3 \quad \text{(for mode III)}$$

$$= 0, \quad \text{(for modes IV and V)} \quad (14)$$

where, z_1, z_2 and z_3 are deflections at one corner of the plate associated with the I, II and III modes, respectively.

The moment due to solar radiation pressure, $\bar{N}_r$, acting on a completely reflecting surface is obtained by substituting Eqs. (11), (12) and (1) into Eq. (7). The resulting integral is simplified to obtain the expression,

$$\bar{N}_r = 2h_o \int_s [(a_2\zeta - a_3\eta')\bar{i} + (a_3\xi' - a_1\zeta)\bar{j} + (a_1\eta' - a_2\xi')\bar{k}]\,s_c d\xi d\eta \quad (15)$$

where, $\xi' = \xi - 0.5$ and $\eta' = \eta - 0.5$

Eq. (15) involves complicated integrals and to find an analytical solution is very difficult. Instead, a numerical evaluation of the integrals involving different modes are carried out and the results are shown in Fig. 3. The plate dimension is considered to be 100mx100m and the deflection at the corner of the plate for each mode is assumed to be $z_1 = z_2 = z_3 = 1.0$m. Similar results are also obtained for a plate having a completely absorbing surface using Eq. (14). The solar incidence angle, θ_i, is varied from 0 to 90°, with $\psi_i = 0$. Only the first three modes give rise to appreciable moments for both the completely absorbing and completely reflecting surfaces. The magnitudes of the moments are seen to be an order of magnitude higher (2×10^{-2}Nt-m) for a completely absorbing surface as compared with the case of a completely reflecting surface (10^{-3} Nt-m). The moments due to modes II and III, and for both completely reflecting and completely absorbing surfaces, can be visualized as extensions of the result obtained for the case of the beam (Ref. 1).

Based on the numerical results shown in Fig. 3, in which ψ_i is varied from 0 to 90° (not shown) the moment expressions for a completely reflecting plate can be written as,

$$\begin{aligned}\bar{N}_r &= h_1 c_o\,(a_o\bar{i}-b_o\bar{j})\,z_1 \qquad \text{(for mode I)}\\ &= h_2 c_o\,(b_o\bar{i}-a_o\bar{j})\,z_2 \qquad \text{(for mode II)}\\ &= h_2 c_o\,(b_o\bar{i}-a_o\bar{j})\,z_3 \qquad \text{(for mode III)}\end{aligned} \tag{16}$$

where, $h_1 = 3.25\times10^{-4}$ and $h_2 = 1.09\times10^{-3}$
Eq. (16) is found to be valid for magnitudes of z_1 to z_3 up to 0.01ℓ. The moments about the x,y and z axes are obtained by collecting the coefficients of $\bar{i}$, $\bar{j}$ and $\bar{k}$, respectively, from Eqs. (14) and (16) as,

$$N_{ax} = h_3\{(a_o/3)z_1 + b_o(z_2+z_3)\}\ ;\ N_{ay} = -h_3\{(b_o/3)z_1 + b_o(z_3-z_2)\}$$
$$N_{az} = (h_3/3)\,(b_o^2-a_o^2)z_1\ ;\ \text{where } h_3 = h_o\ell^2 c_o \tag{17}$$

$$N_{rx} = c_o\{h_1 a_o z_1 + h_2 b_o(z_2-z_3)\}\ ;\ N_{ry} = -c_o\{h_1 b_o z_1 + h_2 a_o(z_2-z_3)\};\ N_{rz} = 0 \tag{18}$$

Eqs. (17) and (18) are now substituted into Eq. (8) to obtain the moment acting on a plate with a surface of general coefficient of reflectivity, ε_r.

3. Modal Forces Due to Solar Radiation Pressure

The effect of the disturbance on the generic mode is obtained by evaluating the integral (Ref. 6).

$$E_n = \int z\,(x,y)\,\bar{k}\cdot d\bar{F} \tag{19}$$

where, $d\bar{F}$ represents the force due to solar radiation pressure per unit area. Also

$$E_n = E_{na} + \varepsilon_r\,(E_{nr}-E_{na}) \tag{20}$$

Eq. (3) is substituted into Eq. (19) and after evaluating the resulting integrals, E_{na} is found to be equal to zero for all modes of the plate. Eq. (6) is used in Eq. (19) to get

$$E_{nr} = 2h_o \int [z(a_o a_1+b_o b_1+c_o)/(a_1^2+b_1^2+1)]\,d\xi d\eta \tag{21}$$

The slopes, $d\theta_n/d\xi$ and $d\psi_n/d\eta$, are assumed to be very small so that $a_1^2+b_1^2+c_1^2 \simeq 1$. Thus, the integral in Eq. (21) can be easily evaluated to show that E_{nr} is also equal to zero for all modes of the plate. Hence, the solar radiation pressure does not give rise to any generic force. The results obtained can now be used in the dynamic model of a flexible plate in the orbit.

4. Effect of Solar Radiation Pressure on a Plate Nominally Oriented Along the Local Vertical

The major surface of the plate is assumed to be perpendicular to the orbital plane (Fig. 4). From the general formulation of Refs. 3 and 5, the equations of motion of the structure are obtained, under the assumption that the transverse deformations are small compared to the characteristic length of the plate. The linearized equations of motion are given by (Ref. 3),

$$\ddot{\psi} = -2\omega_c\dot{\phi} + \omega_c^2\psi + N_x/J_x \; ; \; \ddot{\phi} = \omega_c\dot{\psi} + N_y/J_y \; ; \; \ddot{\theta} = -3\omega_c^2\theta + N_z/J_z \; ;$$

$$\ddot{\varepsilon}_n + (\Omega_n/\omega_c)^2 \varepsilon_n = 0 \qquad (22)$$

where ψ, ϕ, and θ refer to the yaw, roll, and pitch modes, respectively, ω_c is the orbital angular rate, Ω_n is the n^{th} modal frequency, ε_n is the non-dimensional modal amplitude, and $J_{x,y,z}$ are the principal plate moments of inertia.

The roll and yaw equations of motion are coupled to each other and the characteristic equation shows a double pole at the origin indicating instability in the roll-yaw motion. However, for an initial condition of $\psi(0) = \phi(0) = 0$, the roll and yaw motions will not build up. To study the effect of solar radiation disturbance, a 100m. square plate whose fundamental frequency is ten times the orbital frequency is considered. Only the first three flexible modes are included in the dynamic model with initial conditions of 0.01 in each mode. The transient response of the plate under the influence of solar radiation pressure is shown in Fig. 5. The torque about the normal to the plate due to the first modal amplitude acts in one direction only (Eq. (14) for ψ_i=0: as the solar incidence angle changes in the orbit, it is seen that the cyclic contribution due to N_{ax} averages to zero. This torque induces a steady drift in the roll angle ($\simeq 1.5^o$ in 6 orbits). The yaw motion is seen to be oscillating with a very small amplitude (0.3^o). The solar radiation pressure disturbance also induces a small amplitude (0.03^o) pitch oscillation. The modal oscillations (not shown) are unaffected in the presence of the solar radiation disturbance. The magnitude of the pitch, roll, and yaw angular motions due to the solar radiation pressure are small because of the stabilizing gravity-gradient forces acting on the plate.

Active control of the flexible platform nominally oriented along the local vertical may be accomplished by using two reaction jets, f_1 and f_2, as illustrated in Fig. 2. Actuator f_2 is assumed to thrust normal to the undeflected plate, whereas f_1 has its thrust axis in the major plane and normal to one of the edges. Control laws are synthesized based on linear quadratic Gaussian techniques (Ref. 7). The effect of including the solar radiation disturbance on the closed-loop dynamic response is illustrated in Fig. 6 where the initial conditions are identical to those in Fig. 5. For this case the solar disturbance is seen to have little effect on the closed-loop response. The roll motion is now seen to be characterized by a damped oscillation. When the flexibility of this plate was increased (reducing the fundamental plate frequency to only 3 times the orbital rate), it was seen that the main effect was to increase the control effort by about 10 percent.

5. Effect of Solar Radiation Pressure on a Plate Nominally Oriented in the Local Horizontal Plane

For this case the undeflected major surface of the platform is nominally perpendicular to the local vertical. Such a structure could be gravitationally stabilized by attaching a rigid light weight dumbbell at the center by a spring loaded hinge which could also provide viscous damping (Fig. 7). The linearized equations of motion for a plate connected to a two-degree-of-freedom gimballed dumbbell were developed and a related stability analysis provided in Ref. 8.

The closed loop transient response for this system with initial modal displacements in the first five flexible modes is illustrated in Fig. 8. For this case the fundamental flexible modal frequency was reduced to three times the orbital rate. The feedback gain values were obtained by the application of the linear quadratic Gaussian method by taking the state penalty matrix, $Q=100I$, and the control penalty matrix, $R=I$ (I = appropriately dimensioned unit matrix). The pitch and the yaw motions are seen to be characterized by relatively large amplitude oscillations (Fig. 8a) in the presence of the solar radiation disturbance. A second set of feedback gain values is obtained by increasing the elements of the penalty matrix, Q, corresponding to the pitch and yaw states. The resulting transient response of the system is shown in Fig. 8b, for the same initial conditions as in Fig. 8a. For this case, the controlled pitch, roll, and yaw motions are seen to be relatively less sensitive to the solar radiation disturbance than for the case shown in Fig. 8a. The effect of penalizing the pitch, roll, and yaw states more heavily is reflected in the larger control effort required, which is about 10% greater than for the case shown in Fig. 8a.

6. Conclusions

The effect of solar radiation pressure interacting with a vibrating orbiting thin plate is modelled. It is seen that only the first three flexible modes of the plate generate a first order net moment about the center of mass, and that the solar radiation pressure does not influence the flexible modes of the plate for small amplitude vibrations. In the absence of control, for a symmetrical homogeneous square platform the solar pressure induces a steady angular drift about one of the (rigid) body principal axis.

For the case of extremely flexible platforms, nominally oriented in the local horizontal plane, it is seen that appreciable rigid modal amplitudes can be induced due to solar radiation, even in the presence of both active and passive control. For this situation, the versatility of the linear quadratic Gaussian technique can be utilized to redesign control laws which provide a compromise between transient performance and control effort required.

References

1. Krishna, R. and Bainum, P.M., "Effect of Solar Radiation Disturbance on a Flexible Beam in Orbit," AIAA 21st Aerospace Sciences Meeting, Reno, Jan. 10-13, 1983. Paper No. 83-0431; to appear, AIAA Journal.

2. Karymov, A.A., "Determination of Forces and Moments Due to Light Pressure Acting on a Body in Motion in Cosmic Space," P.M.M., No. 5, Vol. 26, 1962, pp. 867-876.

3. Reddy, A.S.S.R., Bainum, P.M., Krishna, R., and Hamer, H.A., "Control of a Large Flexible Platform in Orbit," Journal of Guidance and Control, Vol. 4, No. 6, Nov.-Dec., 1981, pp. 642-649.

4. "ICES STRUDL II, the Structural Design Language," Massachusettes Institute of Technology, V2M2, 1972.

5. Warburton, G.B., "The Vibration of Rectangular Plates," Proceedings of the Institute of Mechanical Engineers, Vol. 168, No. 12, 1954, pp. 371-394.

6. Kumar, V.K. and Bainum, P.M., "Dynamics of a Flexible Body in Orbit," Journal of Guidance and Control, Jan.-Feb., 1980, Vol. 3, No. 1, pp. 90-92.

7. Armstrong, E.S., "ORACLS - A System for Linear Quadratic - Gaussian Control Law Design," NASA Technical Paper 1106, April 1978.

8. Bainum, P.M. and Kumar, V.K., "Dynamics of Orbiting Flexible Beams and Platforms in the Horizontal Orientation," Acta Astronautica, Vol. 9, No. 3, 1982, pp. 119-127.

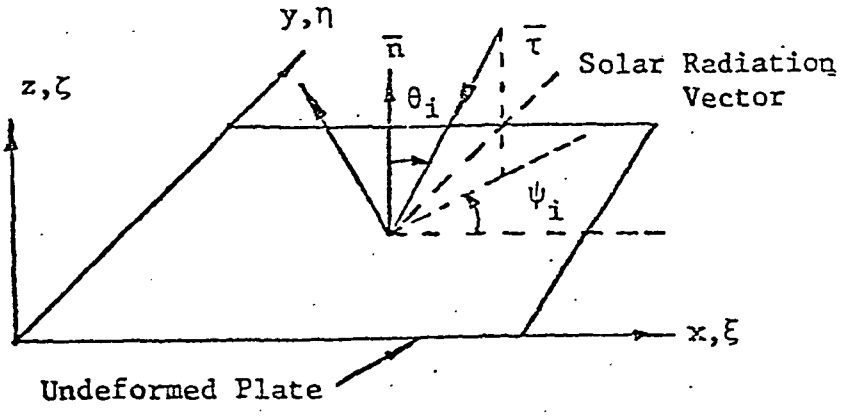

Fig. 1. A Thin Plate Exposed to Solar Radiation Pressure.

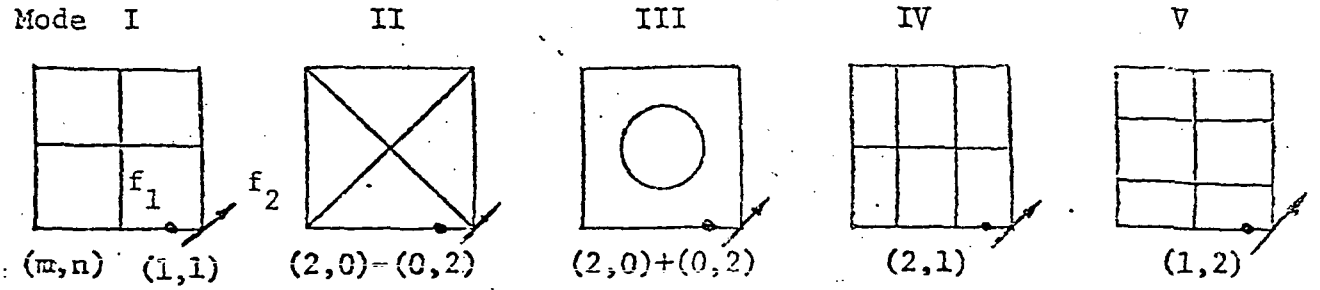

Fig. 2. The First Five Mode Shapes of a Square Plate.

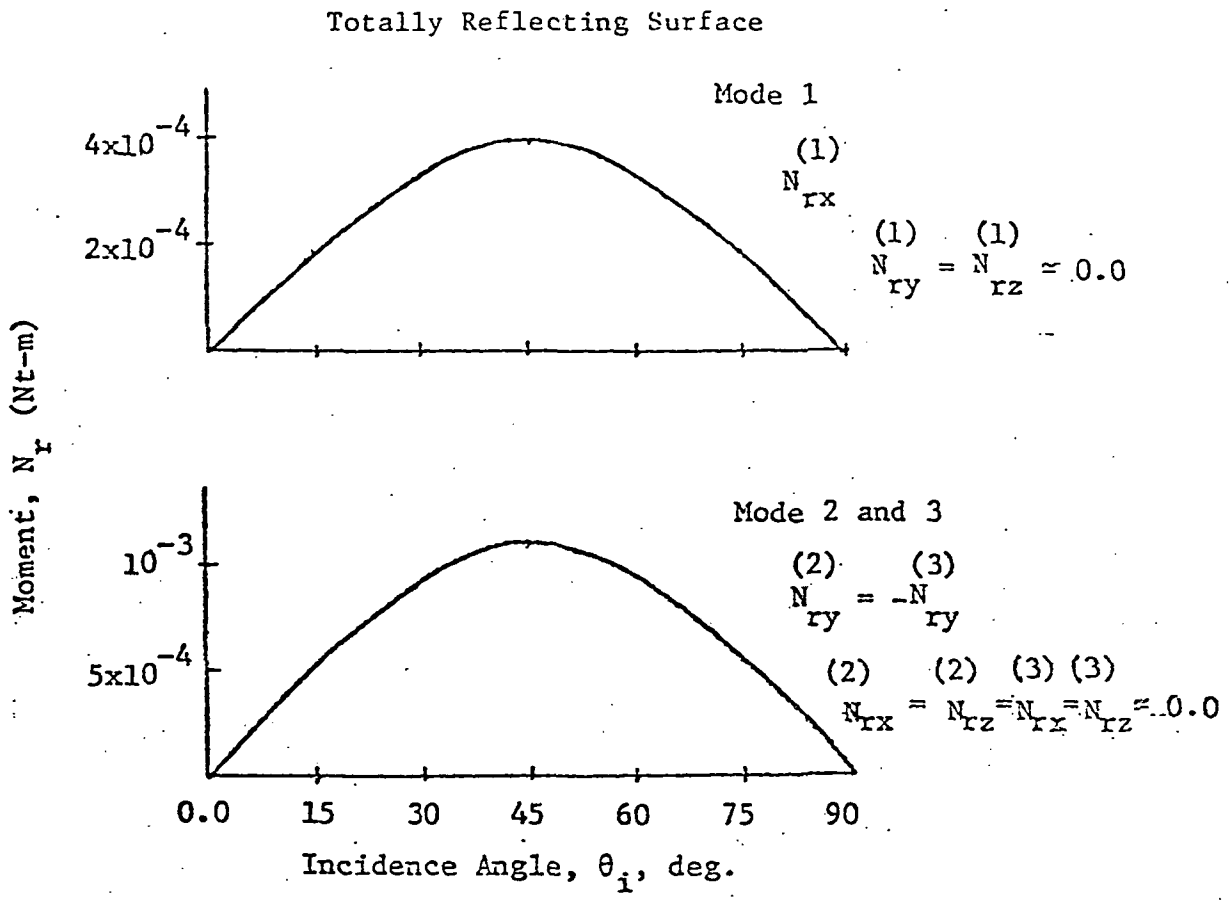

Fig. 3. Moment Due to Solar Radiation Pressure on a Plate ($\psi_i = 0.0$).

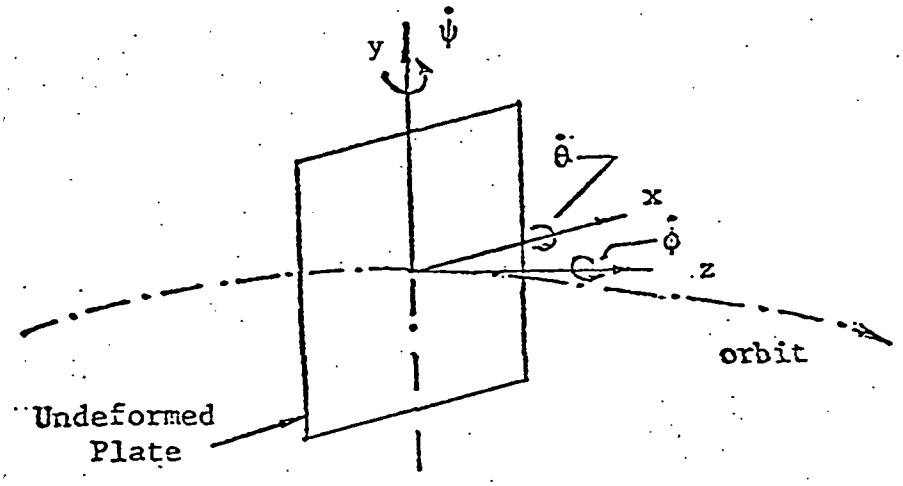

Fig. 4. A Square Plate in Orbit Nominally Along the Local Vertical.

I.C.'s $\psi(0) = \phi(0) = \theta(0) = 0$, $\varepsilon_1(0) = \varepsilon_2(0) = \varepsilon_3(0) = 0.01$

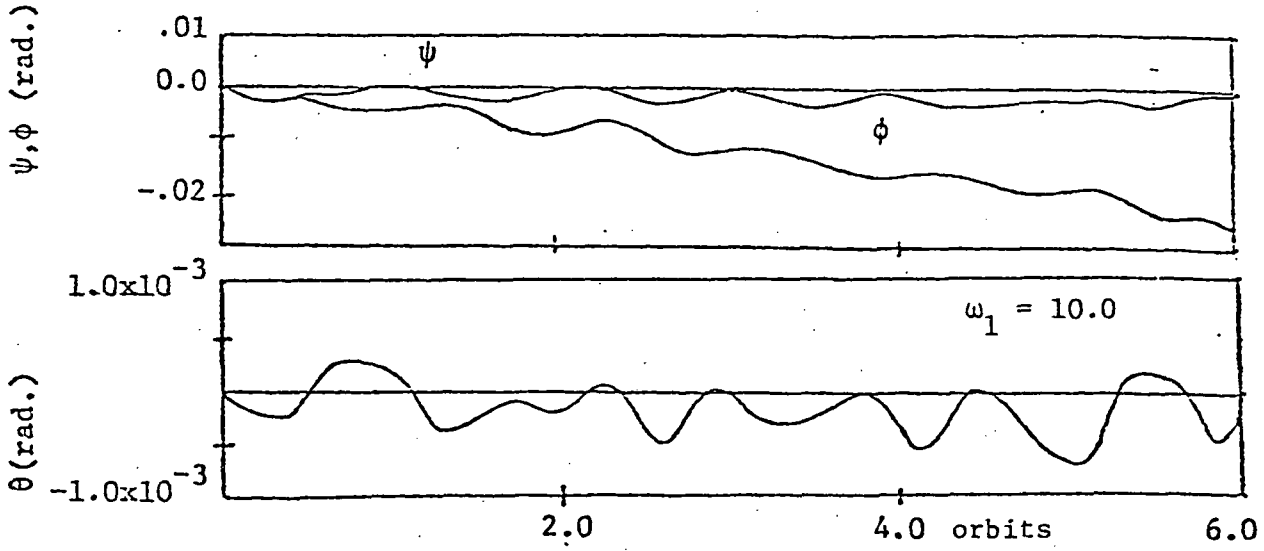

Fig. 5. Time Response of the Plate Nominally Oriented Along the Local Vertical Under the Influence of Solar Radiation Pressure.

Without Disturbance - - -
With Disturbance ———

$(F_1)_{max}$ = 6 Nt.
$(F_2)_{max}$ = 5 Nt.

Q = diag [100.0]
R = diag [1.0]
Control Based on LQG

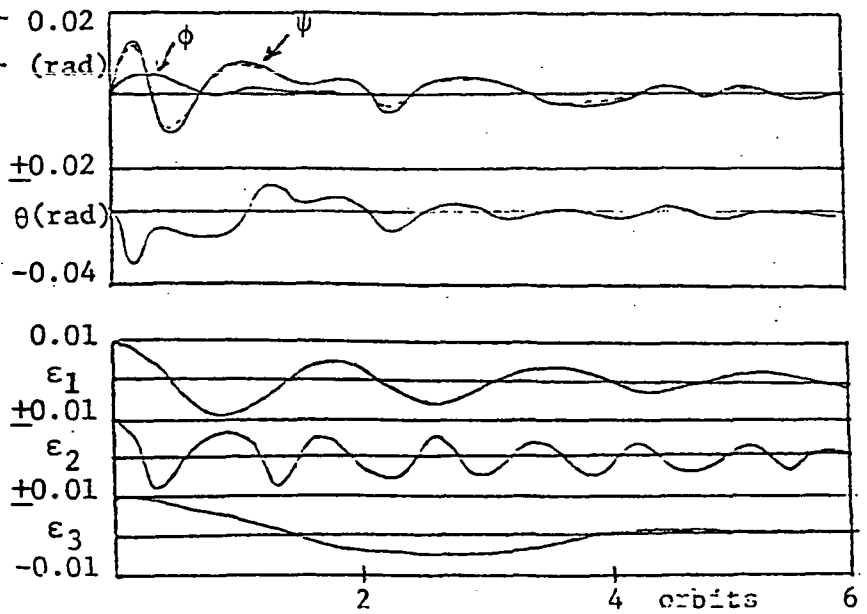

Fig. 6. Controlled Response of the Plate Nominally Oriented Along the Local Vertical ($\omega_1 = 10.0$).

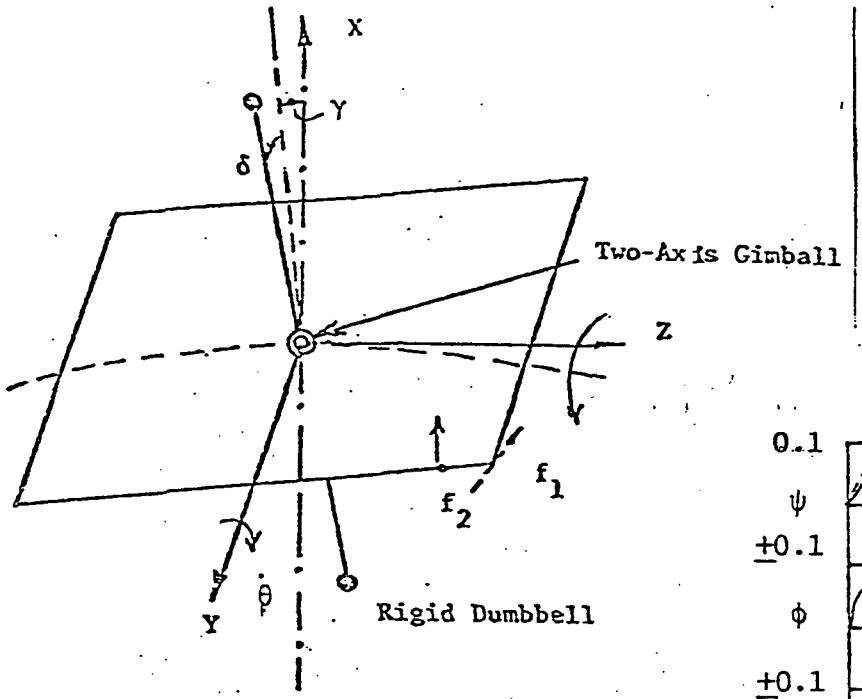

Fig. 7. Dumbbell Stablized Plate.

$$F_c = |\bar{f}_1| + |\bar{f}_2|, \text{ Nt.}$$

Fig. 8. Time Response of Dumbbell Stabilized Plate (Control Based on LQG).

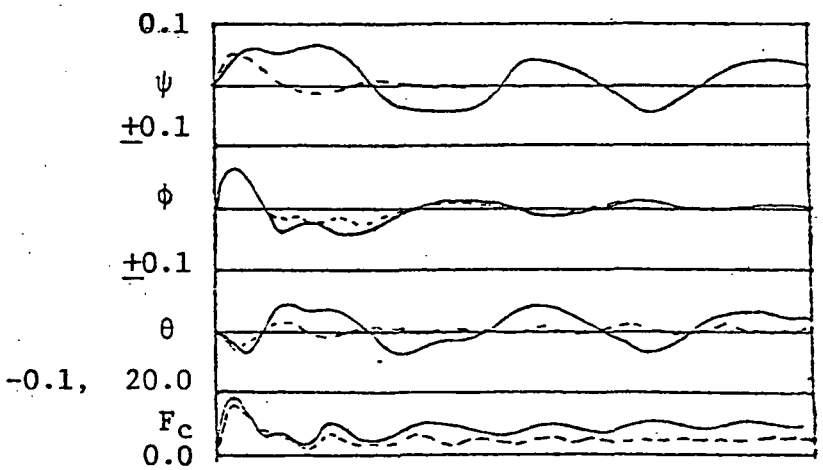

(a) Q = diag [100] R = diag [1.0]

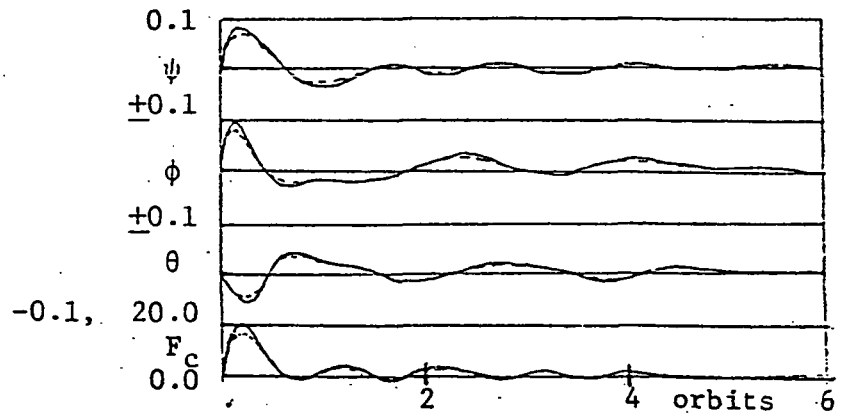

(b) Q = diag [100.0] R = diag [1.0]
except Q(1,1) = Q(2,2) = Q(3,3)=10,000

V. DYNAMICS AND CONTROL OF ORBITING FLEXIBLE BEAMS AND PLATFORMS UNDER THE INFLUENCE OF SOLAR RADIATION AND THERMAL EFFECTS

Abstract

Expressions for thermal deflections of uniform thin beams and plates exposed to solar heating are obtained as a function of the properties of the material and the solar incidence angle. The major effect of the solar radiation pressure interacting with the thermally deformed structure is found to give rise to disturbance moments on the structure. The thermal deformations of the structures are assumed to be within 0.1% of the characteristic length of the structure. With the assumed thermal deformations, the resulting uncontrolled transient responses of these geosynchronous orbiting structures to the solar radiation pressure induced disturbances are simulated. The resulting rigid modal oscillations are found to be an order of magnitude larger than for those cases previously considered in which only the solar radiation pressure effect on vibrating structures was treated. Modifications of control laws and/or the feedback gain values are considered in order to improve the transient response characteristics under the thermally induced disturbances.

I. Introduction

The major environmental disturbances on proposed orbiting large space structural systems are expected to be due to the solar radiation pressure and solar heating effects. The dynamics and control of a flexible beam and a flexible plate in the presence of disturbances due to the solar radiation pressure acting on the vibrating structure were considered previously.[1-3] It was seen that the major effect of the solar radiation pressure interacting with an elastically deformed (vibrating) orbiting structure was to produce moments on the structure resulting primarily in rigid modal oscillations. For the case of extremely flexible structures the amplitudes of these modes may be appreciable, even in the presence of both active and passive control.[1-3] In some situations the control laws previously developed by ignoring environmental effects may have to be redesigned. For simple lower order systems feedback gain values may be suitably adjusted; however, for large order systems the versatility on the linear Gaussian technique can be used to redesign control laws which provide a compromise between transient performance and the required control effort.[1-3]

Another important aspect of the environmental effect is the thermal gradients resulting in the structure due to the solar radiation heating. The deformations caused by the thermal gradients can be very large resulting in the dynamic instability of the structures.[4-6] Furthermore, the solar radiation pressure interacting with the thermally deformed structure gives rise to another form of environmental disturbance. The deformations caused by the solar heating depend on the thermal properties of the material and the geometric shape of the structure. Selection of materials with desired thermal properties and careful structural designs are required to minimize the thermal deformations of the structure to an acceptable level. The thermal deformations of the structure will occur as long as the structure is in the sunlit orbit and the continuous removal of this deformation using active control may not become practicable. The thermal deformations will have to be minimized by careful consideration of the thermal properties of the material in the preliminary structural design process. The objective of the present paper is to consider the effect of solar radiation pressure on the beams and the plates which are thermally deflected due to solar heating. (To the authors' knowledge, this is the first attempt to incorporate such effects into the modelling and simulation of the dynamics of large flexible orbiting systems). Motions of the beams and plates about: (i) the local vertical orientation; and (ii) the local horizontal nominal orientation (the latter carrying a rigid gimballed dumbbell to provide gravity stabilization) will be considered for the study (Figs 1 and 2).

Expressions for the thermal deflections of beams and plates exposed to solar heating will be developed. Subsequently, a mathematical model for the solar radiation induced torque on the thermally deflected structure will be obtained. The uncontrolled and controlled dynamics of the orbiting structures will then be simulated by considering the combined effect of the solar radiation pressure on the thermally deflected and vibrating structure. Modification of the control law and the feedback gain values to control the shape and orientation of the structure will be proposed, where required. In this study, the statically induced thermal deflections will be assumed small relative to the characteristic structural dimensions. In addition, the other major assumptions made here are: (a) the reflected solar radiation by the earth (albedo) can be neglected; (b) the inherent time lags in the heat transfer process are very small compared with the orbital period and are ignored; (c) the radiation from the edge surfaces can be neglected; and, (d) the beams and plates have uniform thickness and thermal properties resulting in a uniform temperature distribution.

The effects of the Earth's shadow and local shadowing due to another part of the structure are not included in the study.

II. Equilibrium Temperatures of Thin Plates and Beams

The cross section of a thin plate (or a beam) exposed to solar radiation is shown in Fig. 3. The solar incidence angle, θ_i, is taken to be a constant during a small interval of time. During this interval the surface facing the sun, s_u, attains a temperature, T_1, and the surface away from the sun, s_1, attains a temperature, T_2. The equilibrium temperatures, T_1 and T_2, can be determined by writing the thermal balance equations. The total heat leaving the beam from the two surfaces, s_u and s_1, should be equal to the heat received by the beam.[7] Therefore,

$$E_1\sigma T_1^4 + E_2\sigma T_2^4 = \alpha_s G \cos\theta_i \qquad (1)$$

where,

E_1 and E_2 are the emissivities of the surfaces, s_u and s_1, respectively

σ = Stefan-Boltzman constant
= 56.7×10^{-12} KW/m^2 K^4

α_s = absorptivity of the surface, s_u

G = intensity of solar radiation = 0.8KW/m^2

The heat flowing through the plate, at equilibrium, is also equal to the heat radiated from the surface, s_1.[7]

$$E_2\sigma T_2^4 = K(T_1-T_2)/t_c \qquad (2)$$

where,

k = thermal conductivity (KW/m K) of the plate material

t_c = thickness of the plate

Equations (1) and (2) can be rearranged as

$$T_1 = T_2 + (E_2\sigma t_c/k)/T_2^4 \qquad (3)$$

$$T_2^4 = (\alpha_s G \cos\theta_i)/E_2\sigma - (E_1/E_2)\, T_1^4 \qquad (4)$$

Eqs. (3) and (4) can now be solved to obtain T_1 and T_2 by assuming an approximate value of T_1 or T_2 and then through numerical iteration. Assuming $E_1 = E_2 = 0.05$ and $\alpha_s = 0.2$ (characteristic of proposed supporting mast material for large space structural systems), the temperature difference, $\Delta T = T_1 - T_2$, is obtained as a function of the solar incidence angle, θ_i, and various parameter ratios of $k_r = k/t_c$, as shown in Fig. 4. A higher value of k_r indicates a larger value of thermal conductivity and, hence, the temperature difference between the two surfaces becomes smaller. A plate of thickness 1 cm and made of polyamide ($k = 0.25\times10^{-3}$ KW/m K) will have a maximum temperature difference of 2.3°K. The temperature gradient is found to vary approximately proportional to $\cos\theta_i$ (Fig. 4). Expressions for deflections of the plate as a function of the temperature gradient are developed in the next section.

III. Pure Bending of Thin Plates and Beams[8]

Fig. 5 shows a beam of length, ℓ and width, b. The temperature of the mid-plane of the beam is denoted by T_n. The temperature of the surface facing the sun, s_u, is then $T_n + (\Delta T/2)$, and the temperature of the surface, s_1, is given by $T_n - (\Delta T/2)$. According to the theory of beam bending analyzed in Ref. 8, we have

$$d^2z/dx^2 = -(\alpha_e/J_y)\int T\, y\, d\,A \qquad (5)$$

where

z is the transverse deflection of the beam,

α_e = coefficient of linear expansion

J_y = moment of inertia of the beam about the y axis

Eq. (5) is rewritten by evaluating the integral

$$d^2z/dx^2 = -\alpha_e(\Delta T/t_c) = \text{a constant} \qquad (6)$$

The expression for the thermal deflection is then given by

$$z = -\alpha_e(\Delta T/t_c)x^2/2 \qquad (7)$$

The thermal deflection can be minimized by selecting a material with a low coefficient of expansion or by using a material of high thermal conductivity. An increase in the thickness of the plate will increase the temperature difference (Fig. 4) and also increase the weight of the plate. Hence, the parameter, t_c, should be as small as possible. The other important properties of materials not reflected in Eq. (7) are the density and the cost of the material as shown in Table 1.[9] For a beam of length 100m and thickness 0.01m, and made of polyamide (a low density and low cost material), the maximum thermal deflection is found to be approximately 7m. If the beam is made of aluminum, the maximum deflection would be about 2mm. Once a tolerable thermal deflection is specified the material can be selected to meet the conflicting requirements of low density, high thermal conductivity, and low cost. In the next section the solar radiation pressure moment resulting from a thermally deflected beam (also applicable to a plate) is discussed.

IV. Effect of Solar Radiation Pressure on Thermally Deflected Beams and Plates

The moment expressions obtained by Karymov[10] are used here to develop the solar radiation disturbance model for thermally deflected beams and plates. The solar radiation moments acting on a completely absorbing surface, $\bar{N}_a$, and a completely reflecting surface, $\bar{N}_r$, are given by[10],

$$\bar{N}_a = h_o\, \bar{\tau} \times \int_s \bar{R}\,(\bar{\tau}\cdot\bar{n})\, ds \qquad (8)$$

$$\bar{N}_r = 2h_o \int_s \bar{n}\times\bar{R}\,(\bar{\tau}\cdot\bar{n})^2\, ds \qquad (9)$$

where

$\bar{\tau} = a_o\bar{i} + b_o\bar{j} + c_o\bar{k}$, is the incident solar radiation vector

$\bar{n}$ = outward unit normal to the elemental surface, ds

$\bar{R}$ = position vector of the surface element, ds, relative to the center of mass

h_o = solar energy constant = 4.64×10^{-6} Nt/m^2.

a_o, b_o, c_o = direction cosines of the incident solar radiation with respect to the directions x,y,z, respectively

The integration over the sunlit area, s, is bounded by the condition, $\bar{\tau}\cdot\bar{n}<0$. The moment on a structure whose surface has an arbitrary coefficient of reflectivity, ε_r, is given by,[10]

$$\bar{N}_{\varepsilon r} = \bar{N}_a + \varepsilon_r(\bar{N}_r - \bar{N}_a) \tag{10}$$

The moment on a thermally deflected beam whose surface completely absorbs all the incident radiation is obtained (after evaluating the integral in Eq. (8)) as,

$$\bar{N}_a = a_o\, c_o\, \delta_o\, \ell\, h_o\, \bar{j} \tag{11}$$

where,

the incident radiation is assumed to lie in the x,y plane ($b_o=0$)

b = width of the surface ($b<<\ell$ for a thin beam)

δ_o = maximum deflection (from Eq. (7)) = z_{max}

The maximum deflection, δ_o, can be obtained as a function of ϑ_1 by selecting a function to represent ΔT in Fig. 4, and then by using the function for ΔT in Eq. (7). The moment acting on a completely reflecting beam surface is obtained through numerical integration, as,

$$\bar{N}_r = -0.05\, a_o\, c_o\, \delta_o\, \ell\, b\, h_o\, \bar{j} \tag{12}$$

The corresponding moment expressions for a plate are obtained as

$$\bar{N}_a = c_o\, \delta_o\, \ell\, b\, h_o(b_o\bar{i} + a_o\bar{j})$$

$$\bar{N}_r = -0.05\, c_o\, \delta_o\, \ell\, b\, h_o(b_o\bar{i} + a_o\bar{j}) \tag{13}$$

The moment on the structural surfaces whose coefficient of reflectivity is, ε_r, can then be obtained by using Eq (10) as,

$$\bar{N}_{\varepsilon r} = c_1\, \delta_o\, \ell\, b\, h_o(b_o\bar{i} + a_o\bar{j})[(1-\varepsilon_r) - 0.05\varepsilon_r] \quad \text{(for a plate)}$$

$$= a_o\, c_o\, \delta_o\, \ell\, b\, h_o\bar{j}\,[(1-\varepsilon_r) - 0.05\varepsilon_r] \quad \text{(for a beam)} \tag{14}$$

V. Dynamics and Control of Beams and Plates under the Influence of Solar Radiation Disturbances due to Thermal Deformations

The dynamic models of beams and plates, for both cases of orbital orientations (Figs. 1 and 2) developed in References 11 and 12 are considered. The nominal local horizontal orientation of beams and plates represents a gravitationally unstable motion due to the unfavorable moment of inertia distribution. Stabilizing gravity-gradient forces on such structures can be obtained by using a rigid dumbbell such that the resulting inertia distribution provides the desired gravity forces. A dumbbell may be attached to the main structure through a hinge which could provide both torsional stiffness and damping. The dynamics of the proposed dumbbell stabilized beam and plate (Figs. 1a and 2a) was considered in Reference 12. Here, the study is extended to consider the disturbances resulting from the interaction of solar radiation pressure with the thermally deformed structure. The disturbance resulting from the solar radiation pressure on the dumbbell will be neglected, since the dumbbell would have a small surface area compared with the main structure. The modified control laws and gain values developed in References 2 and 3 will be used to obtain closed-loop transient responses of these structures by incorporating the disturbance expressions (Eq. (14)) into the structural models of the beams and plates.[1-3,11,12] The maximum thermal deflection for each case is assumed to be 0.001ℓ, based on the calculation of deflections for a 100m long, 0.01m thick beam made of polyamide and aluminum, respectively (Table 1). The beams and plates are assumed to have a fundamental frequency equal to ten times the orbital frequency with the orbital frequency corresponding to a geosynchronous orbit. Initial conditions are assumed to be zero for all the modes in order to highlight the thermally induced disturbance effect. For those cases in which the transient responses appear to be unacceptable further modifications in the control law and/or the gain values are proposed.

V.1 The Beam Along the Local Vertical

The effect of the thermally induced disturbance on the pitch motion of the beam is shown in Fig. 6(a). The disturbance (without control) has no effect on the flexible modal oscillations and hence these are not depicted in the figure. It is seen that the pitch response has a maximum amplitude of 2.4 degrees as a result of the disturbance. Application of the previously developed control law and the gain values[2] for the case of two actuators, located at the beam center and at one of the nodal points of the first symmetric mode, shows (Fig. 6(b)) pitch amplitude oscillations of less than 0.24^o amplitude. The peak control forces required are only of the order of 10^{-3} Nt. for each actuator. By increasing the gain value proportional to the pitch rate by a factor of 10, a further reduction of the pitch amplitude to approximately 0.03^o is illustrated (Fig. 6(c)). Correspondingly, the peak force requirement in actuator number 1 increases to 0.01 Nt.

V.2 The Dumbbell Stabilized Beam

The transient response of the dumbbell stabilized beam due to the solar radiation pressure acting on the thermally deformed beam is shown in Fig. 7 (only the pitch mode is depicted). The pitch oscillations are seen to have approximately 2.4^o amplitudes in the absence of control. With the application of the control law previously developed in Reference 3 (and indicated in the figure), the amplitude of the pitch oscillations is reduced to 0.24^o (Fig. 7). The peak control force required is about 0.01 Nt.

The gain values can easily be modified further to meet any specific requirement on the pitch motion of the beam.

V.3 The Plate Oriented Along the Local Vertical

The uncontrolled and the controlled transient responses of the 100m square thin plate nominally oriented along the local vertical and with the disturbance caused by the thermal deflection of the plate are shown in Fig. 8. The same order of magnitude thermal deflections are assumed here as for the beam in sections V.1 and V.2. The pitch, roll and yaw rotations of the plate exceed the linear range in less than an orbit. Application of the linear quadratic Gaussian control technique with the penalty matrices, $Q = 100I$ and $R = I$, results in a transient responses in which steady state oscillations with amplitudes of about 0.02 radians are seen in all three rotational modes of the plate (Fig. 8). Modal oscillations (non-dimensionalized) in all the three flexible modes remain within an amplitude of 10^{-5} (10^{-3}m). An improvement in the transient response was obtained by employing a split weighting state penalty matrix ($Q = 100$ I, except for $Q(1,1) = Q(2,2) = Q(3,3) = 10{,}000$) where the rotational modes were penalized more heavily. The transient response of the plate in the rotational modes for this case is shown in Fig. 9. The steady state oscillations are reduced by an order of magnitude in comparison with Fig. 8. However, the peak control forces increased from 7 Nt. to 12 Nt. The total control effort required also increased by approximately 60%.

V.4 The Dumbbell Stabilized Plate

The closed-loop transient response of the dumbbell stabilized plate is considered. The magnitude of the pitch, roll and yaw angles are seen to be within 0.02 radians in the absence of any solar radiation pressure induced disturbance (Fig. 10(a)). For the same case, the effect of the solar radiation pressure disturbance resulting from the thermally deformed plate ($\delta_{th} = 0.001\ell$, $\ell = 100$m) is shown in Fig. 10(b). The pitch and the yaw oscillations are seen to exceed the linear range even with the control. The control effort required (3×10^5 Nt. - secs.) was nearly ten times more than that for the case without the disturbance (Fig. 10(a)). The transient response characteristics for this case are therefore unacceptable.

A redesign of the control is attempted with penalty matrices selected as: $Q = 10{,}000I$ and $R = 100I$. (Both the state as well as the control are now penalized more heavily by increasing both sets of elements by two orders of magnitude). The transient response of the dumbbell stabilized plate with this control is shown in Fig. 11. The pitch, roll and yaw amplitudes are well within 0.02 radians even in the presence of the disturbance. The peak control force required is approximately 14Nt. in both actuators (or an RMS value of a little less than 30Nt.).

Thus, the thermal deformations of the structures can be of greater concern than the deformations of the structure due to structural vibrations (considered in Refs. 2 and 3) in modelling the disturbances arising from the solar radiation pressure. This study shows the need to further minimize thermal deformations ($<< 0.001\ell$) from the view point of reducing the radiation pressure disturbance effects. This can be accomplished with cost and strength constraints primarily by increasing the thermal conductivity.

Conclusions

The dynamics and control of thermally deformed orbiting beams and plates interacting with the solar radiation pressure are studied. The major effect of the solar radiation pressure is found to result in net moments on the structure. Modifications of control laws and/or feedback gain values previously obtained by not considering the thermal disturbances are suggested in order to improve the transient response characteristics under the thermally induced effects.

In general, the effect of solar radiation pressure acting on the thermally deformed structures is found to be more important than the effect of solar radiation pressure on the vibrating structures. In order to reduce the disturbances resulting from the interaction of solar radiation pressure with the thermally deformed structure, further minimization of the thermal deformations is recommended.

References

1. Krishna R. and Bainum, P.M., "Effect of Solar Radiation Disturbance on a Flexible Beam in Orbit," AIAA Journal, Vol. 22, No. 5, May 1984. pp. 677-682.

2. Krishna, R. and Bainum, P.M., "Orientation and Shape Control of an Orbiting Flexible Beam Under the Influence of Solar Radiation Pressure," AAS/AIAA Astrodynamics Conference, Lake Placid, N.Y., Aug. 22-24, 1983, Paper No. 83-325; also in Astrodynamics 1983, Advances in the Astronautical Sciences, Vol. 54, Part I, pp. 221-238.

3. Bainum, P.M. and Krishna, R., "Control of an Orbiting Flexible Platform in the Presence of Solar Radiation," Fourteenth International Symposium on Space Technology and Science, Tokyo, May 28 - June 2, 1984.

4. Frisch, H.P., "Thermally Induced Response of Flexible Structures: A Method for Analysis," Journal of Guidance and Control, Vol. 3, No. 1, 1980, pp. 92-94.

5. Ayer, F., and Soosar, K., "Structural Distortions of Space Systems Due to Environmental Disturbances," AIAA International Meeting and Technical Display, "Global Technology 2000," May 6-8, 1980, Baltimore, Md., Paper No. AIAA-80-0854.

6. Shu, C.F., and Chang, M.H., "Integrated Thermal Distortion Analysis for Satellite Antenna Reflectors," AIAA 22nd Aerospace Sciences Meeting, Jan. 9-12, 1984, Reno, paper No. AIAA-84-0142.

7. Gray, W.A. and Muller, R., Engineering Calculations in Radiative Heat Transfer, Pergamon Press, N.Y., 1974.

8. Burgreen, D., Elements of Thermal Stress Analysis, C.B. Press, N.Y., 1971.

9. Ashton, J.E., Halpin, J.C., and Petit, P.H., Primer on Composite Materials Analysis, Technomic Publication, Conn., 1970.

10. Karymov, A.A., "Determination of Forces and Moments Due to Light Pressure Acting on a Body in Motion in Cosmic Space," P.M.M., No. 5, Vol. 26, 1962, pp. 867-876.

11. Kumar, V.K. and Bainum, P.M., "Dynamics of a Flexible Body in Orbit," Journal of Guidance and Control, Jan. - Feb. 1980, Vol. 3, No. 1, pp. 90-92; also AIAA Preprint No. 78-1418.

12. Bainum, P.M. and Kumar, V.K., "On the Dynamics of Large Orbiting Flexible Beams and Platforms Oriented Along the Local Horizontal," Acta Astronautica, Vol. 9, No. 3, 1982, pp. 119-127.

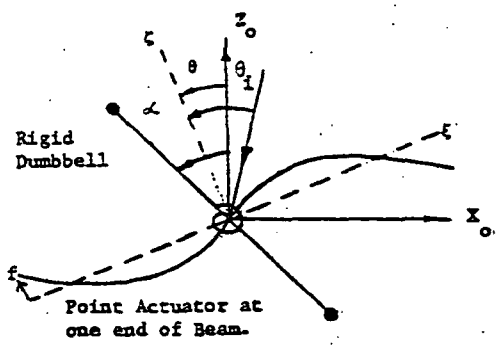

Fig. 1(a). Dumbbell Stabilized Flexible Beam Nominally Oriented Along the Local Horizontal

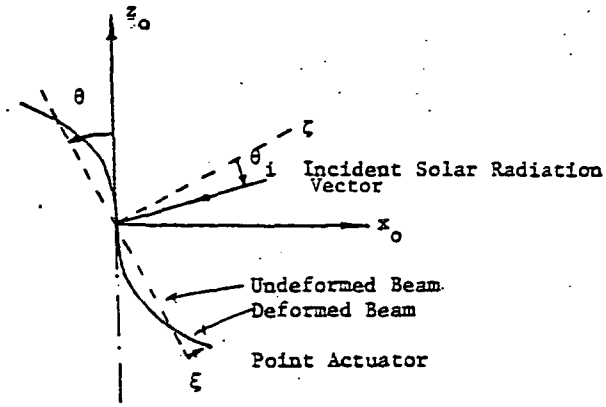

Fig. 1(b). Uniform Flexible Beam Nominally Oriented Along the Local Vertical

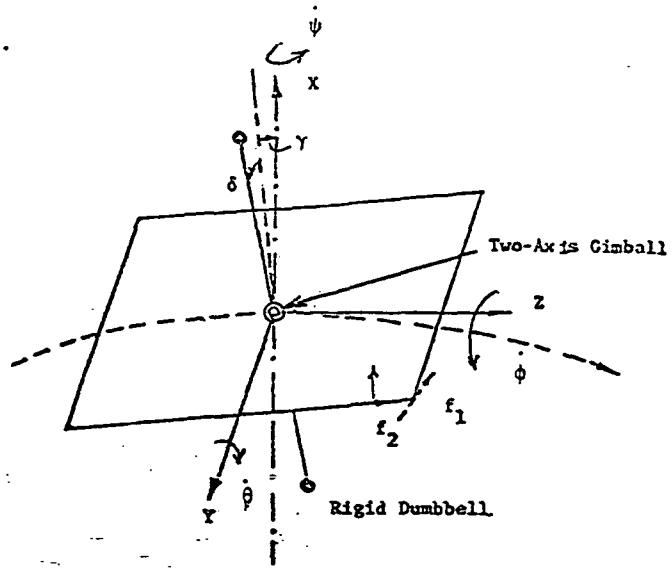

Fig. 2(a) Dumbbell Stabilized Plate in Orbit.

Table I. Properties of Representative Materials[9]

Material	Density (kg/m^3)	Expansion Coefficient, α_e (m/m^oC)	Thermal Cond. K KW/m- K	Cost ($/Kg)	δ_{max} (m)
Graphite	$1.5x10^3$	$8.3x10^{-5}$	$8.65x10^{-3}$	500	10^{-4}
Beryllium	$1.8x10^3$	$3.5x10^{-6}$	$12.25x10^{-3}$	10,000	10^{-4}
Aluminum	$2.7x10^3$	$2.1x10^{-6}$	$28.8x10^{-3}$	1.1	10^{-5}
Polyamide	$1.13x10^3$	$25x10^{-6}$	$2.45x10^{-3}$	15	7

δ_{max}: maximum thermal deflection of a plate with sides equal to 100m and thickness equal to 0.01m.

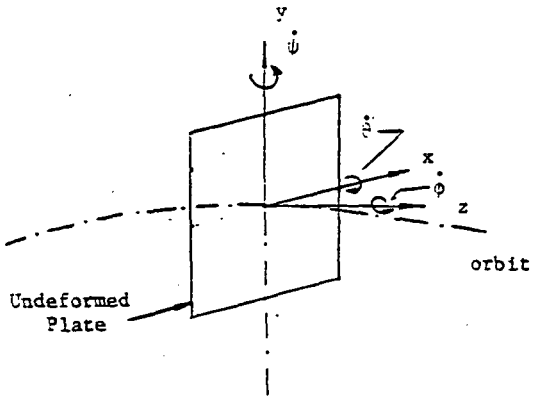

Fig. 2(b). Plate in Orbit Nominally Oriented Along the Local Vertical.

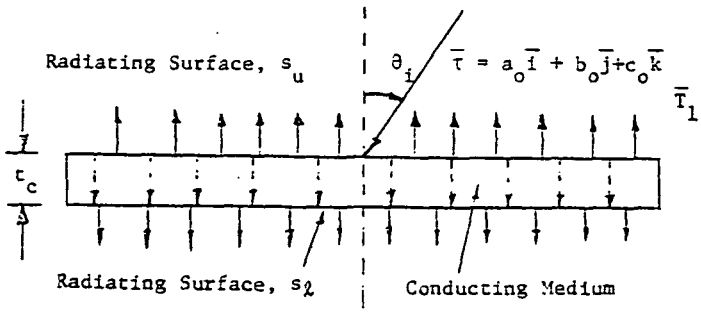

Fig. 3. Thermal Gradient in a Beam Due to Solar Radiation Heating.

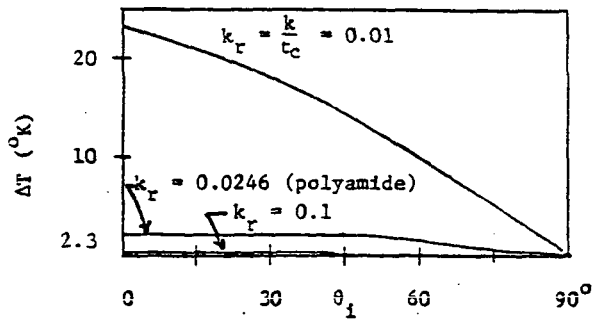

Fig. 4. Thermal Gradient in a Beam as a Function of Solar Incidence Angle and Thermal Conductivity.

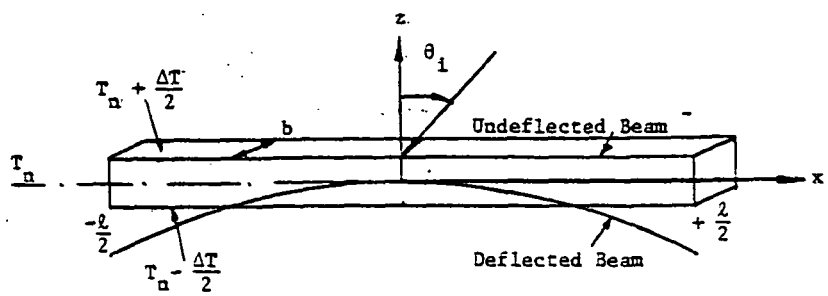

Fig. 5. Beam Bending Due to Solar Radiation Heating

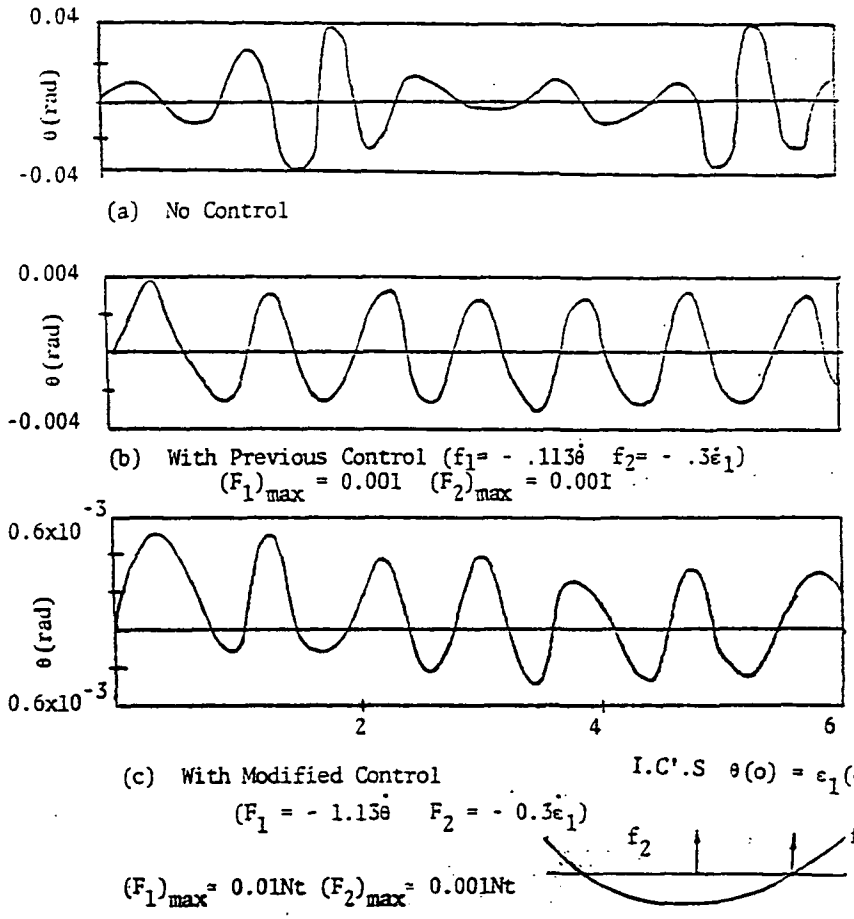

Fig. 6. Response of the Beam Nominally Oriented Along the Local Vertical Under the Influence of Solar Radiation Disturbance Caused by Thermal Deformation of the Beam ($\delta_{th} = 0.001\ell$).

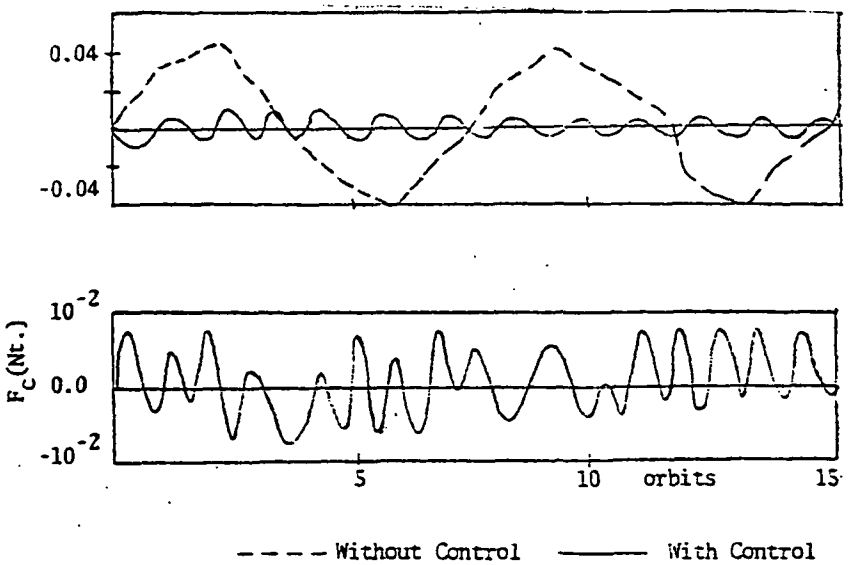

$F_c = -0.07\,\vartheta - 0.005\,\dot{\vartheta} - 0.1\dot{\varepsilon}_1 - 0.03\dot{\varepsilon}_2$

(Single actuator at one end of the beam)

Fig. 7. Response of the Dumbbell Stabilized Beam Under the Influence of Solar Radiation Disturbance Caused by Thermal Deflection of the Beam ($\delta_{th} = 0.001\ell$, $\ell = 100m$).

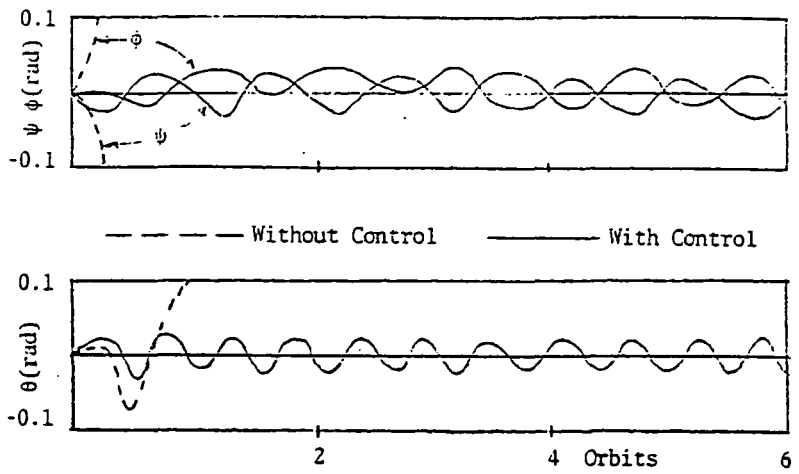

Initial conditions in all the modes are zero.
ε_1 to ε_3 have very small amplitudes (less than 10^{-5})
$(F_1)_{max}$ = 7Nt. $(F_2)_{max}$ = 6Nt.

Fig. 8. Response of the Plate Nominally Oriented Along the Local Vertical Under the Influence of Solar Radiation Disturbance Caused by Thermal Deflection of the Plate (δ_{th} = 0.001ℓ) ℓ = 100m. Control Law Q = 100I, R=I

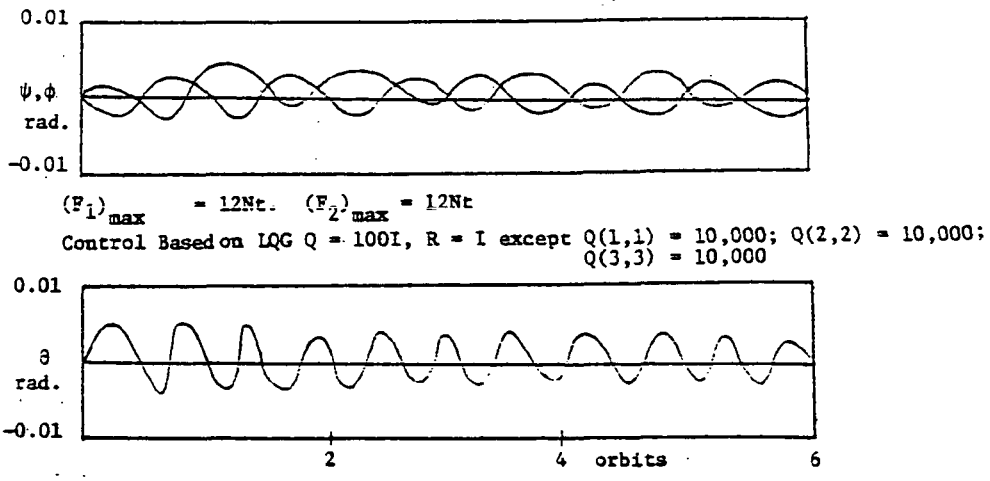

$(F_1)_{max}$ = 12Nt. $(F_2)_{max}$ = 12Nt
Control Based on LQG Q = 100I, R = I except Q(1,1) = 10,000; Q(2,2) = 10,000; Q(3,3) = 10,000

Fig. 9. Response of the Plate Nominally Oriented Along the Local Vertical Under the Influence of Solar Radiation Disturbance Caused by Thermal Deflection of the Plate (δ_{th} = 0.001ℓ) ℓ= 100m, ω_1 = 10

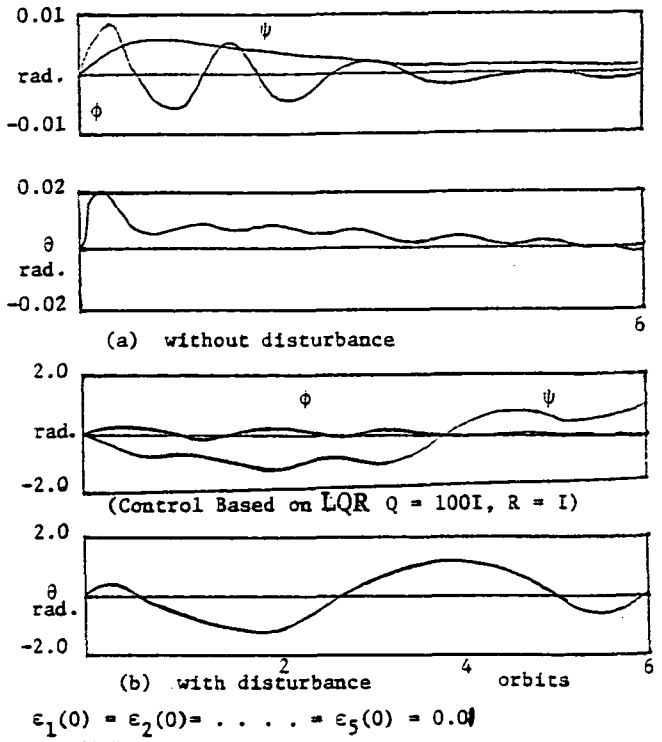

Fig. 10. Response of the Dumbbell Stabilized Plate Under the Influence of Solar Radiation Disturbance Caused by Thermal Deflection of the Plate ($\delta_{th} = 0.001\ell$) $\ell = 100m$, $\omega_1 = 10$

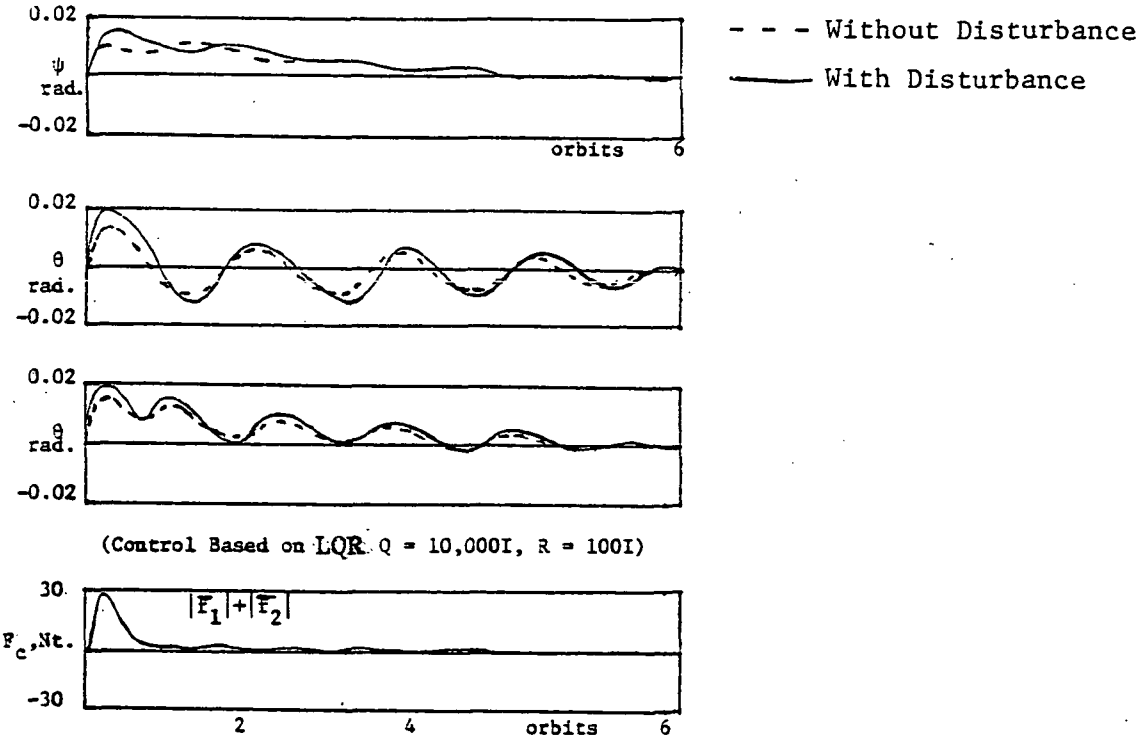

Fig. 11. Response of the Dumbbell Stabilized Plate Under the Influence of Solar Radiation Disturbance Caused by Thermal Deflection of the Plate ($\delta_{th} = 0.001\ell$) $\ell = 100m$, $\omega_1 = 10$

VI. ANALYSIS OF A CONTROL SYSTEM FOR A LARGE SPACE ANTENNA SYSTEM IN THE PRESENCE OF PLANT AND MEASUREMENT NOISE

Abstract

This paper considers the problem of controlling a stochastic linear system by minimization of a quadratic performance index, appropriately weighted in both the state variables as well as the control inputs. A finite element model of a proposed large space structure - the Hoop/Column structural system, is taken as the basis for the controls analysis. The control law is designed for a set of proposed actuator arrangements which include torquers and point actuators along the mast and a single actuator on the hoop. Linear quadratic Gaussian techniques have been used for the development of the control laws. The controls analysis is carried out assuming co-located sensors and actuators. The sensor and plant noises are assumed to be uncorrelated zero-mean white noises. Results indicate a general degradation in the deterministic system performance due to noise characteristics. Increasing elements in the state weighting matrix does not bring as noticeable an improvement in the transient performance as it did in the deterministic case. A definitive improvement in the performance can be obtained by decreasing the plant noise and either: (1) increasing the measurement noise suitably or (2) increasing both the measurement noise and elements in the control weighting matrix.

NOMENCLATURE

A = System state matrix

B, B_c = Control influence matrices

C = Control gain matrix

E = Expectation/value operator

F = Filter gain matrix

F_c = Control vector

G = Plant noise influence matrix

H = Observation matrix

I = Identify matrix

J = Cost function

K = Stiffness matrix

K_1 = Solution of steady state control Riccati differential equation

K_i = i^{th} generalized stiffness

M = Mass (inertia) matrix

m_i = i^{th} generalized modal mass

P = Solution of filter matrix Riccati differential equation

Q = Positive semi-definite state weighting matrix

q = modal co-ordinates

$\dot{q}, \ddot{q}$ = modal velocities and accelerations

R = Positive definite control weighting matrix

t_o = Initial time

t_f = Terminal time

$U(t)$ = Vector representation of the control input

$V(t)$ = Co-variance of measurement noise

$\underline{v}(t)$ = Measurement noise vector

$W(t)$ = Co-variance of plant noise

$\underline{w}(t)$ = Plant noise vector

$X(t)$ = State vector

$\hat{X}(t)$ = State vector estimate

$Y(t)$ = Measurement vector

Z = Matrix consisting of displacements and rotations in the nodal points

ϕ = Modal transformation matrix

I. Introduction

Orbiting large flexible space systems have been considered for use in future communications and other fields. As the size of the spacecraft increases and the ratio of weight to area of the spacecraft decreases, flexibility considerations become very important. This is in contrast to small space structures which are assumed to be rigid. One such large flexible space structure which has been proposed for future space missions is the Hoop/Column antenna system.

The Hoop/Column antenna system[1], depicted in Fig. 1 in deployed configuration, contains the deployable (telescoping) mast system connected to the hoop by support cables under tension. The hoop contains 48 rigid sections to be deployed by motor drive units. The desired shape of the RF relective mesh is produced by a secondary drawing surface using surface control cables. The reflective mesh is connected to the hoop by quartz or graphite stringers. At one end of the mast the electronic feed assemblies are positioned, whereas at the other end are the principal solar arrays connected to the main bus-based control.

The finite element model (FEM) representation of the Hoop/Column antenna system has been taken as the basis for the controls analysis.

The controls analysis of the Hoop/Column antenna system requires specification of the type of actuators and their locations and orientations in

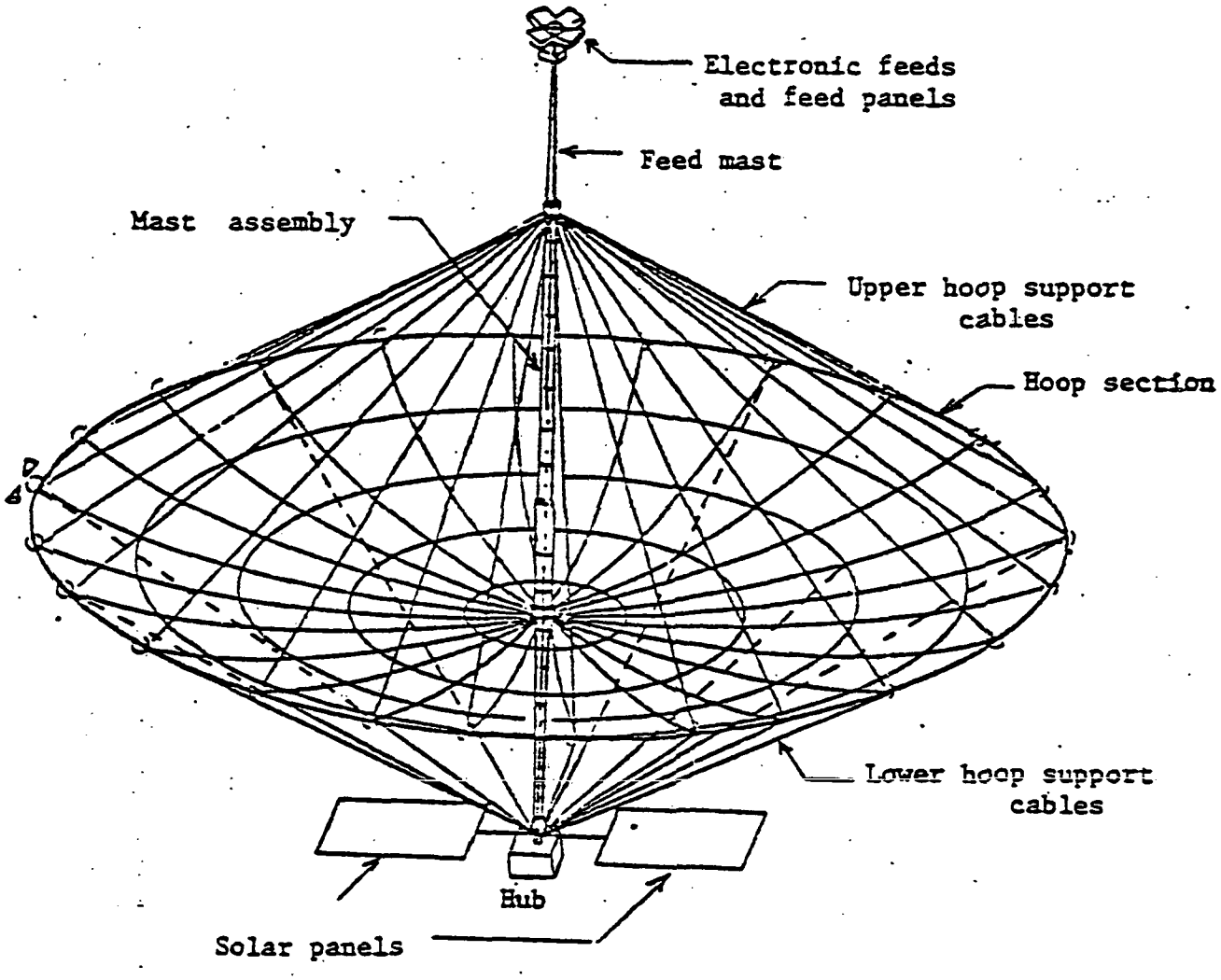

Fig. 1. THE HOOP/COLUMN ANTENNA SYSTEM.

the structure. For this study point thrusters and/or torquers are assumed to generate the required control forces and torques. The location and orientation of these thrusters depend on the mode shapes of the structure and which modes in particular are to be controlled. The first thirteen modes corresponding to the data provided by NASA-Langley will be included in the controls analysis and, hence, it is convenient here, to choose thirteen actuators in this analysis. Each actuator is selected to have a principal effect on a particular mode, but the same actuator may help to control a different mode as well. Controllability considerations of the Hoop/Column system based on the proposed location of the thirteen actuators as shown in Fig. 2 have been established using graph theoretic techniques[2]. Further, the earlier analyses of the Hoop/Column system considered either a deterministic linear system with noise-free plant and sensors[3], or a stochastic linear system (with plant and measurement noise) but with the restriction that only torque actuators on the feed mast were considered in the controls analysis[4], where extensive transient performance was not simulated. The purpose of this paper is to synthesize a control law and simulate transient performance characteristics, based on stochastic optimal control theory, which can be realized by combination of the Kalman filter and linear feedback techniques and under the assumption of co-located sensors and actuators.

II. Mathematical Formulation of the Problem

The dynamic model of the Hoop/Column structural system in the absence of damping can be represented as[3]

$$M\ddot{Z} + KZ = F_c \qquad (1)$$

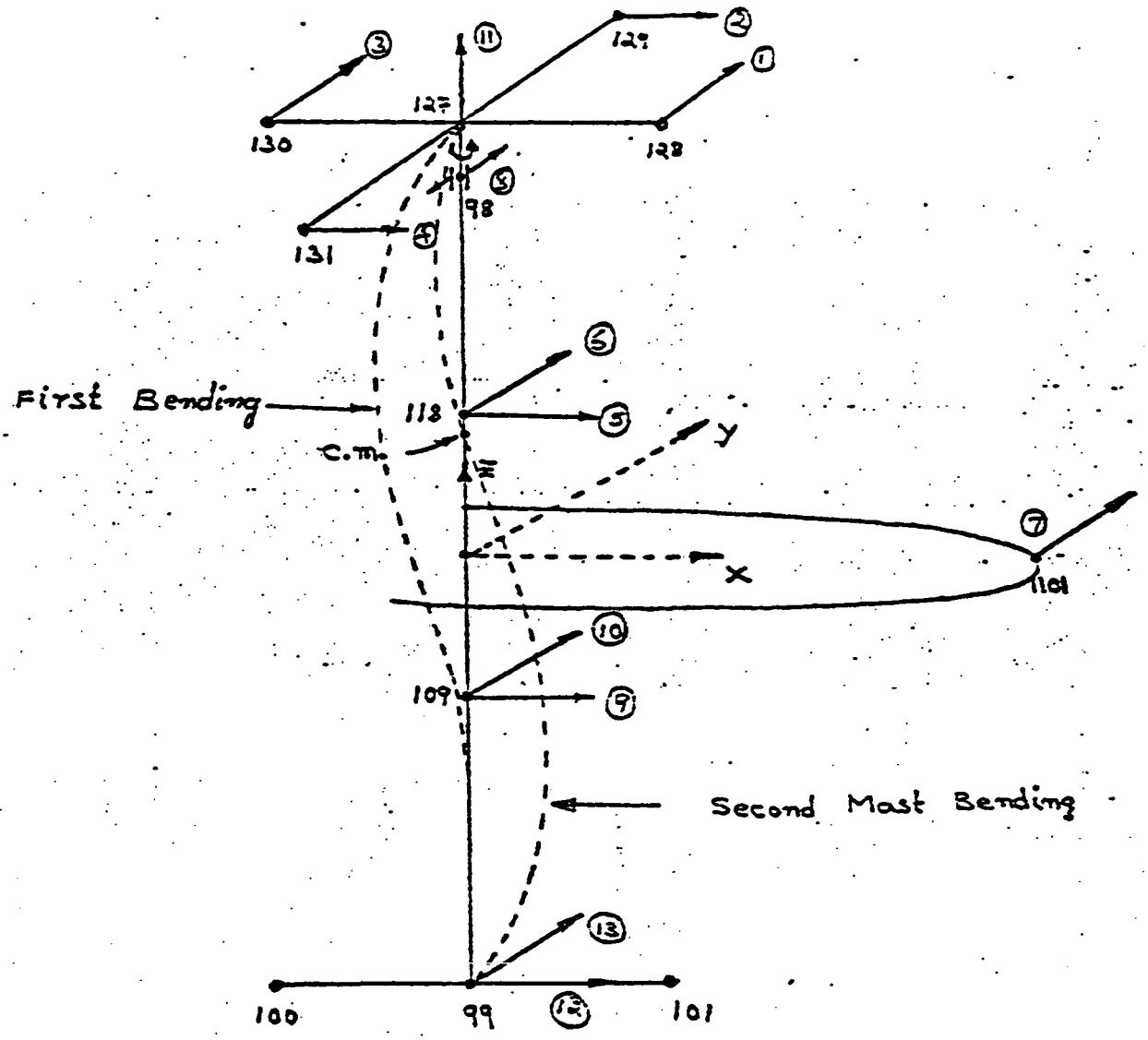

Actuator no. (circled)	Mode being affected
1 2 3 and 4	Feed Mast Torsion (12)
5	First Bending (about y axis) (8)
6	First Bending (about x axis) (9)
7	Surface Torsion (10)
8	Yaw (rotation about z axis) and First Torsion (7)
9	Translation along x } Also second (11)
10	Translation along y } Mast bending (13)
11	Translation along z
12	Pitch (rotation about y axis)
13	Roll (rotation about x axis)

Fig. 2 PROPOSED ARRANGEMENT OF ACTUATORS - HOOP/COLUMN ANTENNA SYSTEM

where

M - 672 x 672 mass/inertia matrix

K - 672 x 672 stiffness matrix

Z - 672 x 1 matrix consisting of the displacements and rotations at the nodal points

F_c - 672 x 1 control vector

$$F_c = B_c U \tag{2}$$

where

B_c - control matrix of order 672 x p

for

p - number of actuators

U - p x 1 matrix associated with the control vector

In general, Z is the state vector containing the generalized co-ordinates of each node and will be of the order (nx6) for n number of nodes and all 6 degrees of freedom; M is the modal mass (inertia) matrix of order (6n x 6n); K is the stiffness matrix of order (6n x bn); and B_c is the control influence matrix of order (6n x p) for p number of actuators to be arranged on the structure. In the present model, represented by equation (1) the number of nodes is equal to 112 (i.e. n = 112), corresponding to the number of nodal (grid) points in the FEM output.

To decrease the dimensionality of the model a modal transformation is carried out defining

$$Z = \phi q \tag{3}$$

where

ϕ is the matrix containing the eigenvectors of equation (1) and is of order (6n x m), for m number of modes and q is a modal vector of order (mxl). In this case, we are considering the first thirteen modes which include all six rigid modes and the first seven flexible modes, so that m = 13.

After using the transformation between the modal co-ordinates given by equation (3) in equation (1), equation (1) can then be rewritten as

$$\phi^T M \phi \ddot{q} + \phi^T K \phi q = \phi^T F_c \tag{4}$$

The left hand side of equation (4) can be rewritten, using the properties of the eigenvalues and associated eigenvectors as

$$[\,m_i\,]\ddot{q} + [\,K_i\,]q = \phi^T F_c \tag{5}$$

where

$$\phi^T M \phi = \text{diag}\,[m_i] = [\,m_i\,]$$

$$\phi^T K \phi = \text{diag}\,[K_i] = [\,K_i\,]$$

The control influence matrix, B_c, in equation (2) is formed as follows:

If there is an actuator that influences the i^{th} node ($1 \leq i \leq 112$) in the j^{th} direction ($1 \leq j \leq 6$), then $B_c(k,L) = 1$ where $k = (i-1) \times 6+j$ and L = the designated number of the actuator. Thus, B_c, consists of zeros and ones, showing the influence of force actuators on the translational degrees of freedom of the various nodes, and the influence of the torque actuators on the rotational degrees of freedom.

Equation (5) can be rewritten in the form

$$\begin{bmatrix} \dot{q}_1 \\ \dot{q}_2 \end{bmatrix} = \left[\begin{array}{cc} 0 & I \\ \hline -[m_i]^{-1}[K_i] & 0 \end{array}\right] \begin{bmatrix} q_1 \\ q_2 \end{bmatrix} + \left[\begin{array}{c} 0 \\ \hline [m_i]^{-1}\phi^T B_c \end{array}\right] U \qquad (6)$$

where the state variables, q_1 and q_2 are denoted,

$$q_1 = q$$

$$q_2 = \dot{q}_1$$

Equation (6) is rewritten in the form:

$$\dot{X} = AX + BU \qquad (7)$$

where

$$X = \begin{bmatrix} q_1 \\ q_2 \end{bmatrix}, \quad A = \begin{bmatrix} 0 & I \\ -[m_i]^{-1}[K_i] & 0 \end{bmatrix},$$

$$B = \begin{bmatrix} 0 \\ [m_i]^{-1}\phi^T B_c \end{bmatrix},$$

Now considering the stochastic problem, the plant noise is included in equation (7) to yield the stochastic linear dynamic system

$$\dot{X} = AX + BU + G\underline{w} \qquad (8)$$

The measurement vector, Y, can be related to the state vector and the measurement noise according to,

$$Y = HX + \underline{v} \tag{9}$$

Equations (8) and (9) together with the following cost function,

$$J = E\left(\lim_{t_f \to \infty} \frac{1}{2t_f} \int_{t_o}^{t_f} (X^T QX + U^T RU)\, dt \right) \tag{10}$$

completely define the stochastic problem.[5] After minimizing the cost function, the optimal control vector U becomes,[5]

$$U = -C\hat{X} \tag{11}$$

where

$$C = R^{-1} B^T K \tag{12}$$

and

K is the steadystate solution of the matrix Riccati differential equation,

$$-\dot{K} = KA + A^T K - KBR^{-1} B^T K + Q \tag{13}$$

The estimate, $\hat{X}$, is obtained from[6]

$$\dot{\hat{X}} = A\hat{X} + BU + F\,(Y - H\hat{X}) \tag{14}$$

with the filter gain, F, expressed as

$$F = PH^T V^{-1} \tag{15}$$

where P is the solution of the filter matrix Riccati differential equation,

$$\dot{P} = AP + PA^T - PH^T V^{-1} HP + GWG^T \tag{16}$$

where

$$V = E\,(\underline{v}\underline{v}^T) \tag{17}$$

Table 1 - Hoop/Column model eigen values

Mode No.	Frequency Hz	Generalized mass, m_i (lb-sec^2/in)	Generalized stiffness, K_i (lb/in)
1	0.0	16.44388	0.0
2	0.0	8.925020	0.0
3	0.0	7.349353	0.0
4	0.0	9.704152	0.0
5	0.0	2.940652	0.0
6	0.0	8.418909	0.0
7	0.1188347	153.1573	85.38542
8	0.2142455	5.232954	9.482657
9	0.2709558	3.073094	8.907021
10	0.5063228	0.3046446	3.083247
11	0.7288725	1.992988	40.88663
12	0.8897594	723.5216	22612.90
13	0.9192313	0.6581203	21.95405

IIC. Possible Arrangement of Actuators for the Hoop/Column System

Twelve actuators consisting of combinations of point actuators and a torquer are assumed to be located at positions along the mast and at selected positions in the feed assembly. The remaining actuator is assumed to be a point actuator mounted on one of the rigid links of the hoop assembly and whose thrust direction is tangential to the hoop circle. Fig. 2 describes the proposed actuator assembly. Actuators numbers 5 and 6 are assumed to provide control over translation along the X and Y directions, respectively, and, in addition, also

and

$$W = E\left(\underline{w}\underline{w}^{T}\right) \tag{18}$$

Substitution of equation (11) into equation (8) will yield

$$\dot{X} = AX - BC\hat{X} + G\underline{w} \tag{19}$$

Furthermore after including equations (9) and (11) in equation (14) the following first order differential equation in the estimated state vector results:

$$\dot{\hat{X}} = (A - FH - BC)\,\hat{X} + FHX + F\underline{v} \tag{20}$$

The simulation of the stochastic optimally controlled system here will involve the simultaneous numerical solution of the sets of differential equations in both the state variables and the estimated state variables, represented by equations (19) and (20). A flow diagram schematic of this configuration is illustrated in Fig. 3, and will be taken as the basis for studying the system behavior. This approach has been selected as being computationally simpler than considering, alternatively, simultaneous differential equations in the state vector together with differential equations in the error vector, $e = X - \hat{X}$. If the latter approach were taken, then at each time step a subtraction of appropriate components of $\hat{X}$ from the corresponding components of X would be required.

IIB. Mass and Stiffness Properties of the Hoop/Column System

The model considered here consists of six rigid body modes (3 translation+ 3 rotation) and the first seven flexible modes. Table 1 indicates the generalized mass, the generalized stiffness, and the frequency at each mode.[3]

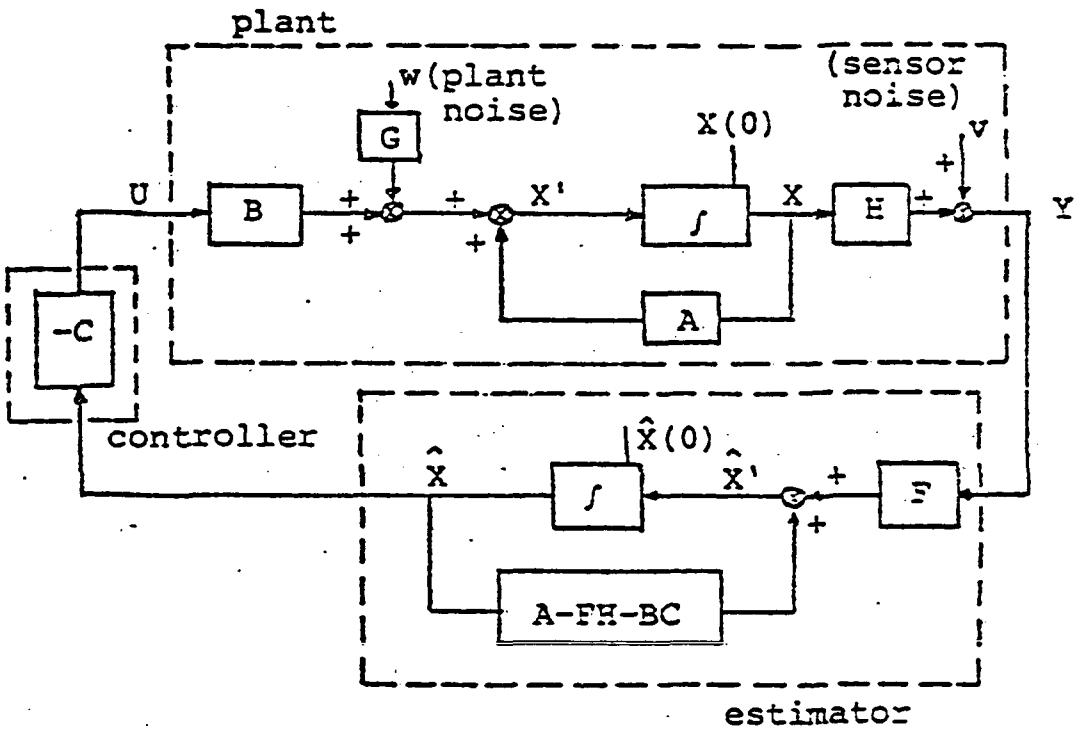

Fig. 3 STOCHASTIC OPTIMAL CONTROL CONFIGURATION

to control the first bending modes (modes 8 and 9). Actuator 11 controls translation along the Z direction, whereas actuators 8,12, and 13 control yaw, pitch and roll motions respectively. Actuators 1,2,3, and 4 are selected so that each actuator could provide independent control of the feed mast torsion (mode 12). Actuators 9 and 10 are selected to control the second mast bending (modes 11 and 13). Actuator 7 controls surface torsion (mode 10) and is the only actuator assumed to be mounted on the hoop. Table 2 indicates the various modes affected by each actuator.

Table 2 - Relationship between actuators and modes directly influenced

Actuator No. (circled in Fig. 2)	Mode being affected
1,2,3 and 4	Feed Mast Torsion (12)
5	First Bending (about Y axis) (8)
6	First Bending (about X axis) (9)
7	Surface Torsion (10)
8 (Torquer)	Yaw (rotation about Z axis) and First Torsion (7)
9	Translation along X axis and Second Mast Bending (11)
10	Translation along Y axis and Second Mast Bending (13)
11	Translation along Z axis
12	Pitch (rotation about Y axis)
13	Roll (rotation about X axis)

III. Numerical Simulations and Synthesis of Control Law

Numerical calculation of the control gains and filter gains and the

simulation of the dynamic transient responses are obtained with the aid of ORACLS.[7] For the proposed 13 actuator model a parametric study was performed showing the effect of varying Q from 100I to 10000I and R from I to 100I on the least damped mode of the system (Fig. 4). It has been concluded that Q = 1000I, R=I is a suitable design point from the stand point of minimizing the least damped modal time constant and maintaining a reasonable control effort.[3] As mentioned earlier, controllability of the proposed system of 13 actuators (Fig. 2) has been verified.[3] Further, it has been established that closed loop eigenvalues of the combined plant and estimator exist for all combinations of Q,R,W and V considered here. As an example, Table 3 shows the closed loop eigenvalues of the combined plant and estimator system for Q=1000I, R=I and Q=10000I, R=I with W=0.00001, V=0.0000025 assumed in both cases. The values of the plant noise are in general of the order of 1.0×10^{-5} $(dn\text{-}cm)^2$. The values of the sensor noise varies with the type of sensor measurement device. For example, some of the angular and linear displacement sensors have noise characteristics of the order of 1.0×10^{-7} $(rad)^2$ and 1.0×10^{-7} $(m)^2$, respectively. Since in our problem more than one type of displacement and/or rate may be required to be sensed, some average values of these plant and measurement noises have been assumed.

Figs (5a-5g) show the transient behavior of the modal coordinates with random noise generated for an initial displacement of 0.01 in all modes. (Figs (6a-6c) indicate the transient behavior of the estimated modal displacement coordinates which have an initial assumed displacement of 0.01. Figs (5a-5g) and Fig (6a-6c) along with Table 4 show that for the same order of control effort,

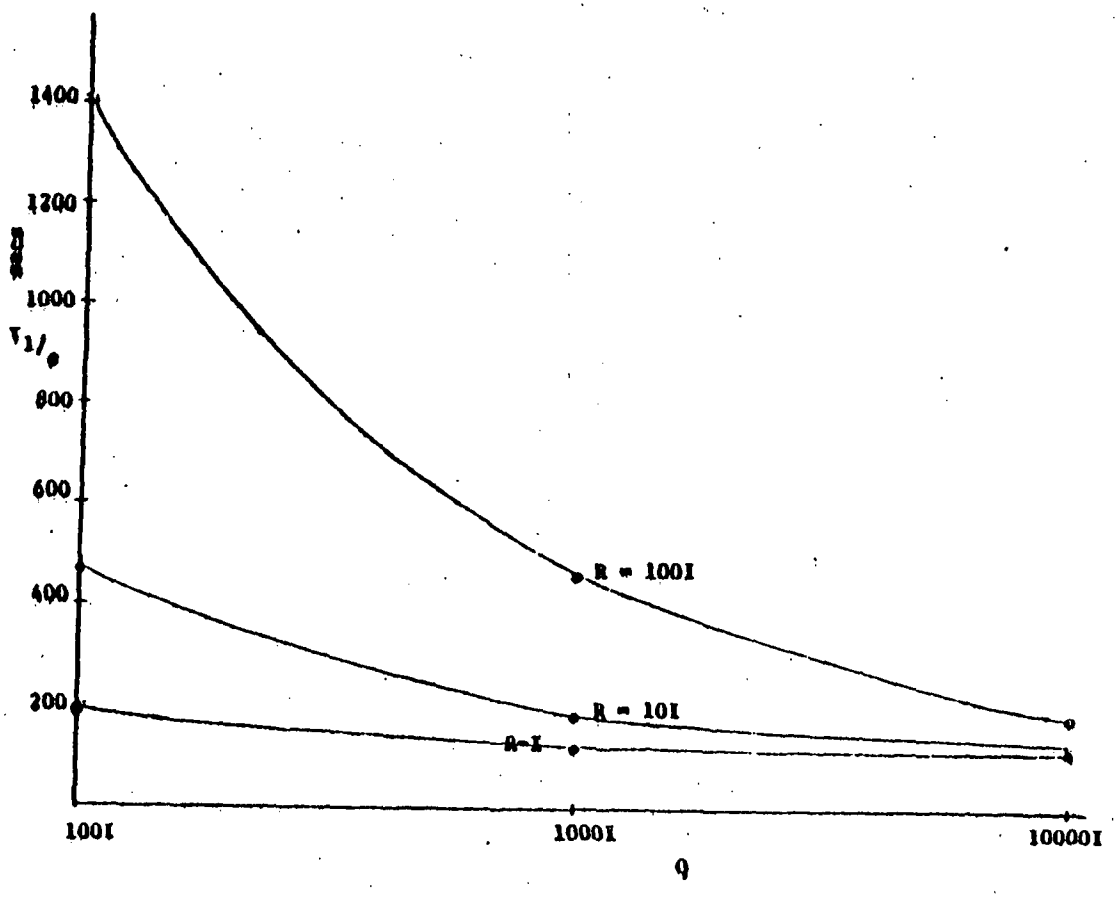

Fig. 4 VARIATION OF THE TIME CONSTANT OF THE LEAST DAMPED MODE WITH Q AND R PENALTY MATRICES

Table 3

Table showing the eigenvalues of the closedloop stochastic system with observation for different state weighting matrices

13 Actuators/ 13 Modes W=0.00001, V=0.0000025

Q=1000I, R=I		Q=10000I, R=I	
(Real) 1/sec	jw(Imaginary)	(Real) 1/sec	jw(Imaginary)
-0.4179	0.4544	-0.5012	0.5193
-0.4179	-0.4544	-0.5012	-0.5193
-1.0058	0.0	-1.0006	0.0
-1.0118	0.0	-1.0011	0.0
-1.0142	0.0	-1.0023	0.0
-1.0248	0.0	-1.0024	0.0
-1.0260	0.0	-1.0082	0.0
-0.7046	0.7785	-1.0086	0.0
-0.7046	-0.7785	-1.0125	0.0
-1.0543	0.0	-1.0142	0.0
-0.6137	0.8688	-1.0544	0.0
-0.6137	-0.8688	-0.6137	0.8688
-0.9666	0.4922	-0.6137	-0.8688
-0.9666	-0.4922	-0.9666	0.4922

Q=1000I, R=I		Q=10000I, R=I	
(Real) 1/sec	jw(Imaginary)	(Real) 1/sec	jw(Imaginary)
-1.0868	0.0	-0.9666	-0.4922
-1.0902	0.0	-1.0902	0.0
-1.0947	0.0	-1.0947	0.0
-1.0987	0.0	-1.1976	0.0
-1.1360	0.4403	-1.1360	0.4403
-1.1360	-0.4403	-1.1360	-0.4403
-1.2914	0.0	-1.3041	0.0
-1.1849	0.6481	-1.3257	0.0
-1.1849	-0.6481	-1.1849	0.6481
-1.5807	0.0	-1.1849	-0.6481
-1.0950	1.4745	-1.0950	1.4745
-1.0950	-1.4745	-1.0950	-1.4745
-2.5134	0.0	-2.5134	0.0
-2.5688	0.0	-2.5688	0.0
-2.1916	1.6704	-2.6843	0.0
-2.1916	-1.6704	-1.1000	2.6437
-1.0244	2.7961	-1.1000	-2.6437
-1.0244	-2.7961	-3.2607	0.0
-3.2607	0.0	-0.0575	3.3319
-0.0575	3.3319	-0.0575	-3.3319
-0.0575	-3.3319	-0.5617	4.4959
-3.9913	0.0	-0.5617	-4.4959
-3.6151	1.7994	-0.9201	5.4912
-3.6151	-1.7994	-0.9201	-5.4912

Q=1000I, R=I		Q=10000I, R=I	
(Real) 1/sec	jw(Imaginary)	(Real) 1/sec	jw(Imaginary)
-0.5617	4.4959	-0.0091	5.5905
-0.5617	-4.4959	-0.0091	-5.5905
-5.4764	0.0	-0.5935	5.7365
-0.9201	5.4911	-0.5935	-5.7365
-0.9201	-5.4911	-6.3792	0.0
-0.0078	5 .5905	-8.7613	0.0
-0.0078	-5.5905	-9.2251	0.0
-0.5935	5.7365	-12.6541	0.0
-0.5935	-5.7365	-13.1993	0.0
-6.2697	0.0	-19.0026	0.0
-9.2251	0.0	-27.1591	0.0
-10.0084	0.0	-32.9847	0.0
-12.4055	0.0	-40.2118	0.0
-30.1863	0.0	-98.5507	0.0

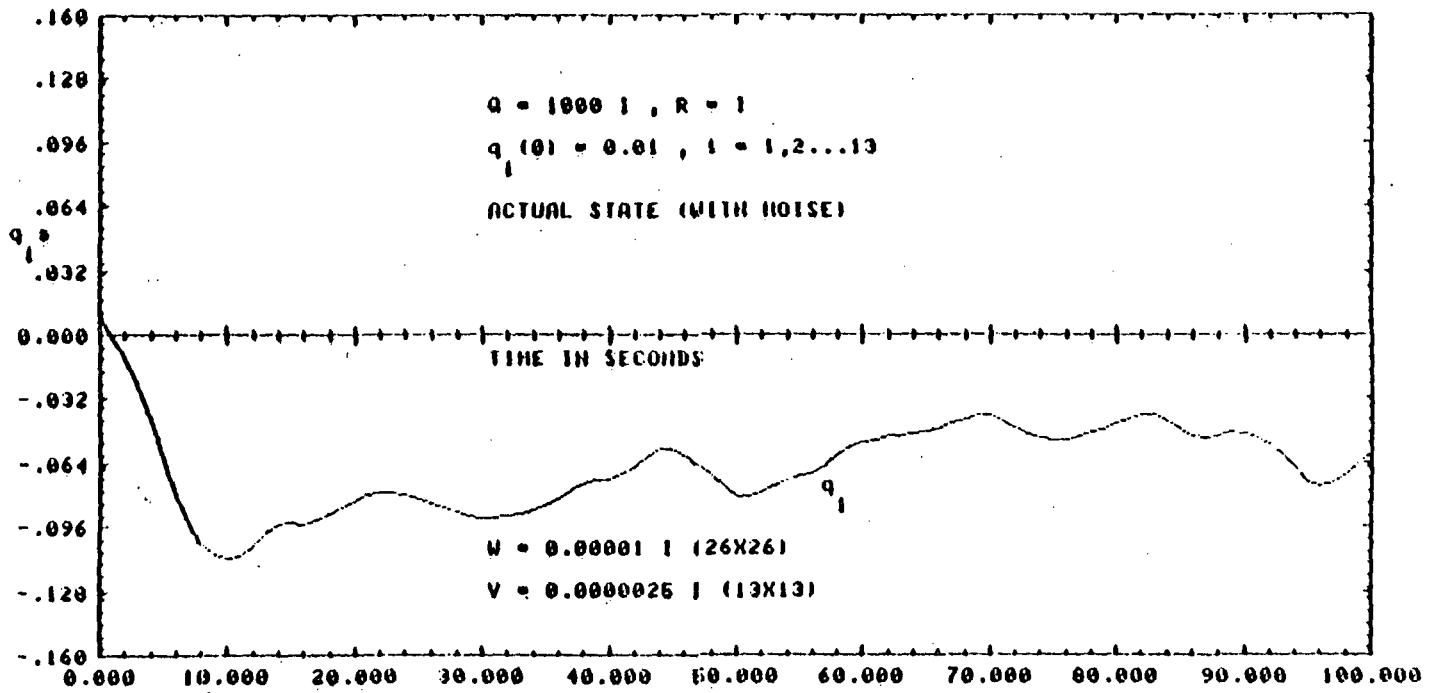

Fig. 5a Transient Response for 100 secs - Hoop / Column Antenna System

13 Actuators / 13 Sensors / 13 Modes - Actual State with Noise

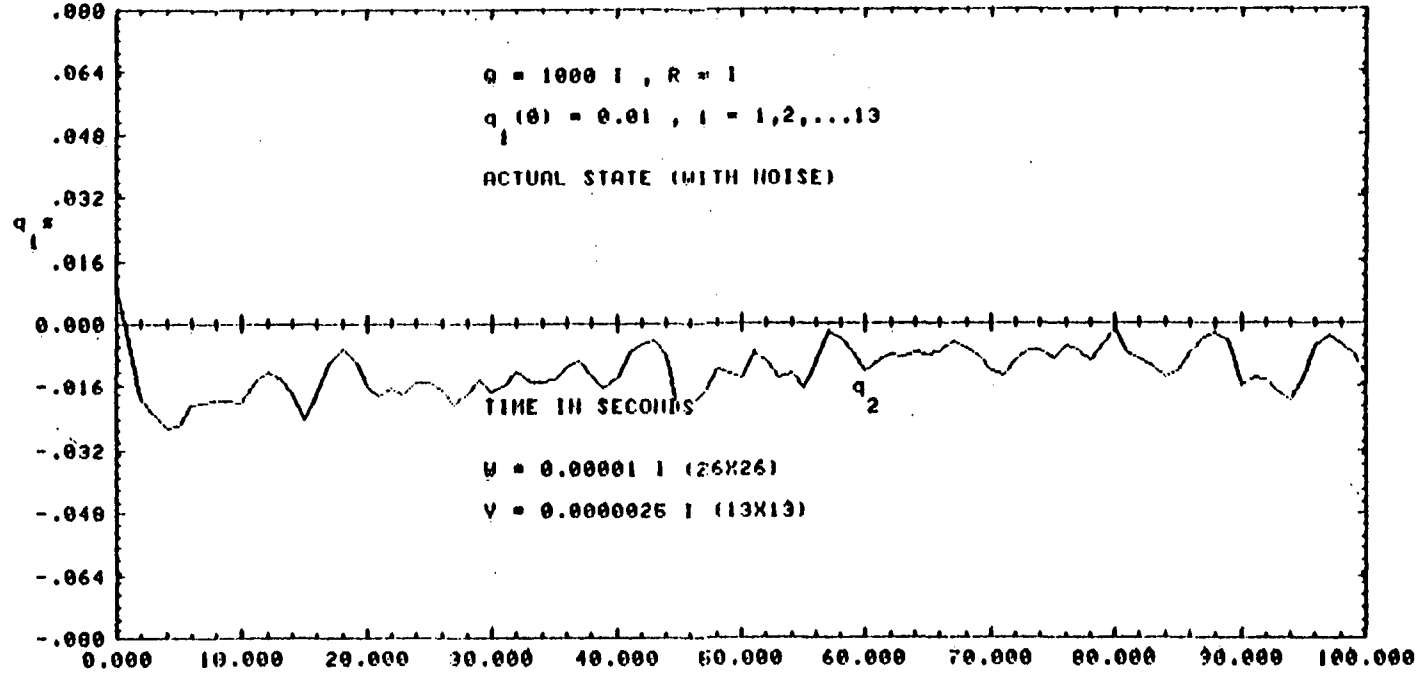

Fig. 5b Transient Response for 100 secs - Hoop / Column Antenna System

13 Actuators / 13 Sensors / 13 Modes - Actual State with Noise

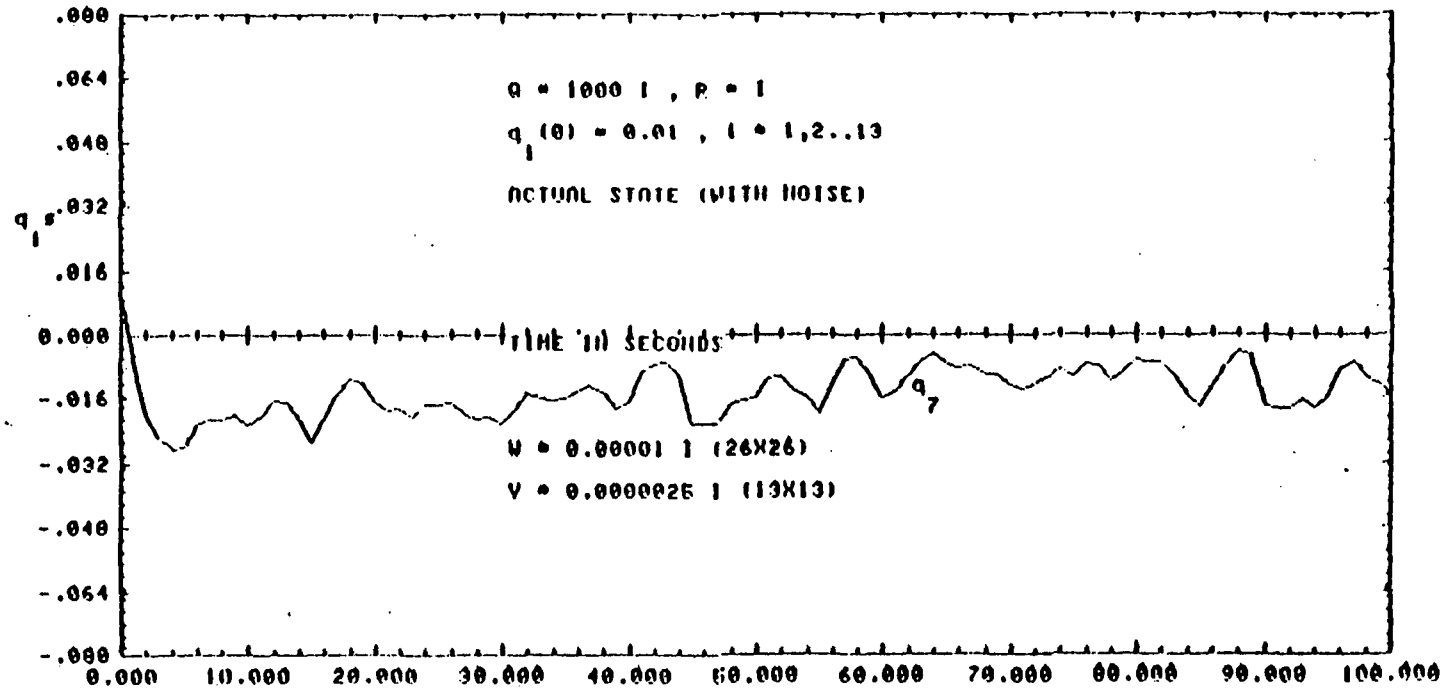

Fig. 5c Transient Response for 100 secs - Hoop / Column Antenna System

13 Actuators / 13 Sensors / 13 Modes - Actual State with Noise

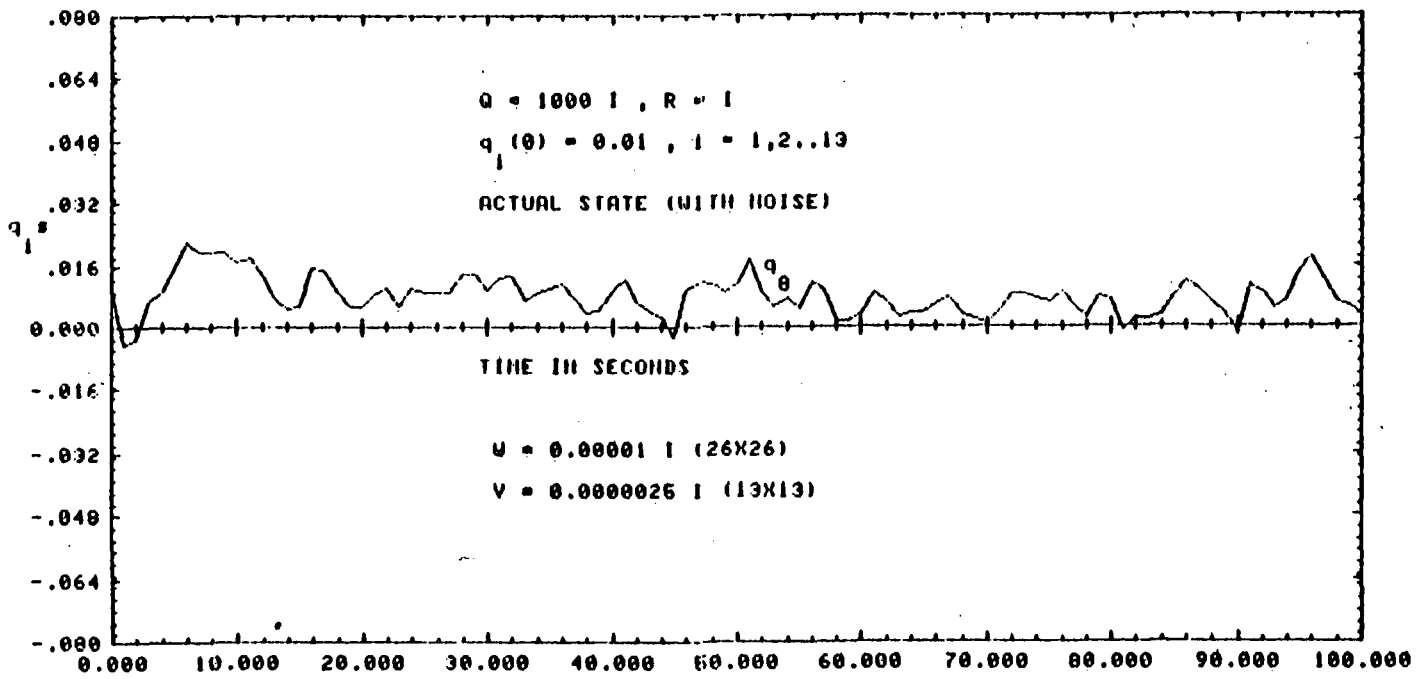

Fig. 5d Transient Response for 100 secs - Hoop / Column Antenna System

13 Actuators / 13 Sensors / 13 Modes - Actual State with Noise

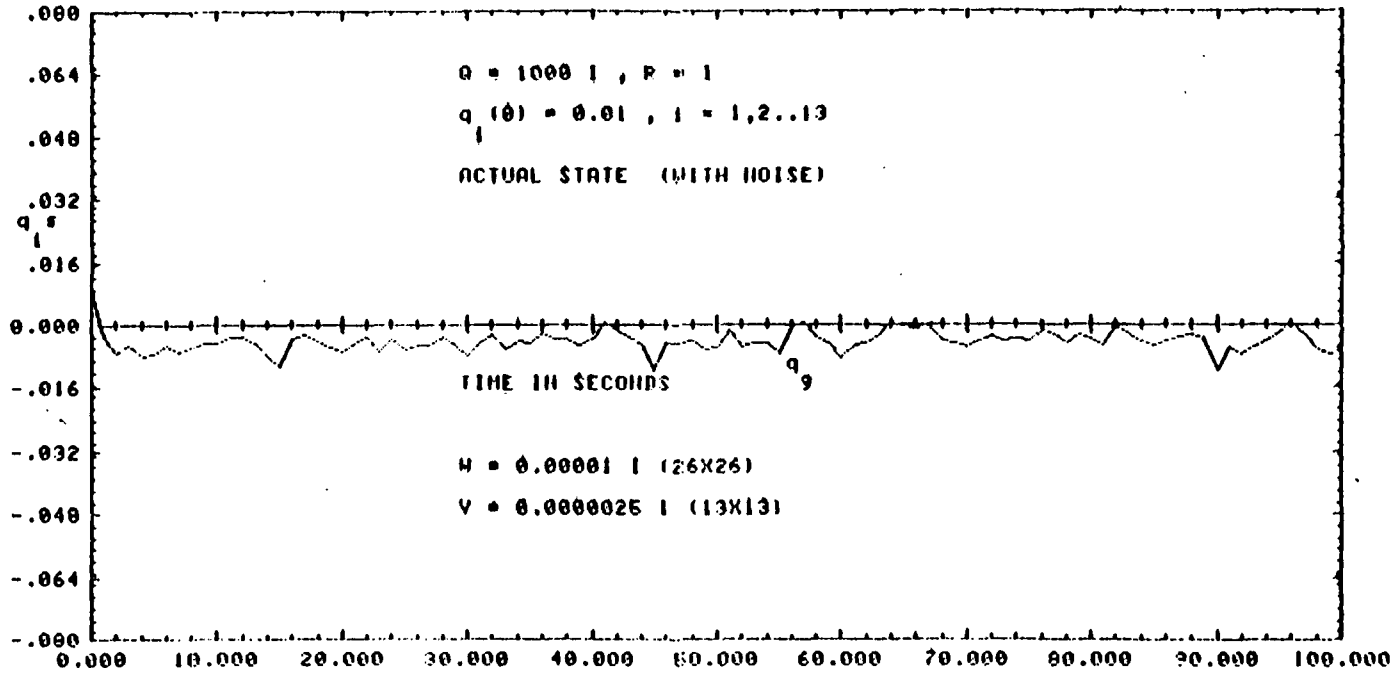

Fig. 5e Transient Response for 100 secs - Hoop / Column Antenna System

13 Actuators / 13 Sensors / 13 Modes - Actual State with Noise

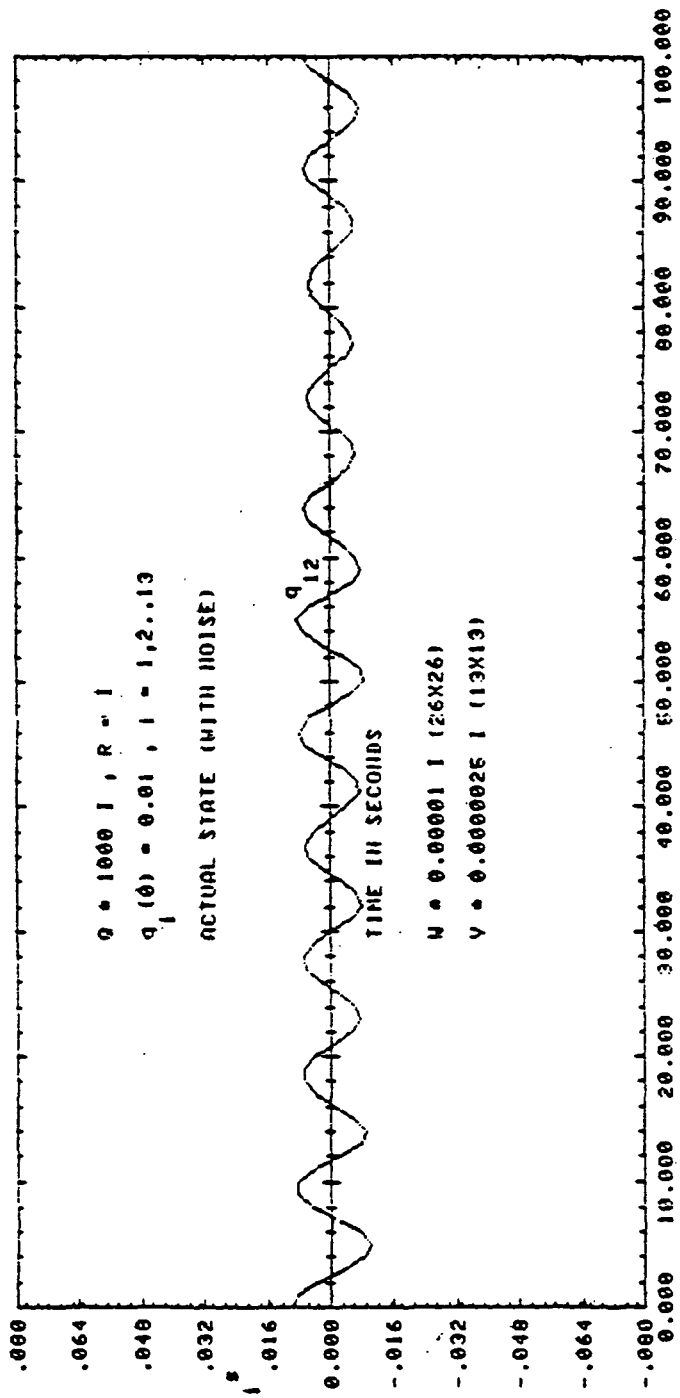

Fig. 5f Transient Response for 100 secs - Hoop / Column Antenna System

13 Actuators / 13 Sensors / 13 Modes - Actual State with Noise

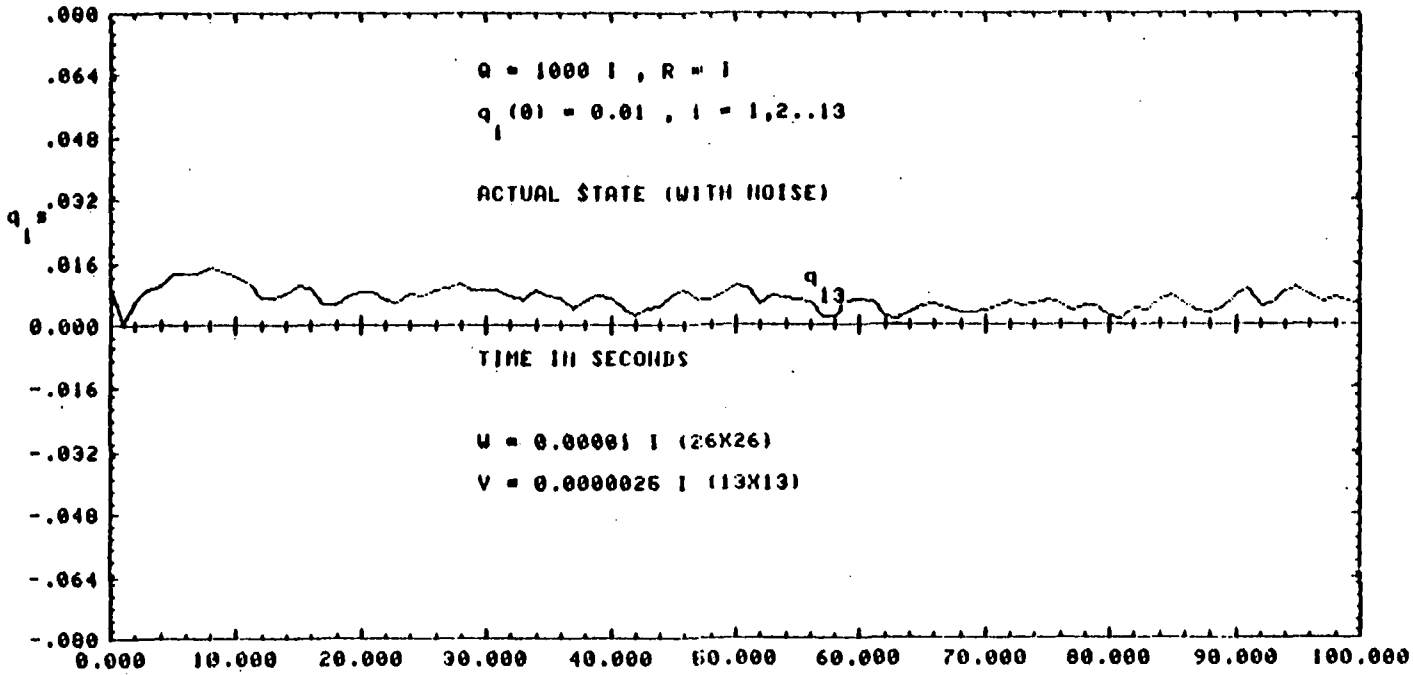

Fig. 5g Transient Response for 100 secs - Hoop / Column Antenna System

13 Actuators / 13 Sensors / 13 Modes - Actual State with Noise

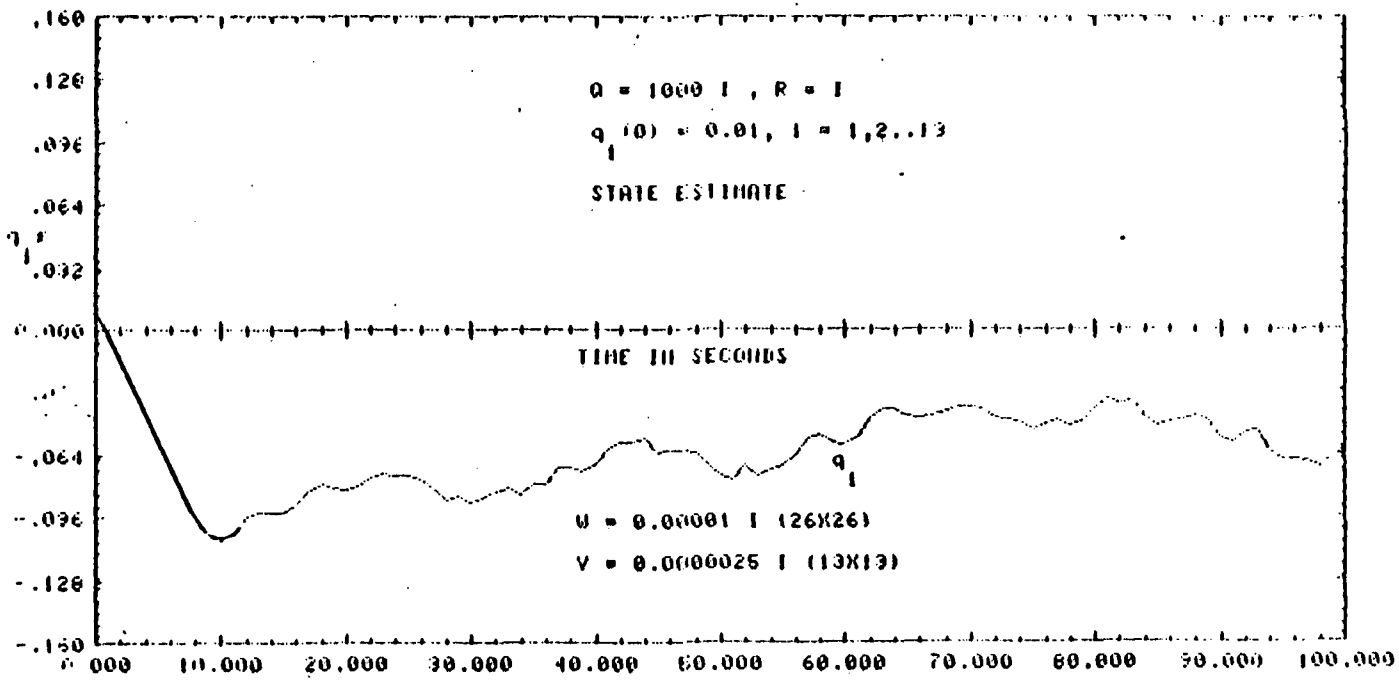

Fig. 6a Transient Response for 100 secs - Hoop / Column Antenna System 13 Actuators / 13 Sensors / 13 Modes - State Estimate with Nominal Weights on State and Control

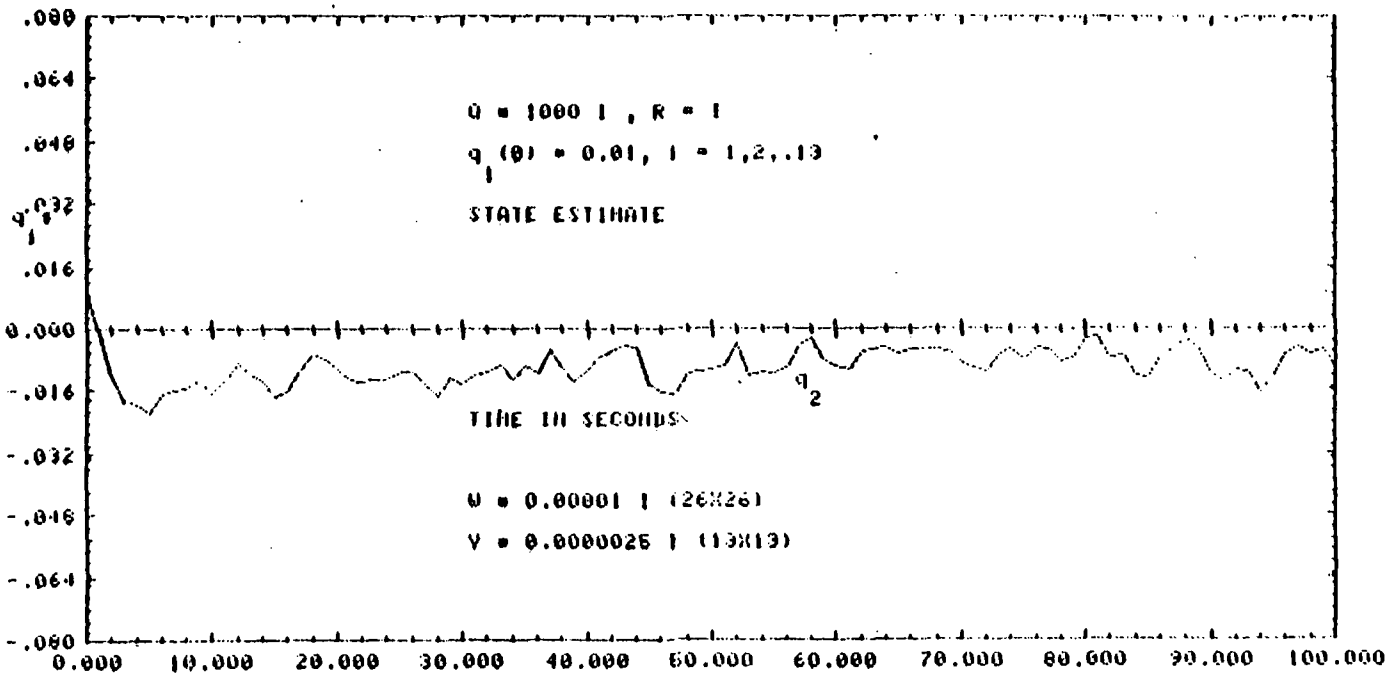

Fig. 6b Transient Response for 100 secs - Hoop / Column Antenna System

13 Actuators / 13 Sensors / 13 Modes - State Estimate with

Nominal Weights on State and Control

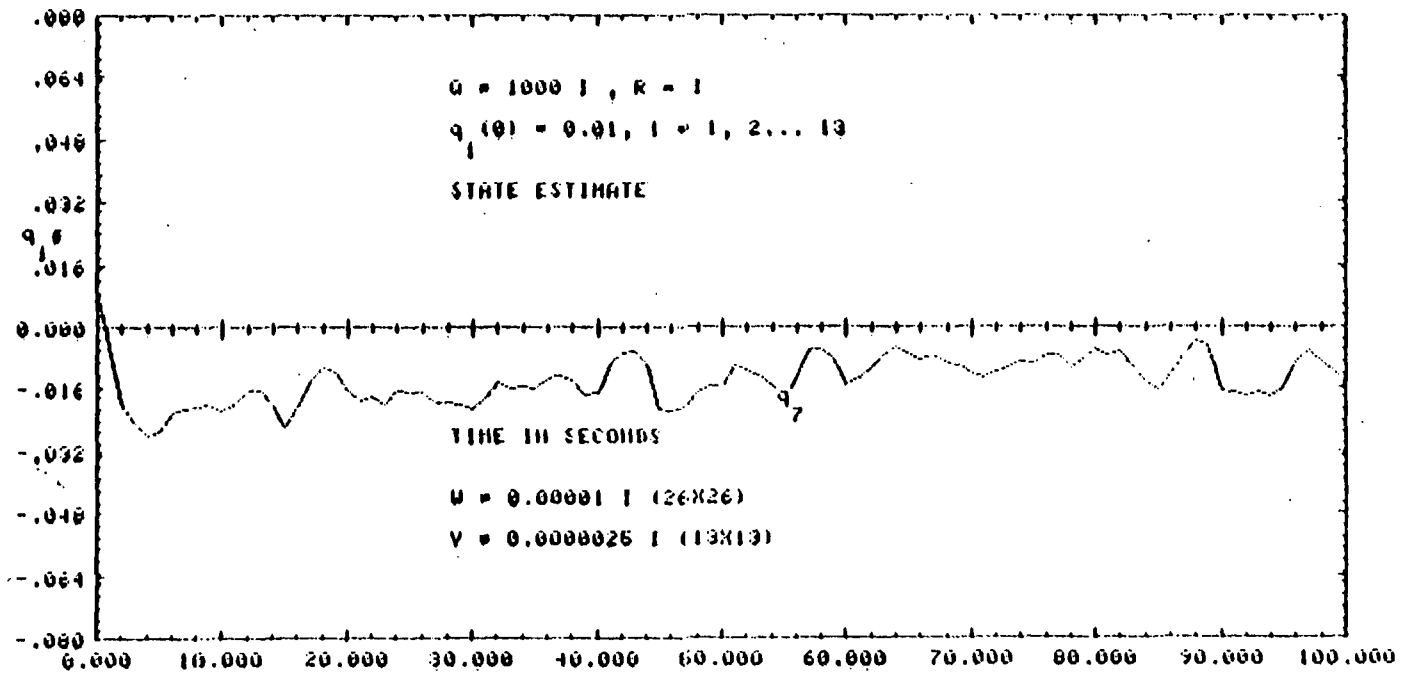

Fig. 6c Transient Response for 100 secs - Hoop / Column Antenna System 13 Actuators / 13 Sensors / 13 Modes - State Estimate with Nominal Weights on State and Control

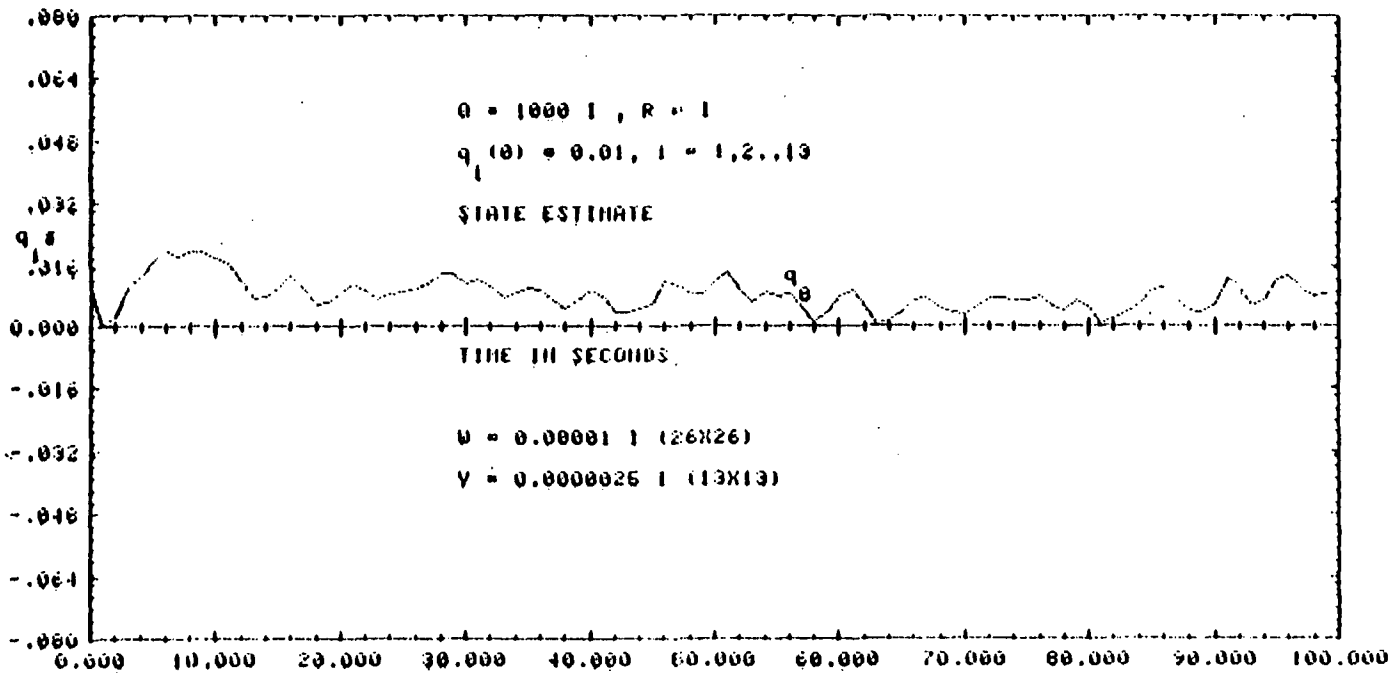

Fig. 6d Transient Response for 100 secs - Hoop / Column Antenna System 13 Actuators / 13 Sensors / 13 Modes - State Estimate with Nominal Weights on State and Control

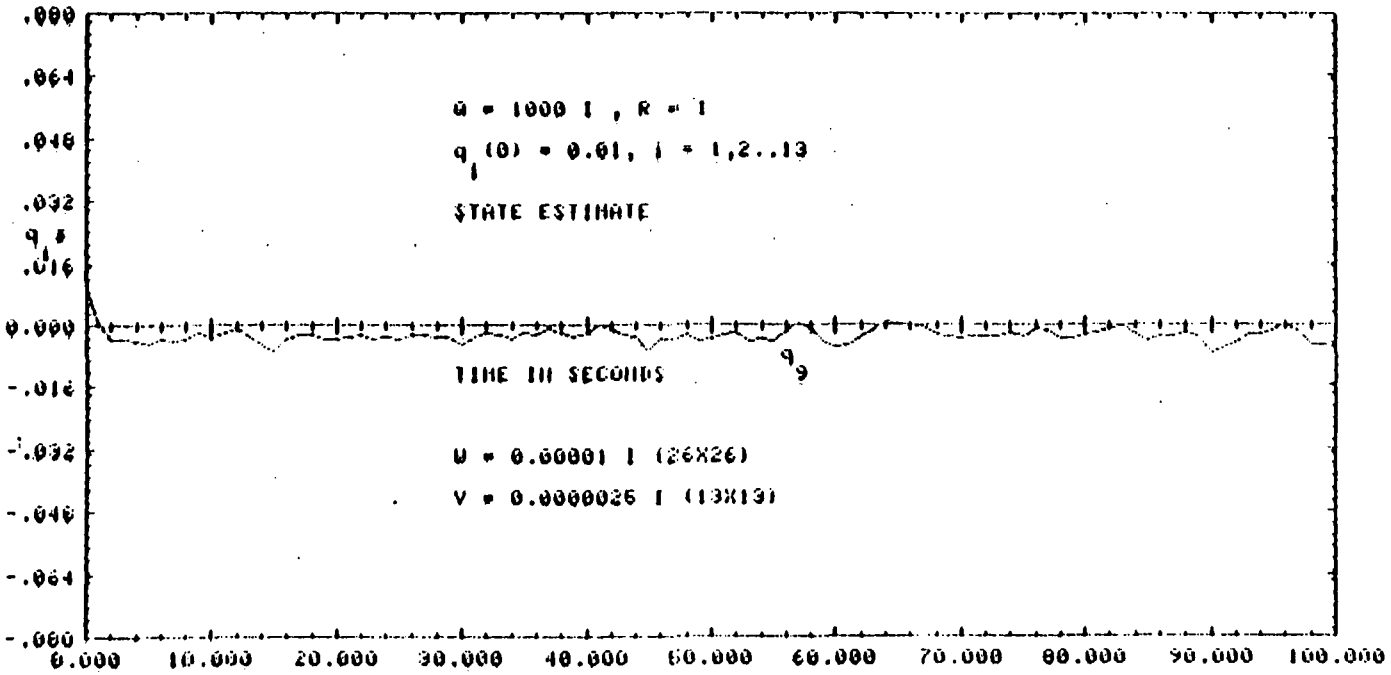

Fig. 6e Transient Response for 100 secs - Hoop / Column Antenna System 13 Actuators / 13 Sensors / 13 Modes - State Estimate with Nominal Weights on State and Control

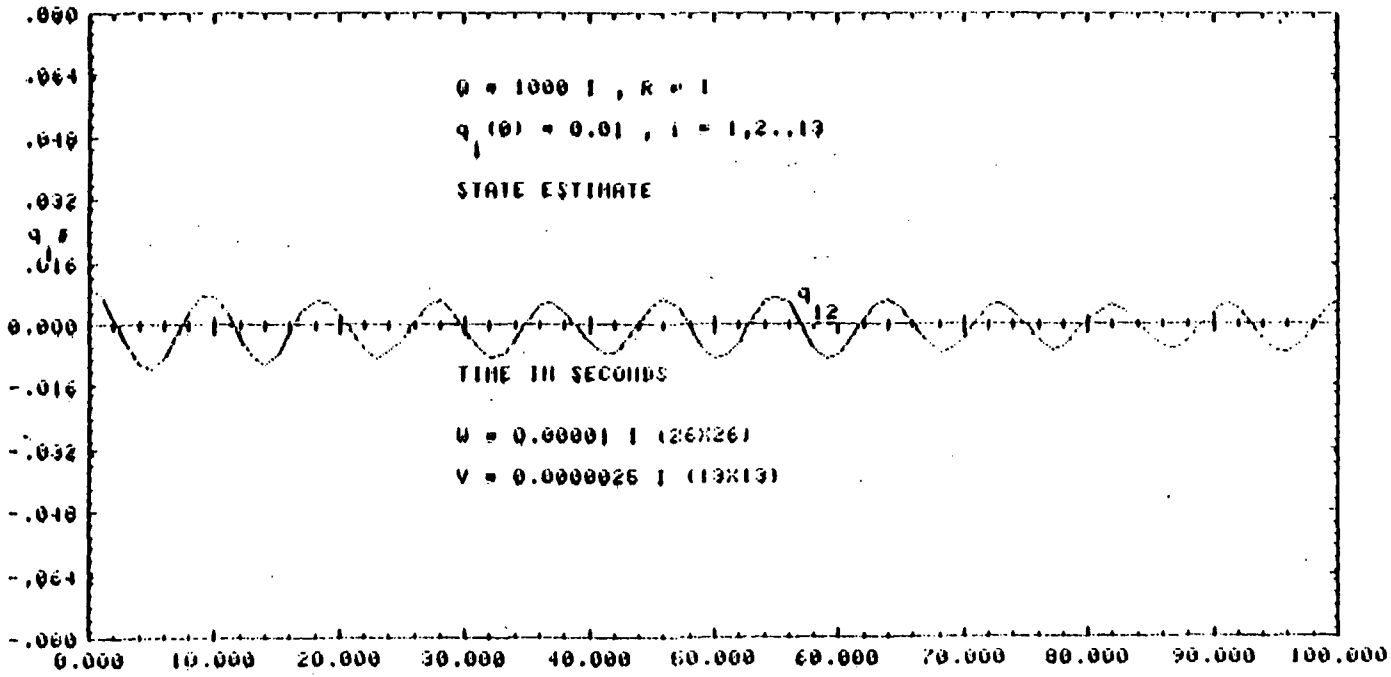

Fig. 6f Transient Response for 100 secs - Hoop / Column Antenna System
13 Actuators / 13 Sensors / 13 Modes - State Estimate with
Nominal Weights on State and Control

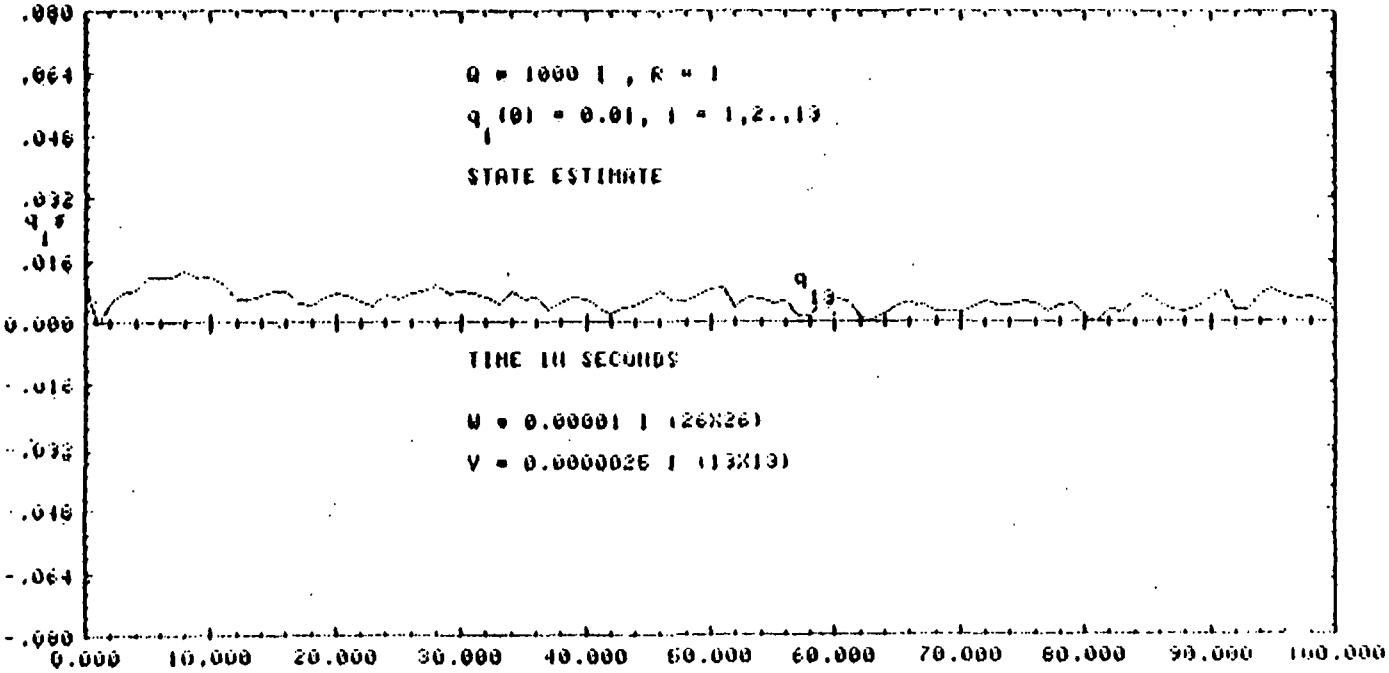

Fig. 6g Transient Response for 100 secs - Hoop / Column Antenna System 13 Actuators / 13 Sensors / 13 Modes - State Estimate with Nominal Weights on State and Control

Table 4

Comparison of maximum actuator force amplitudes

$Q = 1000I$, $R = I$, $q_i(0) = 0.01$, $i = 1, 2 \ldots, 13$. 13 Actuators/ 13 Modes

Maximum actuator force amplitudes (pounds)	Actual State with Noise	Stochastic case W = 0.00001 V = 0.00000.25
f_1	0.3500	0.3330
f_2	0.0569	0.0570
f_3	0.3030	0.2681
f_4	0.0569	0.0570
f_5	1.3000	1.3028
f_6	0.2830	0.2865
f_7	1.2700	1.2310
f_8 (in-lb)	0.0124	0.0140
f_9	0.2360	0.2859
f_{10}	0.1570	0.1574
f_{11}	0.4060	0.4086
f_{12}	0.3520	0.3521
f_{13}	0.0688	0.0660

the estimate of the state closely follows the actual system dynamics thus ensuring a satisfactory estimation process. The assumed initial displacements of 0.01 in the modal coordinates correspond to the expected maximum perturbations in the linear range from the nominal operating required RMS displacements, obtained through calculation of equation (3).

Figs. (6a-6c) and Figs. (7a-7c) together with Table 5 show that increasing the elements of the state weighting matrix increases the control effort required by an order of magnitude, but does not cause a significant improvement in the transient response. [But, it was found in the deterministic case that increasing the elements of the state weighting matrices causesa significant improvement in the transient response (Ref. 3).] Other results (not shown) in which only some of the state weighting elements are inceased, also indicate that this technique of increasing the elements of the state weighting matrix will not result in a marked improvement.

A separate study was conducted to determine the effect of varying the plant and sensor noise characteristics for a fixed set of penalty matrices. In Fig. 8 the measurement noise co-variance has been increased to 0.00025, while the plant noise has been reduced to 0.0000001 (both changes involve two orders of magnitude), as compared with Figs. (6a-6c). For comparison purposes only a few of the modes are depicted in Fig. 8. It can be seen that a great improvement in transient performance is realized, with the same order of control effort (Table 6). Increasing the elements of the control weighting matrix along with the sensor noise for the same weighting matrix is also found to bring about a significant improvement in the transient response as could be seen from a comparison of Figs. (6a-6c) with Fig. 9.

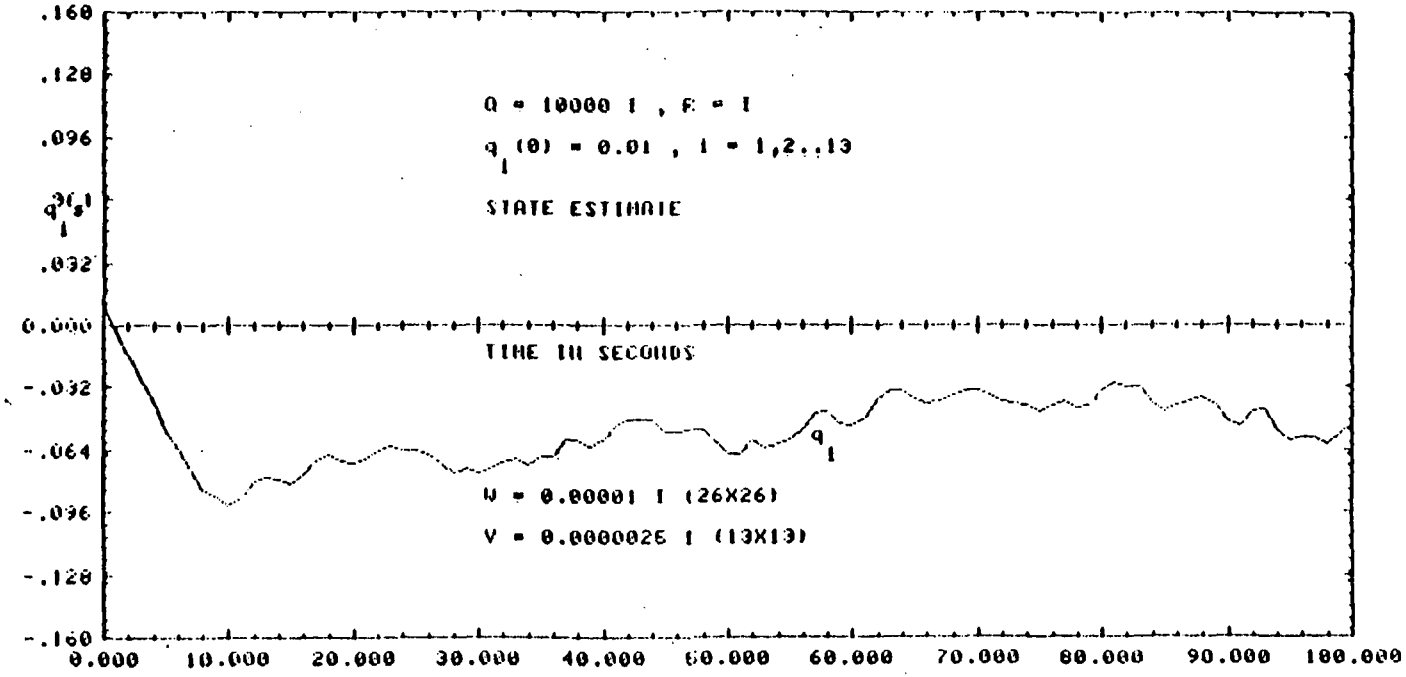

Fig. 7a Transient Response for 100 secs - Hoop / Column Antenna System 13 Actuators / 13 Sensors / 13 Modes - State Estimate with Increased Penalty on the State

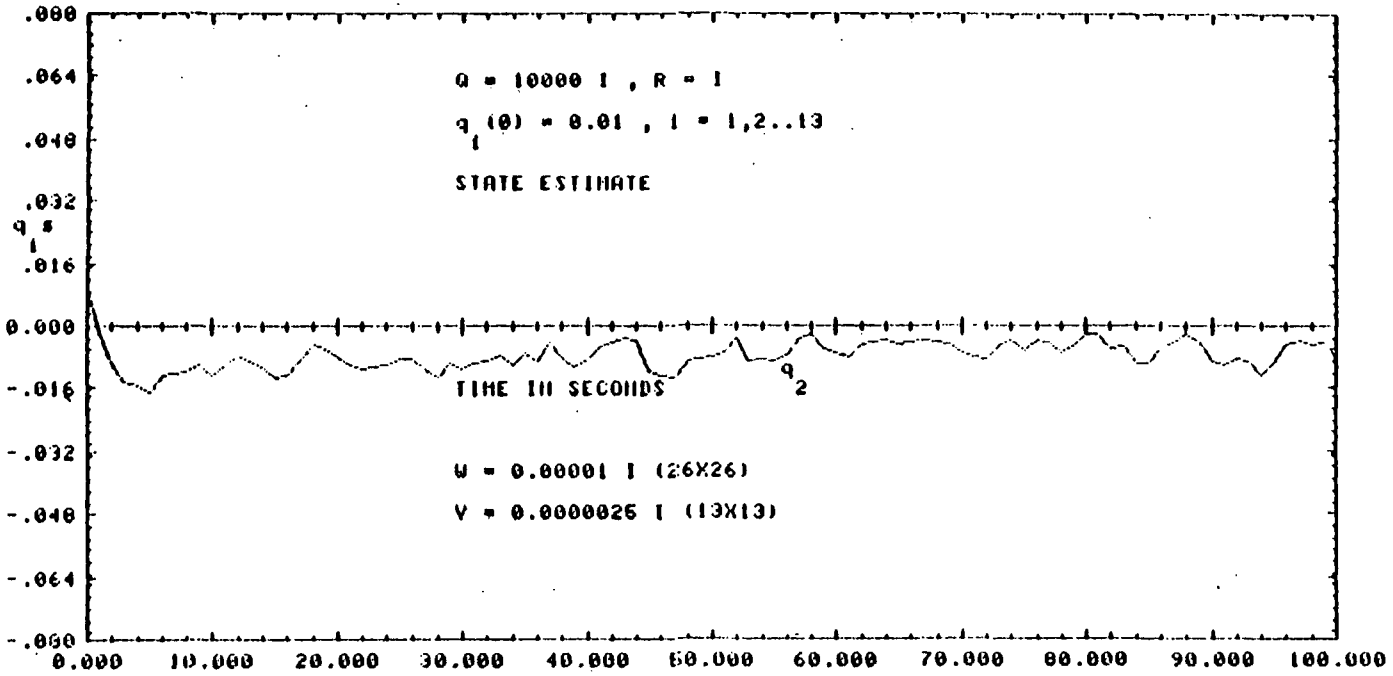

Fig. 7b Transient Response for 100 secs - Hoop / Column Antenna System 13 Actuators / 13 Sensors / 13 Modes - State Estimate with Increased Penalty on the State

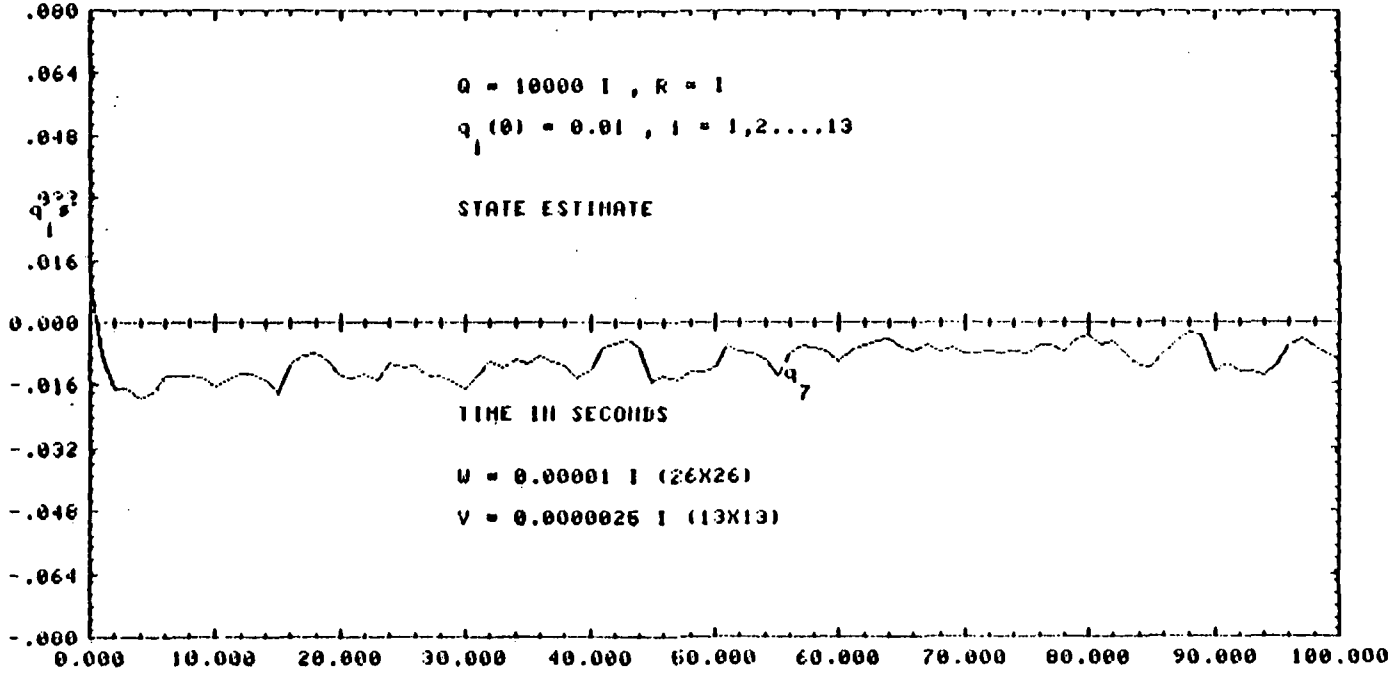

Fig. 7c Transient Response for 100 secs - Hoop / Column Antenna System

13 Actuators / 13 Sensors / 13 Modes - State Estimate with

Increased Penalty on the State

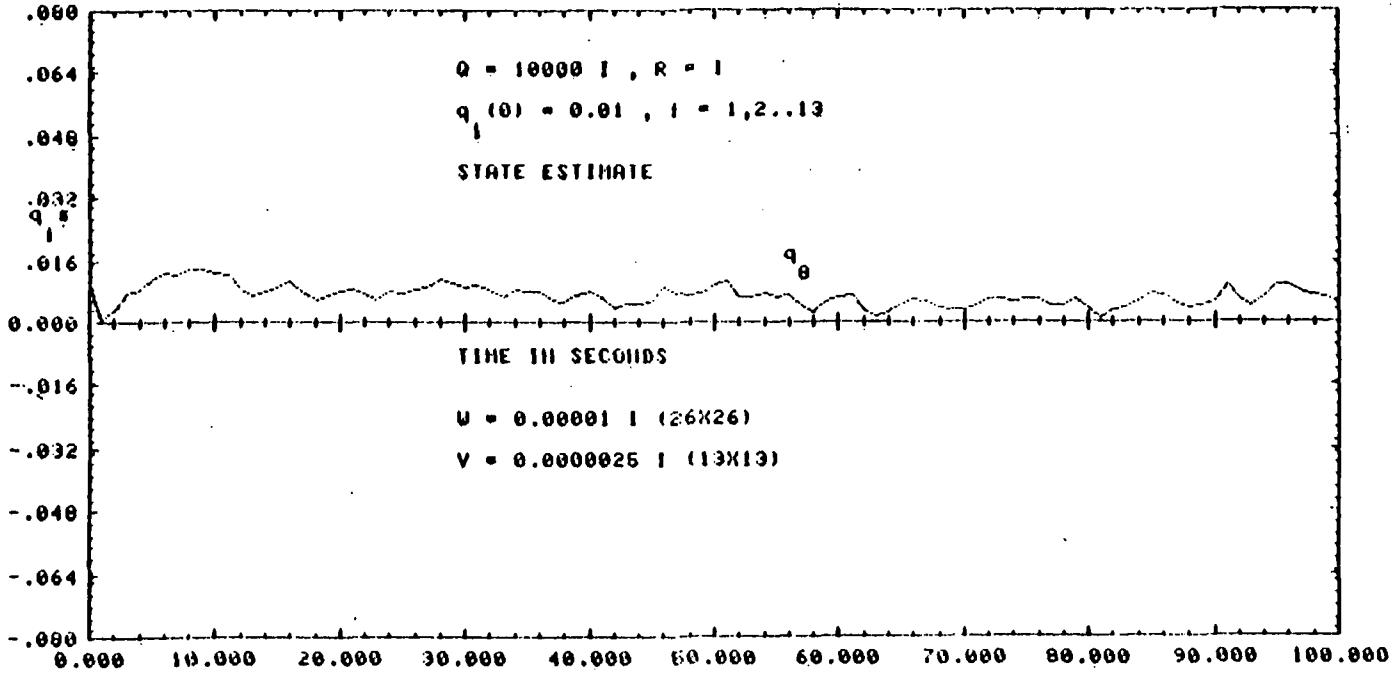

Fig. 7d Transient Response for 100 secs - Hoop / Column Antenna System 13 Actuators / 13 Sensors / 13 Modes - State Estimate with Increased Penalty on the State

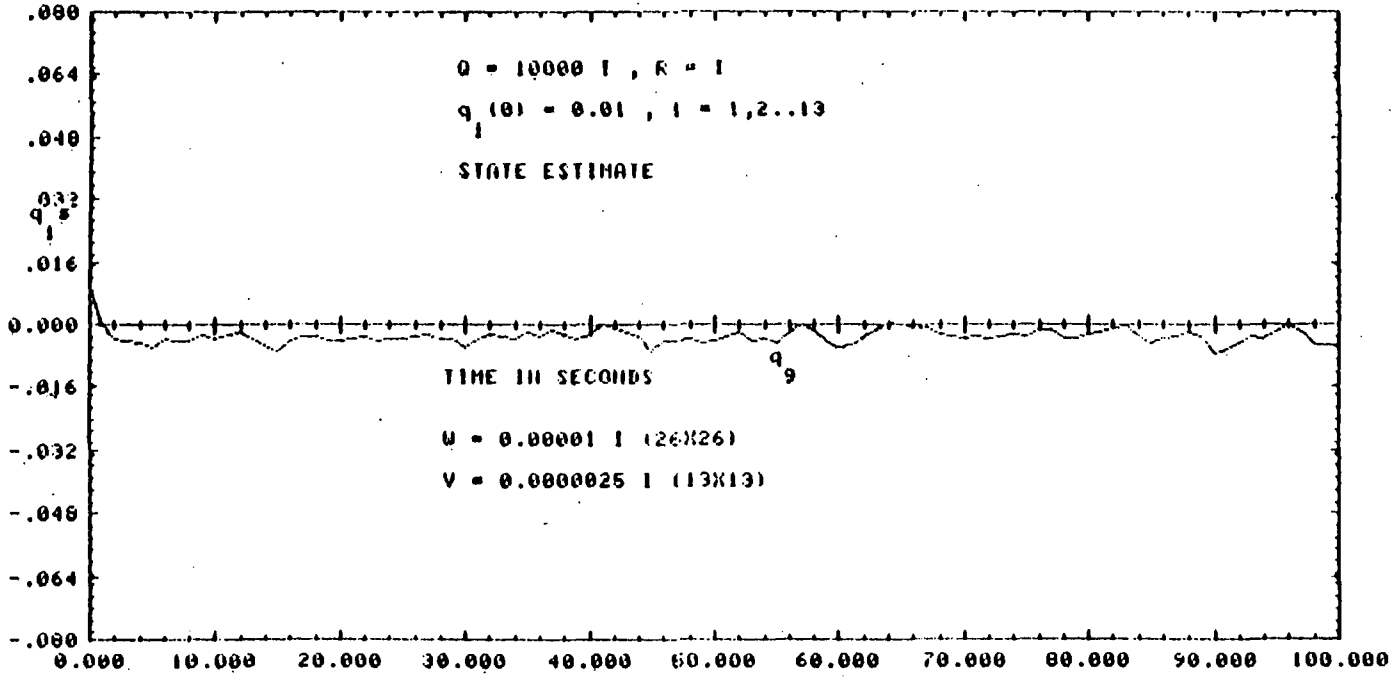

Fig. 7e Transient Response for 100 secs - Hoop / Column Antenna System 13 Actuators / 13 Sensors / 13 Modes - State Estimate with Increased Penalty on the State

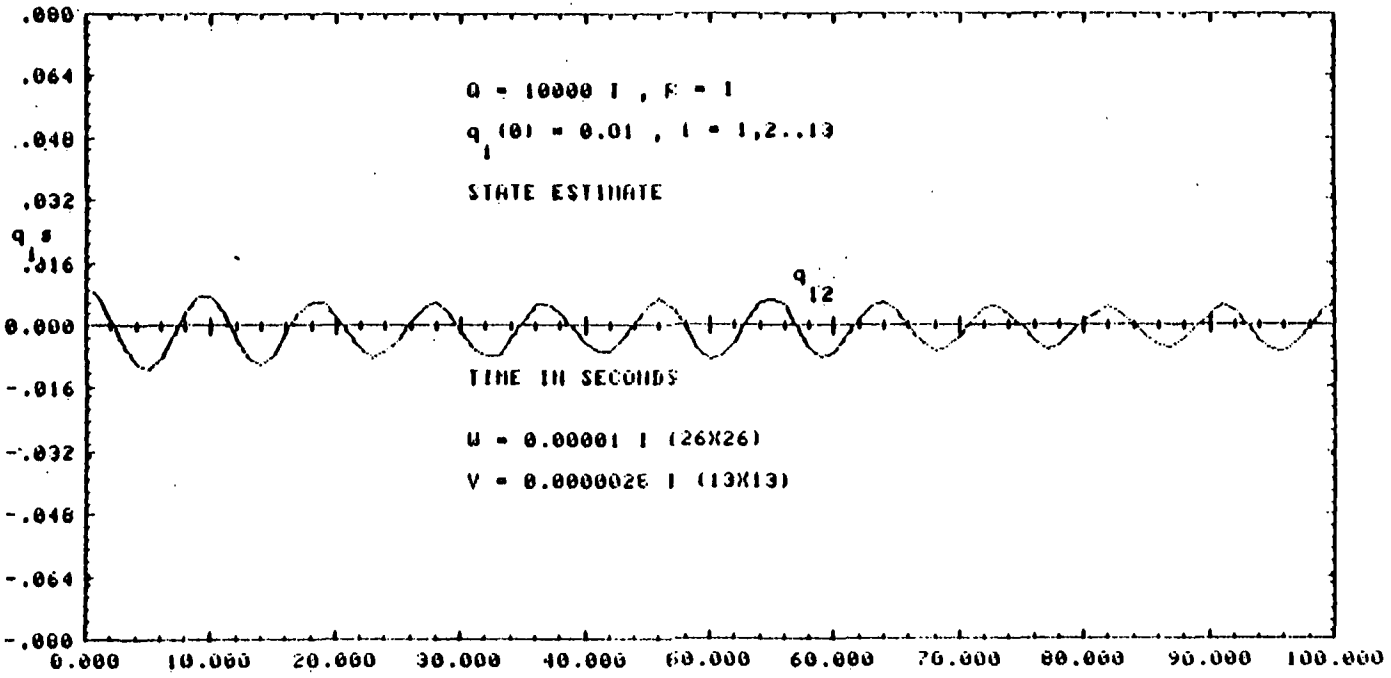

Fig. 7f Transient Response for 100 secs - Hoop / Column Antenna System 13 Actuators / 13 Sensors / 13 Modes - State Estimate with Increased Penalty on the State

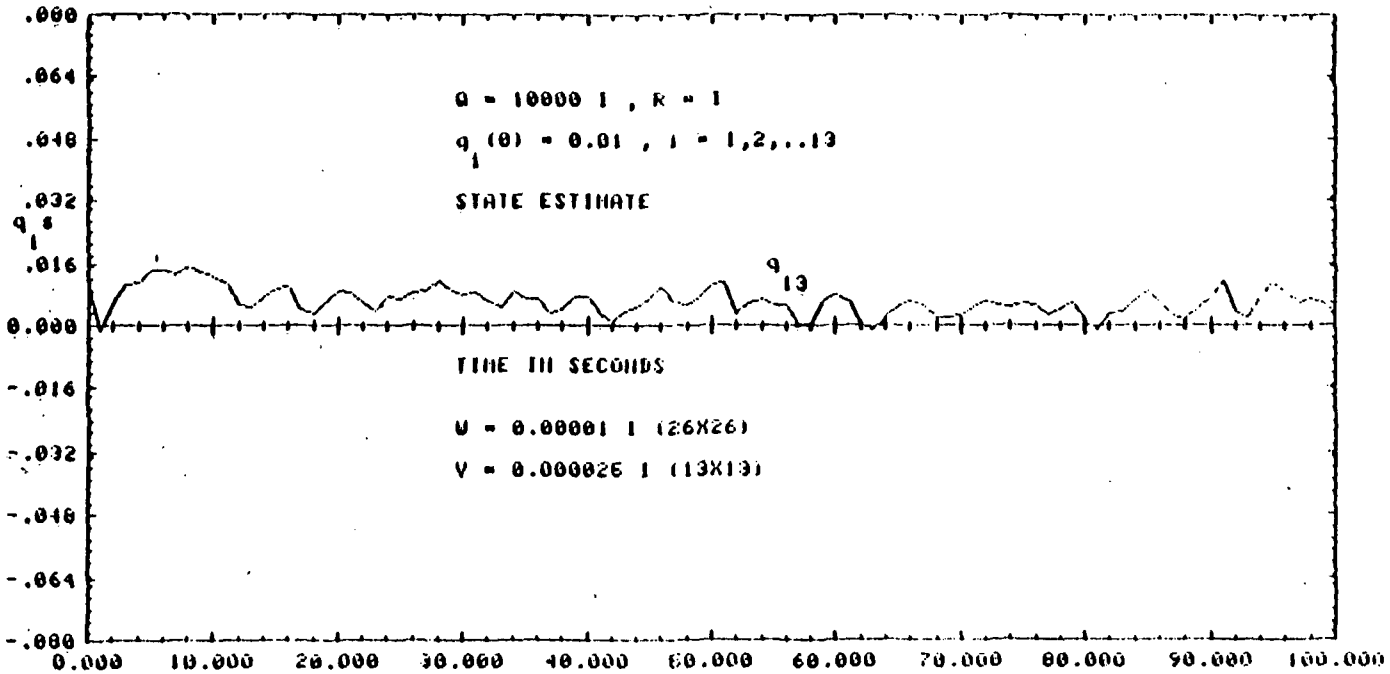

Fig. 7g Transient Response for 100 secs - Hoop / Column Antenna System 13 Actuators / 13 Sensors / 13 Modes - State Estimate with Increased Penalty on the State

Table 5

Comparison of maximum actuator force amplitudes

$q_i(0)=0.01$, $i=1,2\ldots,13$. 13 Actuators/ 13 Modes

Maximum actuator force amplitudes (pounds)	Stochastic case W=0.00001 V=0.000025 Q=1000I R=I Fig.6	Q=10000I R= I Fig.7
f_1	0.3330	1.5759
f_2	0.0570	0.1915
f_3	0.2681	1.4151
f_4	0.0570	0.1915
f_5	1.3028	3.6022
f_6	0.2865	0.8400
f_7	1.2310	3.0046
f_8 (in-lb)	0.0140	0.1184
f_9	0.2859	0.8483
f_{10}	0.1574	0.6483
f_{11}	0.4086	1.3481
f_{12}	0.3521	0.9442
f_{13}	0.0660	0.2342

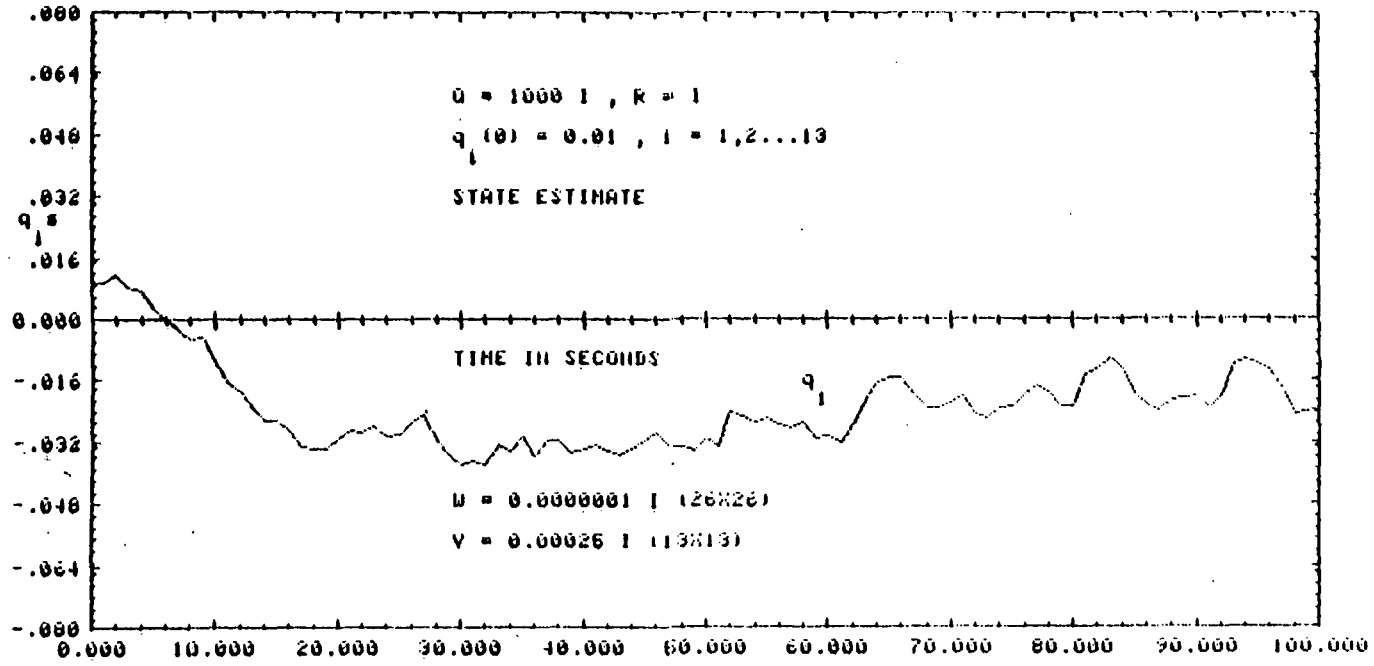

Fig. 8a Transient Response for 100 secs - Hoop / Column Antenna System 13 Actuators / 13 Sensors / 13 Modes - State Estimate, Effect of Changing Noise Parameters

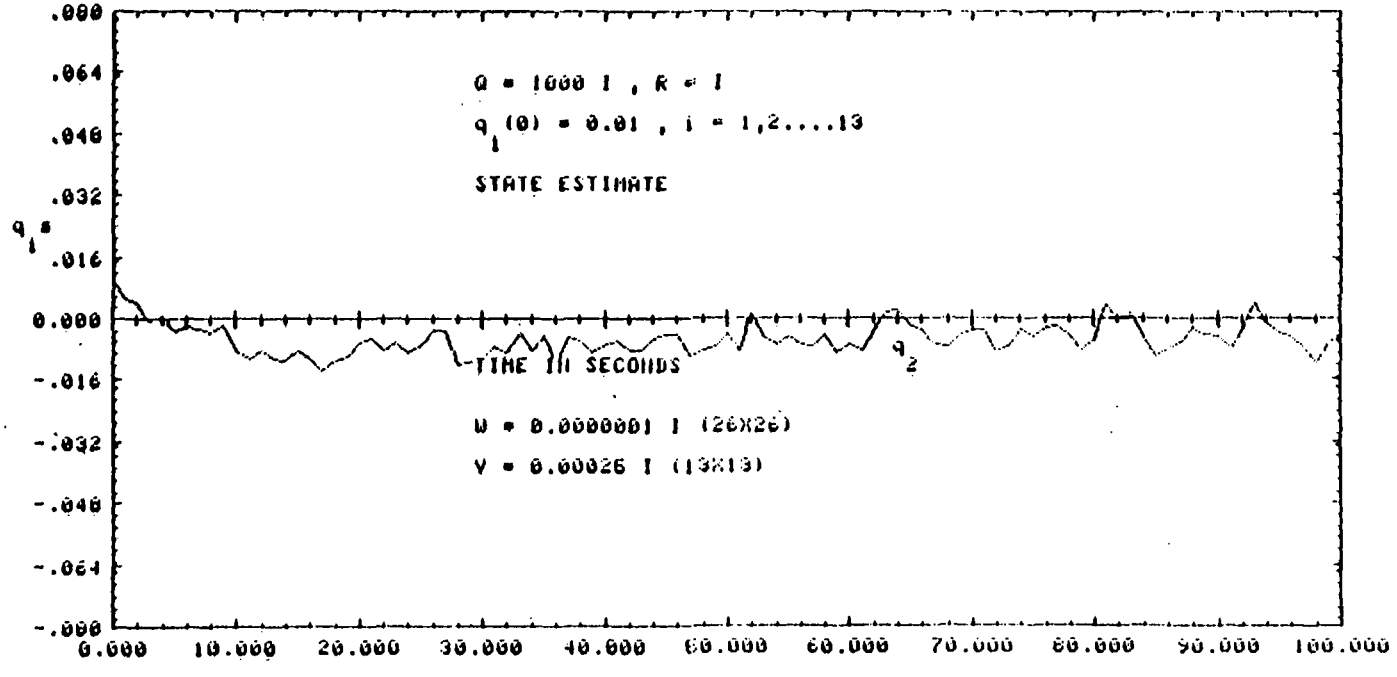

Fig. 8b Transient Response for 100 secs - Hoop / Column Antenna System 13 Actuators / 13 Sensors / 13 Modes - State Estimate, Effect of Changing Noise Parameters

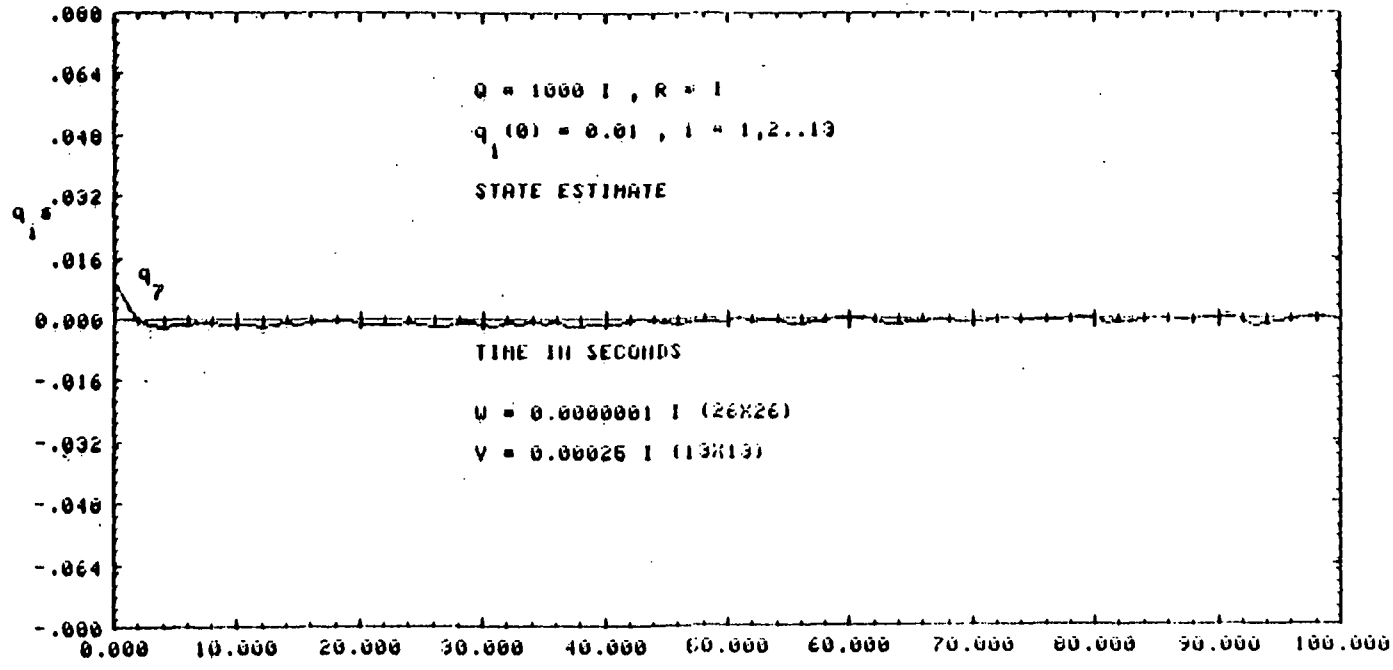

Fig. 8c Transient Response for 100 secs - Hoop / Column Antenna System 13 Actuators / 13 Sensors / 13 Modes - State Estimate, Effect of Changing Noise Parameters

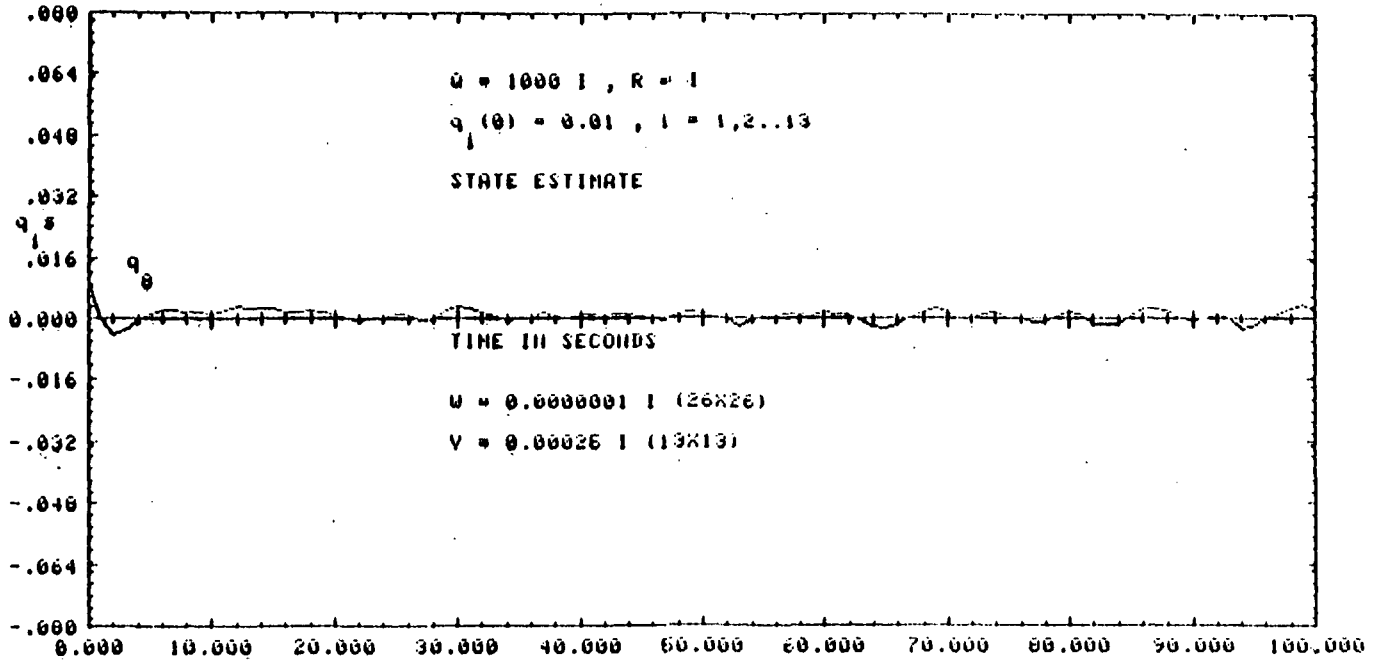

Fig. 8d Transient Response for 100 secs - Hoop / Column Antenna System 13 Actuators / 13 Sensors / 13 Modes - State Estimate, Effect of Changing Noise Parameters

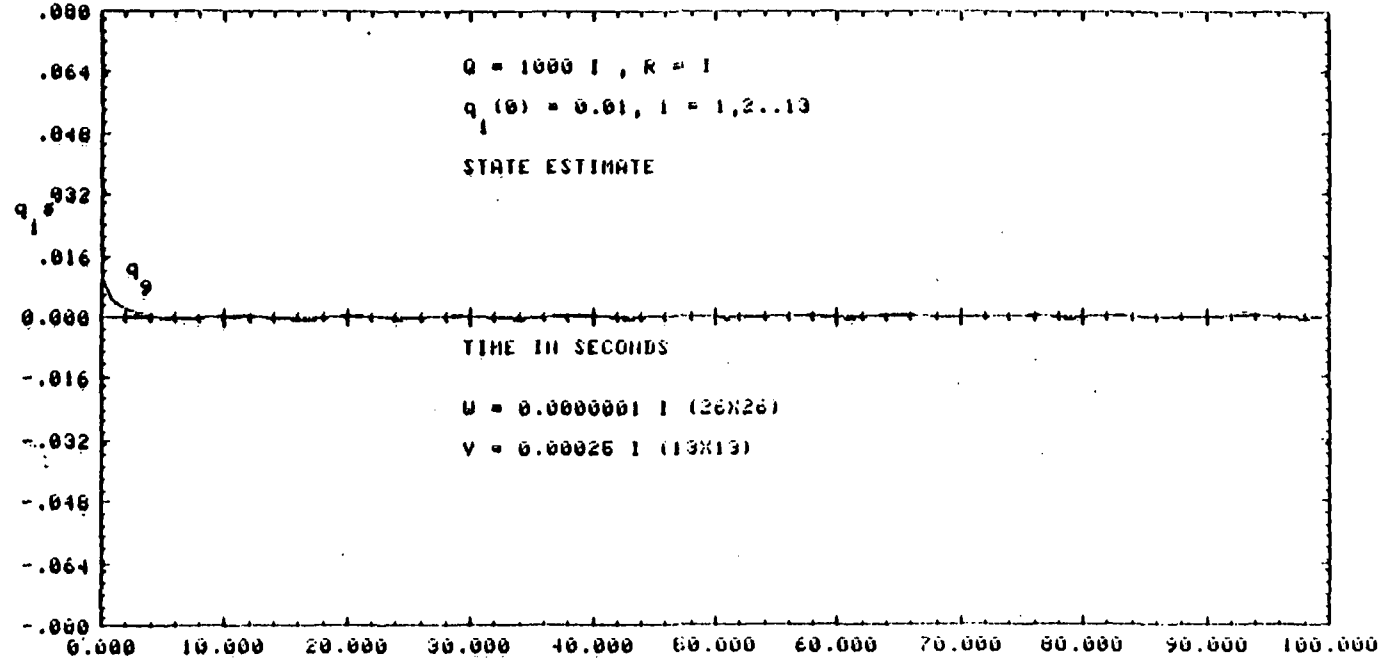

Fig. 8e Transient Response for 100 secs - Hoop / Column Antenna System 13 Actuators / 13 Sensors / 13 Modes - State Estimate, Effect of Changing Noise Parameters

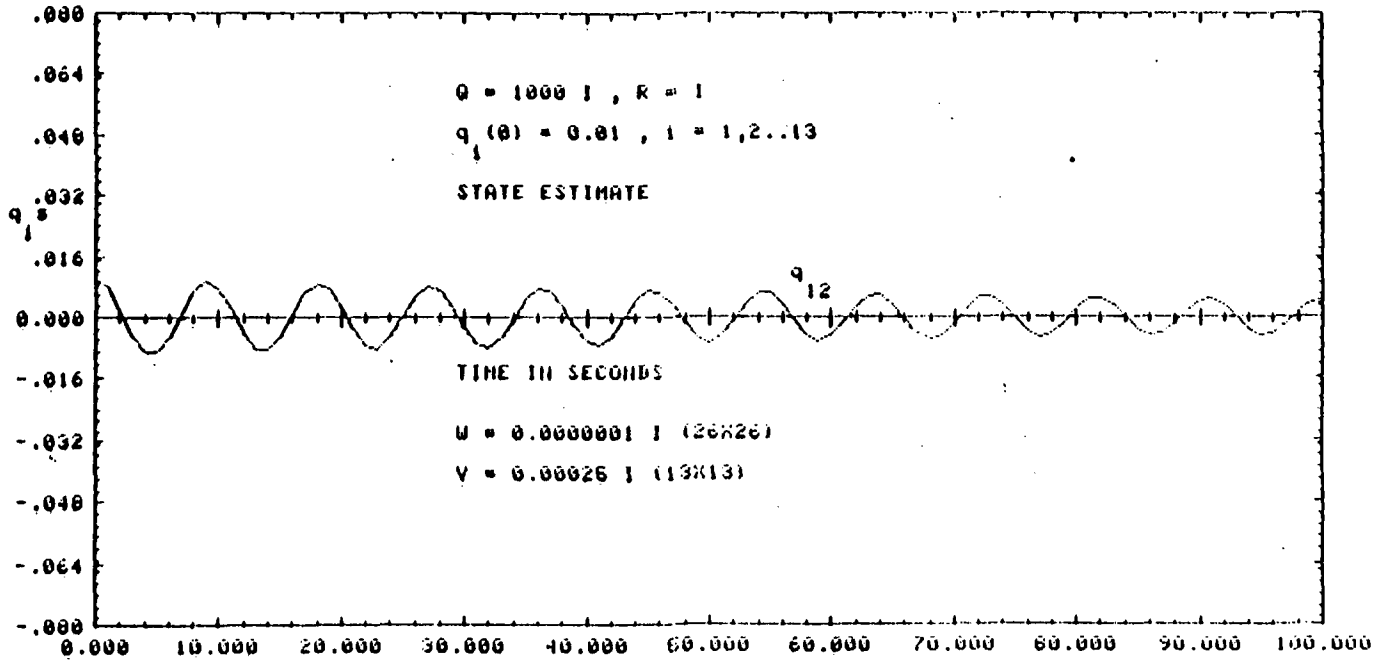

Fig. 8f Transient Response for 100 secs - Hoop / Column Antenna System 13 Actuators / 13 Sensors / 13 Modes - State Estimate, Effect of Changing Noise Parameters

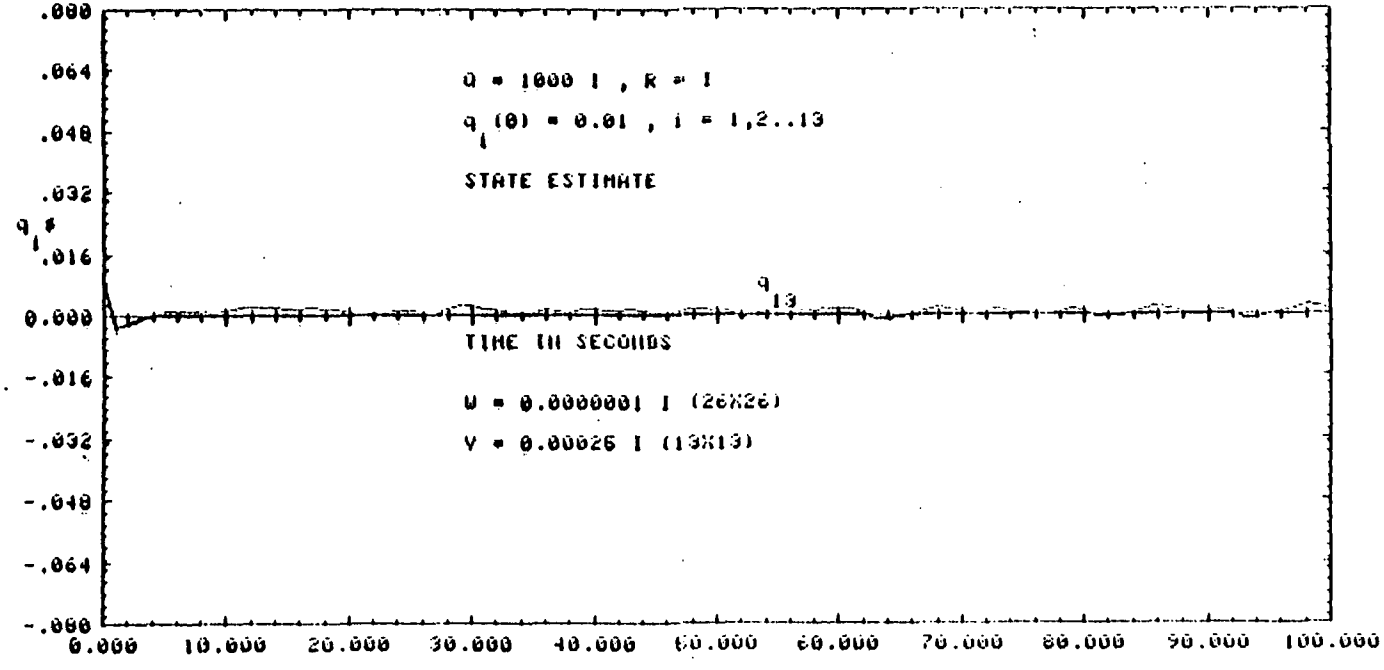

Fig. 8g Transient Response for 100 secs - Hoop / Column Antenna System 13 Actuators / 13 Sensors / 13 Modes - State Estimate, Effect of Changing Noise Parameters

Table 6

Comparison of maximum actuator force amplitudes

$Q=1000I$, $R=I$, $q_i(0)=0.01$, $i=1,2...,13$. 13 Actuators/ 13 Modes

Maximum actuator force amplitudes (pounds)	Stochastic case	
	W=0.00001	W=0.0000001
	V=0.0000025	V=0.00025
	Fig.6	Fig.8
f_1	0.3330	0.3490
f_2	0.0570	0.0570
f_3	0.2681	0.3010
f_4	0.0570	0.0569
f_5	1.3028	1.3028
f_6	0.2865	0.2865
f_7	1.2310	1.2310
f_8 (in-lb)	0.0140	0.0127
f_9	0.2859	0.2606
f_{10}	0.1574	0.1574
f_{11}	0.4086	0.4086
f_{12}	0.3521	0.3521
f_{13}	0.0660	0.0870

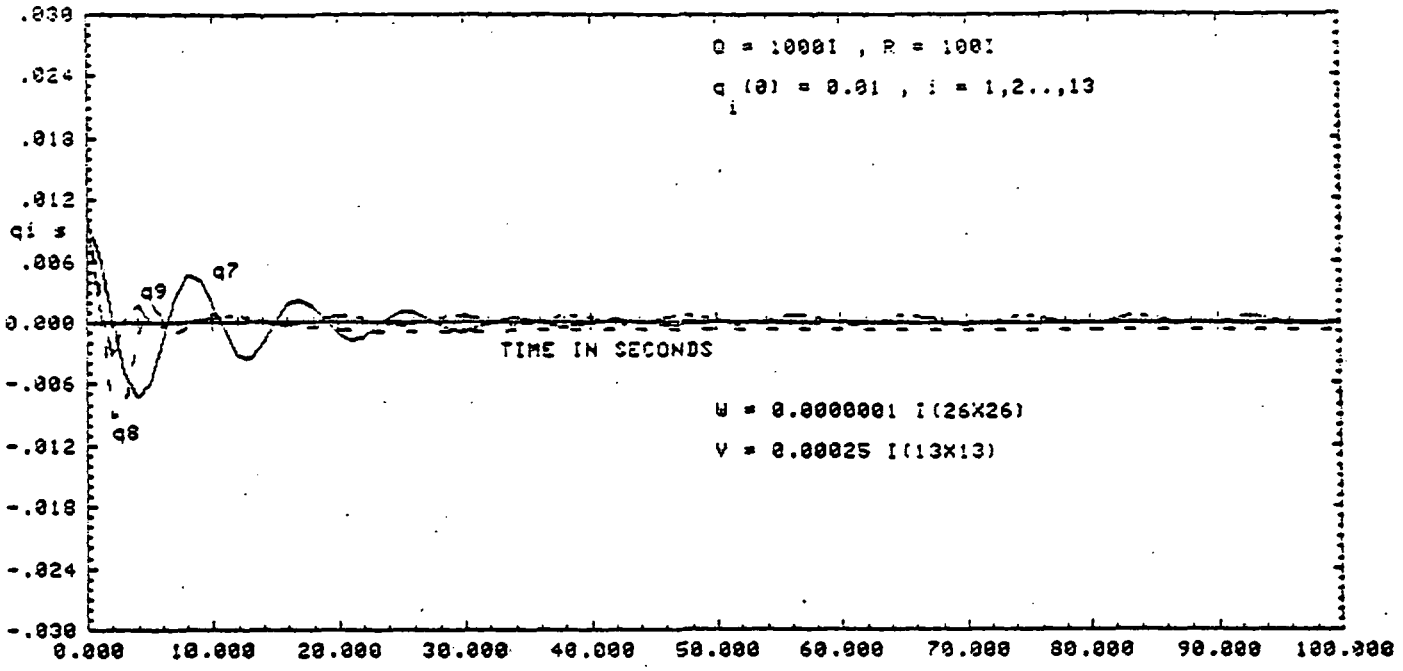

TRANSIENT RESPONSE FOR 100 SECS - HOOP/COLUMN

13 ACTUATORS - 13 MODES

STOCHASTIC CASE

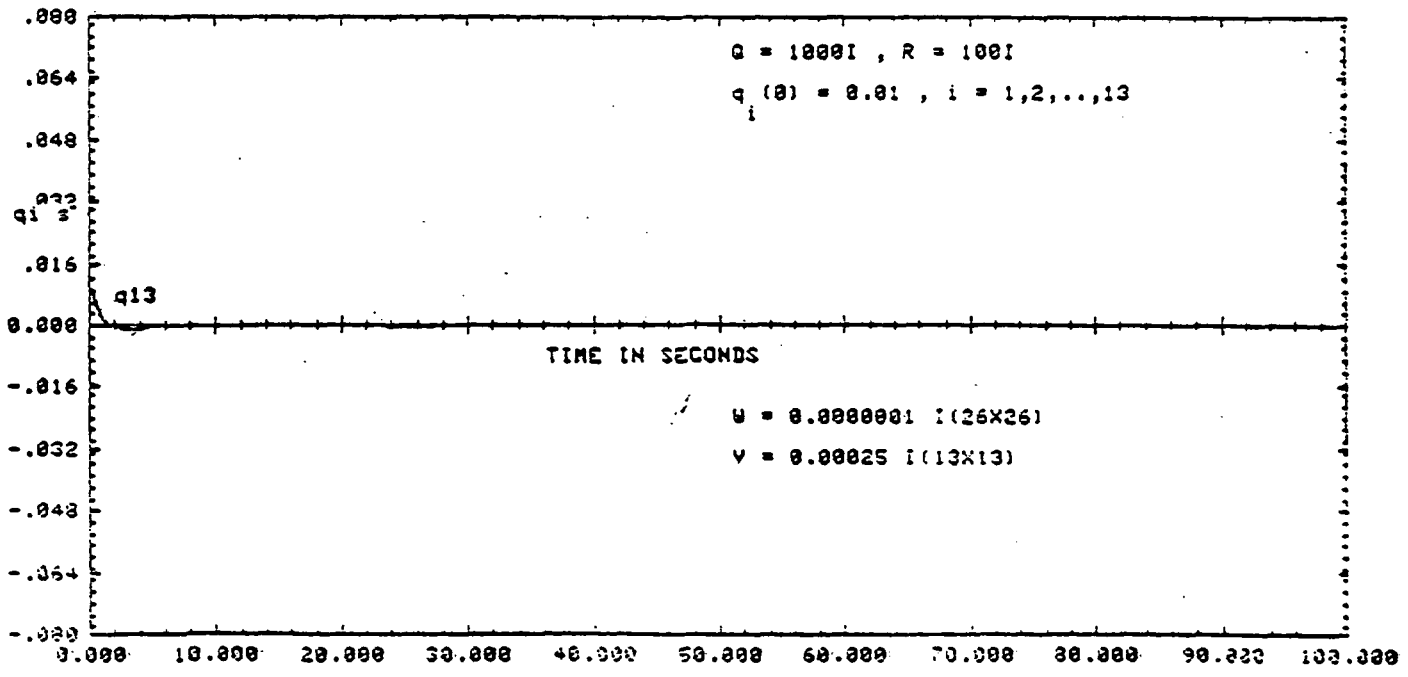

Fig. 9

IV. Concluding Comments

For all cases considered here the estimate of the state closely correlates with the actual (RMS) system dynamics. Some improvement in the transient performance may be achieve by increasing the sensor noise because the filter gain depends upon the inverse of the sensor noise covariance. As the sensor noise covariance is increased, the filter gain decreases and the matrix (A - FH - BC) increases causing a faster decay of the transients. However, one cannot increase the sensor noise covariance indefinitely since large values of sensor noise may affect the performance of the sensor itself, and thus, the estimation process. Plant noise can be reduced by incorporating appropriate filtering devices and this may also result in improved transient performance; here a definite trade-off exists between the increased complexity, cost, weight and reliability of the filter, and the possible gain in system performance. Further studies in this area are recommended.

When there is no or only limited flexiblity in altering the stochastic properties of the plant and the sensors, then one should consider the possible relocation of the actuators and /or sensors. It is suggested that this could form the basis for further research on this problem.

References

1) Sullivan, M.E., "Maypole (Hoop/Column) Concept Development Program, "Large Space Systems Technology - 1981, Third Annual Technical Review, NASA Langley Research Center, Nov. 16 -19, 1981, NASA Conference Publication 2215, Part 2, pp. 503 - 5550.

2) Reddy, A.S.S.R. and Bainum, P.M., "Controllability of Inherently Damped Large Flexible Space Structure," 33rd International Astronautical Congress,

Paris, Sept. 27 - Oct. 2, 1982, Paper No: IAF 82 - 319; also, Acta Astronautica, Vol. 10, No. 5 - 6, pp. 357 - 363, 1983.

3) Bainum, P.M. and Reddy, A.S.S.R.,"On the Controllability and Control Law Design for an Large Flexibile Antenna System", 34th International Astronautical Congress, Budapest, Hungary, Paper No. 83 - 340 (Oct. 10 - 15, 1983).

4) Joshi, S.M.,"Control Systems Synthesis for a Large Flexible Space Antenna", XXXIII rd Congress of the International Astronautical Federation, Paris,France, Paper No. 82 - 320 (Sept. 26 - Oct. 2, 1982).

5) Gelb, A.E.,(Editor) Applied Optimal Estimation, The M.I.T. Press,Massachusetts Institute of Technology, Cambridge, Massachusetts, 1974. (pp. 356 - 365).

6) Bryson, A.E. and Ho, Y.C., Applied Optimal Control, Blaisdell Publishing Co., Waltham, Massachusetts, 1969. (pp 414 - 418).

7) Armstrong, E.S., ORACLS - A Design System for Linear Multivariable Control (Volume 10), Marcel Dekker Inc., New York, 1980.

8) DeLorenzo, M.L.,"Selection of Noisy Sensors and Actuators for Regulation of Linear Systems", Purdue University, School of Aeronautics and Astronautics, West Lafayette, Indiana 47907. Technical Report prepared under grant AFOSR 82-0209 for The Air Force Office of Scientific Research .

VII. CONCLUSIONS AND RECOMMENDATIONS

The two dimensional model of the SCOLE configuration developed here will be extended to the three dimensional situation and control synthesis initiated for both linear systems analysis as well as for slewing maneuvers outside of the linear range. The ultimate goal of such an analysis will be to support the actual design of a scale model laboratory experiment to be prepared by the Flight Dynamics and Control Division at NASA Langley.

At this stage of our preliminary review of the stability of large ordered space structure systems with input delays, it is not completely conclusive that such large ordered systems under general oscillatory motions could be stabilized by a time delayed feedback. Further work in this area is anticipated together with a sample numerical example computation and is proposed for the next grant year.

It is found that for extremely flexible large orbiting platforms, especially those nominally oriented in the local horizontal plane, that appreciable amplitudes in the rigid modes may be induced by solar radiation pressure even in the presence of (active and/or passive) control. When this situation is suspected, linear quadratic regulator techniques offer a versatile means of redesigning control laws previously synthesized without compensating for environmental disturbances.

In general, thermal deformations of simple beam and platform type structures in orbit may be of greater concern than the deformations due to structural vibrations when modelling the disturbances arising from solar radiation pressure.

Within cost and weight constraints materials should be selected and designed so as to minimize the expected thermal deformations.

Our analysis of the stochastic optimal control of the proposed Hoop/Column antenna system indicates that increasing the appropriate elements in the state weighting matrix may not bring as noticeable improvement in the transient performance as it did for the deterministic case. A definitive improvement in both transient and steady state (RMS) performance can be realized by decreasing the plant noise and (1) suitably increasing the measurement noise or by (2) selectively increasing the measurement noise and also selected elements in the control weighting matrix.